

Editorial

Demonstration of controlled nuclear chain reaction by Fermi in 1942 paved the way for nuclear technology and ultimately culminating into construction of nuclear power reactors and research reactors. The Brookhaven Graphite Research Reactor (BGRR), world's first research reactor, came into operation in 1950. There are a large number of research reactors all over the world. Research reactors are simpler than power reactors, smaller in size and needs enriched fuel or efficient moderator and good reflectors. The primary purpose of a research reactor is to provide a neutron source for research. Neutrons have magnetic moment and no charge. De Broglie wavelength of thermal neutrons is around an Å. These properties make neutron an ideal probe for studies in condensed matter. Additionally, neutron induces reactions in the entire periodic table making it a good projectile for isotope production and activation analysis. Structure and dynamics of materials are studied using neutron beams; Material under real world conditions like varying temperature, pressure and magnetic field are probed using neutron scattering. Neutron activation is a sensitive and reliable technique to determine macro, micro and trace constituents of different matrices. Medicinally and industrially important isotopes are produced using research reactors. In addition research reactors are very useful in training and education. In view of innumerable applications, an issue on the utilization of research reactors is being brought out. It is impossible to cover all the aspects and therefore, it is limited to include articles on condensed matter physics research, activation analysis and production of radioisotopes. Accordingly Dr. S.M. Yusuf, guest editor chose the topics and experts to write the articles. My thanks are due to Dr. Yusuf for his excellent inputs and Dr. M. Ramanadham for providing guidance. I thank all the authors for excellent cooperation in giving the articles.

Special thanks are due to Dr. S.K. Sikka for giving Focus to this issue. I feel that it is a privilege for members of IANCAS to have an article from former DAE Chairman, Dr. R. Chidambaram who has been encouraging the activities of our Association. I am hopeful that readers will find this thematic bulletin useful.

CONTENTS

| | |
|-------------------------------------------------------------------------------------------------|------------|
| President's Message | iii |
| From the Secretary's Desk | iv |
| IANCAS News | v |
| Announcement - NUCAR 2003 | vi |
| Focus | 1 |
| Guest Editorial | 2 |
| National Facility for Neutron Beam Research (NFNBR) | 3 |
| <i>M. Ramanadham and S.M. Yusuf</i> | |
| Neutron Diffraction Studies of Hydrogen Bonded Crystals | 9 |
| <i>M. Ramanadham, S.K. Sikka and R. Chidambaram</i> | |
| Neutron Crystallographic Investigation of Ferroic and Electro-Optical Systems | 15 |
| <i>Rajul Ranjan-Choudhury, R. Chitra and P.U. Sastry</i> | |
| Neutron Diffraction Study of Crystals, Liquids and Glasses | 21 |
| <i>P.S.R. Krishna, S.M. Yusuf, S.K. Paranjpe, Keka R. Chakraborty and M. Ramanadham</i> | |
| Magnetism with Neutrons | 27 |
| <i>S.M. Yusuf, Keka R. Chakraborty and S.K. Paranjpe</i> | |
| Small-Angle Neutron Scattering at Trombay | 33 |
| <i>S. Mazumder, D. Sen, A.K. Patra, P.S. Goyal, V.K. Aswal and Ekta Seth</i> | |
| Inelastic Neutron Scattering for the Study of Atomic Vibrations and Magnetic Excitations | 39 |
| <i>Mala N. Rao, R. Mittal and S.L. Chaplot</i> | |

Contd.

CONTENTS (Contd.)

| | | | |
|----------------------------------------------------------------------------------|-----------|-----------------------------------------------------------------------------------------------|-----------|
| Neutron Quasi-elastic Scattering in Material Science | 45 | Neutron Detection Techniques in Neutron Scattering and Radiography Experiments | 66 |
| <i>S. Mitra and R. Mukhopadhyay</i> | | <i>A.M. Shaikh</i> | |
| Neutron Reflectrometry : An Ideal Tool for Thin Film Characterization | 50 | Large Scale Radioisotope Production | 72 |
| <i>Saibal Basu</i> | | <i>M. Ananthakrishnan, S.V. Thakare and K.V.S. Sastry</i> | |
| Neutron Interferometry and Optics | 54 | Prospects and Challenges in Production of Radionuclides for Therapy | 78 |
| <i>A.G. Wagh and Veer Chand Rakhecha</i> | | <i>V. Meera, M.R.A. Pillai and N. Ramamoorthy</i> | |
| Neutron Activation Analysis | 60 | | |
| <i>A.V.R. Reddy, R. Acharya and A.G.C. Nair</i> | | | |



President's Message

Since Chadwick first produced free neutrons in 1932, neutrons have been used in scientific investigation in varied fields such as, physics, chemistry, material science, agriculture engineering and biology. Till the discovery of nuclear fission and subsequent development of nuclear reactors, neutron source strengths were limited to $\sim 10^5 - 10^6$ n/sec. With advancement in reactor technology, now research reactors with neutron flux in the range of $10^{12} - 10^{15} \text{ cm}^{-2} \text{ s}^{-1}$ are currently in operation. Some of the properties of neutron which make it a versatile research tool are high penetration in matter, relatively good cross section for absorption and scattering for isotopes across the periodic table, its magnetic moment which leads to interaction with unpaired electrons and de Broglie wavelength of the same order as that of inter atomic distances in solids/liquids. Thus a research reactor is very useful tool for scientific research. One of the major uses of research reactors is production of radioisotopes which find application in almost all branches of science. These reactors can also be used as a tool for teaching and growing public awareness in the areas of nuclear technology. Students of basic sciences such as chemistry, physics, biology and medicine can be initiated into nuclear science applications at research reactors. The teaching programme in the area of radiation protection and radiological safety can also be effectively carried out using research reactors. Some of the areas connected with basic science are covered in this issue as contributed articles by scientists working in the respective fields. I would like to add to this by way of listing some of the applications which are not covered.

High flux of neutrons and gamma rays make a reactor useful for irradiation induced transmutation effects in varieties of materials. One of the promising applications is that of neutron transmutation doping of high purity silicon. This method is superior to any other technique as it produces a uniform phosphorous doping over the entire volume of irradiated silicon. Value addition by enhancing the colour of diamonds by neutron/gamma irradiation is another important area. Neutron radiography produced images in films have been used in many areas of R&D e.g., radiography of irradiated fuels. One such facility KAMINI has been now created at IGCAR. Irradiation of seeds by neutron /gamma rays for mutation is being carried out in BARC over a long period. Research reactors are also useful in geological dating by Ar/K determination as well as fission track measurements using solid state nuclear track detectors. Positrons are very useful for materials study. Research reactors based positron beam facilities can add to its versatility by way of defect depth profiling. The positrons can be created by activation of a source (such as Cu) as well as by capture gamma ray conversion. Positron intensities of the order of 10^6 to 10^7 p/s could be produced which can further be converted in to beam of tunable energy. Neutron capture therapy using $B(n,\alpha)$ reaction for cancer treatment is yet another exciting application of research reactors.

In short the research reactor has a multidimensional uses and one such facility can effectively be used by hundreds of scientists for quality research. I am thankful to Dr. S.M. Yusuf, guest editor and Dr. A.V.R. Reddy, Editor for their efforts in bringing out this excellent volume and Dr. S.K. Sikka for giving focus to this issue.

S.B. Manohar

From the Secretary's Desk



Dear Members,

Greetings to the members,

The use of research reactors as a steady neutron source showed the practicality of generating radioisotopes on a large scale and the utility of the neutron as a powerful tool to characterize the structure of matter. Further efforts on intensifying the utilization of neutron evolved in to the development of neutron-scattering techniques for application to many areas of research in nuclear and non-nuclear science and technology. Department of Atomic Energy with its multi-disciplinary strength has gainfully employed the three research reactors at Trombay for various applications in and outside the Atomic energy establishments. In view of the steadfast encouragement from the DAE, the academic users are expected to be enthused in engaging the neutron in myriad of applications such as material analysis, basic research in solid-state physics, activation analysis, studies on magnetic materials and production of innumerable number of radioisotopes.

Dr. Yusuf has put noteworthy efforts as the guest editor of this issue in the selection of the articles and the respective contributors.

The Southern Chapter of IANCAS at Kalpakkam is now geared up to establish itself under the guidance of Dr.P.R.Vasudeva Rao, Associate Director, Chemical Group, IGCAR and with the active involvement of our members to serve the cardinal objective of the Association in popularizing the subject in that region. I appeal to all the members once again to update their mailing addresses including the email ID to help IANCAS to bring out a member directory.

I am happy to inform the members that BITS, Pilani has obtained the clearance from AERB to set up a radiochemical laboratory by appointing a Radiation Safety Officer on the basis of his participation in BRNS-IANCAS National Workshop held at Pilani during 2000. I take pleasure in sharing with the members that Registrar of News Papers for India, Delhi allotted the Registration Number to our Bulletin for its objective of functioning for social cause. IANCAS gratefully acknowledges the kind help from Sri P.S.Parihar, our colleague from AMD, Delhi in pursuing the matter with the Delhi office.

IANCAS continues to receive invitations for organizing BRNS-IANCAS National Workshops from universities and institutes and the resource persons utilize this opportunity to visit the schools and colleges in the vicinity of the Workshop to expose the children to this exciting science through simple lectures, video-shows and conducting experiments on radioactivity measurement.

BRNS has been supportive of one of the major activities of IANCAS, namely organizing the National Workshops on 'Radiochemistry and Applications of Radioisotopes'. IANCAS is grateful to BRNS for its appreciation of these thematic bulletins with generous grants every year.

G.A.Rama Rao

Announcement

DAE-BRNS Symposium on Nuclear and Radiochemistry (NUCAR 2003)

The sixth biennial symposium "Nuclear and Radiochemistry" (NUCAR 2003) is being organised by the Board of Research in Nuclear Sciences (BRNS), Department of Atomic Energy at Bhabha Atomic Research Centre, Mumbai, during February 10-13, 2003. The objective of the symposium is to provide a forum for effective interaction among the scientists in the areas of Nuclear and Radiochemistry and Applications of Radioisotopes for the advancement of these disciplines. It is hoped that scientists engaged in research in these areas from National Laboratories, Universities and Research Institutes from India and abroad, will actively participate in large numbers.

Scope

- Nuclear chemistry
- Chemistry of actinides and reactor materials
- Spectroscopy of actinides
- Radioisotope applications
- Chemistry of fission and activation products
- Radioanalytical chemistry
- Radioactivity in environment
- Nuclear instrumentation

*The scientific programme of the symposium will include invited talks by eminent scientists as well as contributed papers. An important feature of this symposium would be half a day special seminar on **APPLICATIONS OF ACCELERATORS INCLUDING ACCELERATOR DRIVEN SUBCRITICAL SYSTEMS, MEDICAL CYCLOTRONS, LOW ENERGY ACCELERATORS** etc.*

Last Date for Receipt of Manuscripts : October 31, 2002

Registration Fee

Rs.100/- for research scholars, delegates from National lab.
Rs.250/- for delegates from PSUs
Rs.500/- for other delegates

Persons to be contacted for further correspondence

Dr. B.S. Tomar
Convener, NUCAR 2003
Radiochemistry Division
Bhabha Atomic Research Centre
Mumbai 400 085, INDIA
Tel. 91-22-559 5011
Fax: 91-22-5505151
E-mail : bstomar@apsara.barc.ernet.in

Shri M.K. Saxena
Secretary, NUCAR 2003
Fuel Chemistry Division
Bhabha Atomic Research Centre
Mumbai 400 085, INDIA
Tel.91-22-559 2456
Fax: 91-22-5505151

IANCAS News

It has been our endeavour to include prominent events and latest scientific news in our Bulletin. Members have been requested to send us brief note on such items. I am glad that one of Life Members of IANCAS, Shri B.K. Bhasin, Senior Adviser (Operations), NPCIL, Mumbai has sent important information about commencement of commercial operation of our nuclear power reactors and nuclear power projects under construction which are given below. I urge members and readers to contribute to IANCAS News.

A.V.R. Reddy

Nuclear Power Reactors in India

| Unit | Installed Capacity (MWe) | Date of Synchroni- zation | Date of Commer- cial Operation |
|---------|--------------------------|------------------------------|--------------------------------------|
| TAPS-1* | 160 | 01.04.69 | 01.11.69 |
| TAPS-2* | 160 | 08.05.69 | 01.11.69 |
| RAPS-1 | 150 | 30.11.72 | 16.12.73 |
| RAPS-2 | 200 | 01.11.80 | 01.04.81 |
| MAPS-1 | 170 | 23.07.83 | 27.01.84 |
| MAPS-2 | 170 | 20.09.85 | 21.03.86 |
| NAPS-1 | 220 | 29.07.89 | 01.01.91 |
| NAPS-2 | 220 | 05.01.92 | 01.07.92 |
| KAPS-1 | 220 | 24.11.92 | 06.05.93 |
| KAPS-2 | 220 | 04.03.95 | 01.09.95 |
| KAIGA-2 | 220 | 02.12.99 | 16.03.2000 |
| RAPS-3 | 220 | 10.03.2000 | 01.06.2000 |
| KAIGA-1 | 220 | 12.10.2000 | 16.11.2000 |
| RAPS-4 | 220 | 17.11.2000 | 23.12.2000 |

Total installed capacity = 2770 MWe

*BWR (Boiling Water Reactors)

All others are PHWR (Pressurised Heavy Water Reactors)

Nuclear Power Reactors under construction

| Project | Rated capacity (MWe) |
|------------|----------------------|
| RAPP-5 | 220 |
| RAPP-6 | 220 |
| TAPP-3 | 500 |
| TAPP-4 | 500 |
| KAIGA-3 | 220 |
| KAIGA-4 | 220 |
| Kudankulam | 2000 (two units) |

Total rated capacity = 3880 Mwe

Received from

Shri B.K. Bhasin, Sr. Adviser (Operations), NPCIL

Utilization of Research Reactors

Guest Editor

Dr. S.M. Yusuf

Solid State Physics Division
Bhabha Atomic Research Centre
Mumbai 400 085



FOCUS

Dr. S.K. Sikka

*Director, Atomic & Condensed Matter Physics Group
Bhabha Atomic Research Centre, Mumbai 400 085*

Neutron is a nuclear particle with zero charge. Thermal neutrons have de Broglie wavelength of $\sim 1 \text{ \AA}$. These properties make the thermal neutrons suitable for probing the positional arrangement of atoms, ions or molecules in condensed matter. Further, the kinetic energy of such neutrons is of the order of meV, which is a typical energy for collective excitation of atomic and molecular vibrations in solids and liquids and thus suitable for studying dynamics in condensed matter. Neutron also possesses a magnetic moment of -1.913 nuclear magnetons, which makes the thermal neutrons an ideal probe to study the structure and dynamics of magnetic materials. Small Angle Neutron Scattering is very useful for studying large inhomogeneities ($\sim 20 - 1000 \text{ \AA}$) that are present in any substance. Neutron reflectometry can be used for a very sensitive and useful non-destructive technique for characterising surfaces, interfaces, multilayers and thin films. Neutron radiography and neutron interferometry & optics are other promising areas in neutron beam research. Neutron activation analysis for multielemental analysis is one of the major applications of a research reactor. Neutrons are also very useful for the production of radioisotopes.

Apsara, CIRUS and Dhruva are the three research reactors in India, which have catered to research and development programs at Trombay, particularly for condensed matter studies, neutron activation analysis and radioisotope production during the past four decades. The first neutron spectrometer installed at Apsara in 1959 laid the foundation. It provided very useful means for training scientists in the initial phases of neutron beam research programmes in India. Currently, it is being used for neutron detector testing, neutron radiography, neutron activation analysis and isotope production. CIRUS reactor was the main facility for nearly three decades (1962-1985) for condensed-matter research, isotope production and training centre. To meet the increasing demands of such research reactors, Dhruva reactor (indigenously designed and built, 100 MW maximum thermal power with corresponding neutron flux at the core of the reactor $\sim 1.7 \times 10^{14} \text{ n/cm}^2/\text{s}$, criticality date: August 8, 1985) was built with better technical facilities. The Dhruva reactor is being used for basic and applied research in various disciplines of condensed matter physics, nuclear physics and nuclear engineering, activation analysis, radioisotopes production, training the scientific and technical personnel in the field of nuclear technology. Neutron scattering research in India has shown a rapid expansion both in the number of users and in the diversity of disciplines and science to which neutron methods are being applied. Fully automated computer controlled neutron instruments were built at Trombay. Radioisotope production programme has been an on-going activity at Trombay for more than four decades. The present requirement of radioisotopes for different applications in medicine, industry, agriculture and research in our country is being met. India ranks high in the list of nations capable of producing large quantity of radionuclides.

I am glad that IANCAS decided to bring out a special issue on Utilization of Research Reactors in India with articles on neutron beam research in condensed matter physics, neutron activation analysis and production of radioisotopes. I am happy to state that Dr. S.M. Yusuf, the guest editor has done a good job in choosing the articles and the authors for the articles. I take this opportunity to compliment all the authors for their valuable contributions, the guest editor and the editor for their efforts in bringing out this issue. This special issue on Research Reactor Utilization is aimed primarily at professionals in different scientific and engineering disciplines who may not be sufficiently aware of the opportunities provided by the research reactors (in particular the Dhruva reactor) in Trombay. I am sure that this issue of IANCAS will be useful to members of the IANCAS and other readers.

Guest Editorial

Dr. S.M. Yusuf

*Solid State Physics Division,
Bhabha Atomic Research Centre, Mumbai 400 085*



The neutron, which was discovered by Chadwick in 1932, has been used in scattering experiments from condensed matter since 1946, starting with the pioneering work of Shull and Wollan. Neutron scattering is one of the most powerful tools to investigate the structure and dynamical properties of condensed matter. Neutron scattering research has spread in physics, chemistry, metallurgy, biology and other fields. Neutrons are also used for production of radioisotopes. In our country, neutron beam research and radioisotope production were initiated at Apsara reactor in 1956 and have grown over the years. A qualitative change has occurred with the full operation of Dhruva reactor since 1988.

It is nice that IANCAS is bringing out this bulletin on “Utilization of Research Reactor”. It was thought to be appropriate to have articles on neutron beam research (NBR) in condensed matter, neutron activation analysis and, production of radioisotopes; the major areas of utilization of research reactors at Trombay.

In this issue, there are eleven articles covering various aspects of neutron beam research in condensed matter physics and one article on neutron activation analysis, which are presently being pursued mainly at Dhruva reactor, Trombay. In addition to this there are two articles on the production of radioisotopes in Trombay, using Apsara, CIRUS and Dhruva reactors. The very first article is on National Facility for Neutron Beam Research, which gives an overview of the neutron beam research program at Trombay. The use of neutrons to study the structure of matter at atomic resolution has been described in more than three articles. The unpolarized and polarized neutron scattering activities for magnetic studies are described briefly in one of the articles. The inelastic and quasielastic neutron scattering for studying the translational, vibrational and rotational motions of atoms and molecules in condensed matter are also included. The principle and application of neutron small angle scattering for studying precipitates, nanocomposites, soft matters etc. are given in an article. The present issue also includes articles on the neutron reflectometry technique for characterization of thin films and, neutron interferometry and optics. The principle and application of neutron activation analysis are described in an article. The principle and use of the neutron detection technique in neutron scattering and radiography experiments have been brought out in one of the articles. Out of two articles on the production of radioisotopes, one deals with the large-scale production of radioisotopes and the other gives the details of the prospects and challenges in production of radionuclides for therapy.

In this bulletin no attempt is made to provide an exhaustive coverage, only a very brief coverage of the present activities in the area of neutron beam research, neutron activation analysis and, production of isotopes in Trombay is given. I am hopeful that these articles are of interest to IANCAS members and other readers.

I thank Dr. A.V.R. Reddy, Editor, IANCAS, for asking me to be the guest editor. I am thankful to Dr. M. Ramanadham, Head, Solid State Physics Division, BARC for his support. I am extremely thankful to Dr. S.K. Sikka, Director, Atomic & Condensed Matter Physics Group, BARC for providing the “focus” to this bulletin. My thanks are due to all the authors of this bulletin for their contributions.

National Facility for Neutron Beam Research (NFNBR)



Dr. M. Ramanadham, currently the Head, Solid State Physics Division, BARC, started his research career at BARC in 1969 in the field of neutron crystallography and hydrogen bonding studies on biomolecules. He obtained Ph.D. degree in 1975 from the University of Mumbai. Subsequently, he worked on x-ray protein structures. His interests include crystallographic computing, statistical analysis of crystallographic data, hydrogen bonding and parallel computing. He served as an elected member of the Computing Commission of the International Union of Crystallography during 1993-96 and 1996-99. Presently, he is the Hon' General Secretary of the Indian Physics Association.

Dr. S.M. Yusuf joined the magnetism section of Solid State Physics Division (formerly Nuclear Physics Division), BARC in 1989 after completing 32nd batch of BARC Training School. He received his M.Sc. degree in Physics from Visva Bharati University in 1987 and Post M.Sc. degree in Physics from Saha Institute of Nuclear Physics in 1988. He was intimately connected with the setting up of the neutron polarization analysis spectrometer at Dhruva reactor for magnetic scattering studies. He has also set up a low temperature laboratory for macroscopic magnetic studies. He acquired the Ph. D. (Physics) degree of the University of Mumbai in 1997 and he was a post doctoral fellow at Argonne National Laboratory, USA during 1997-1998. Dr. Yusuf has published a large number of papers in international scientific journals. He has received Best Young Physicists Award from Indian Physical Society and N.S. Sathya Murthy Award from Indian Physics Association in 1996 in recognition of his contributions to neutron scattering from magnetic materials. He is a member of American Physical Society.



Neutron beam research in condensed matter physics is one of the most important R&D activities of the Department of Atomic Energy (DAE) in general, and Bhabha Atomic Research Centre (BARC), in particular. This activity at BARC, over the last four and a half decades, has resulted in excellent basic research, both in terms of in-house research, and national and international collaborations. This article attempts to provide a brief, bird's eye view of neutron beam research at BARC.

Thermal Neutrons: Production, Detection and Utilization

Neutron is a spin-1/2 nuclear particle, having a mass of $1.674929 (1) \cdot 10^{-27}$ kg (equal to

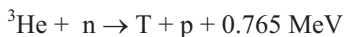
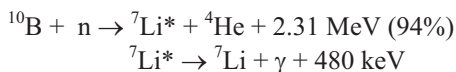
$1.00866490(1)$ amu, or, $939.5656(3)$ MeV). Though electrically neutral, a neutron possesses magnetic dipole moment, $\mu_n = -1.9130428(4)$ nuclear magnetons. Wavelength associated with a neutron of energy, E , is given by $\lambda = (0.286/\sqrt{E})$, where the wavelength and energy are expressed, respectively, in Å units (10^{-10} m) and electron volts (eV). For example, wavelength associated with neutrons of energy 36.4 meV is 1.5 Å. The velocity and frequency associated with these neutrons are, respectively, 2637 m/s and 1.76×10^{13} Hz. Thus, neutrons with their energies in the milli electron volt range, known as thermal neutrons, are ideally suited to study the structure of matter at atomic resolution, as well as dynamics of atoms in materials. The added advantage of the neutron having a magnetic dipole

Dr. M. Ramanadham, Dr. S.M. Yusuf, Solid State Physics Division, Bhabha Atomic Research Centre, Trombay, Mumbai 400 085;
E-mail : ramu@magnum.barc.ernet.in; smyusuf@apsara.barc.ernet.in

moment makes it an ideal probe to study the structure and dynamics of magnetic materials also.

Two very important, high-intensity sources of neutrons for condensed matter physics research are, fission reactors and spallation sources. In nuclear fission reactors, the ^{235}U isotope undergoes fission, producing, two, or three neutrons, in addition to fission fragments. These neutrons, initially of high energies, are slowed down to thermal energies, using moderators, such as heavy water (D_2O). A coolant removes the heat generated in the reactor. Either H_2O , or D_2O is used mostly for this purpose. The equilibrium energy distribution of neutrons in a thermal reactor is Maxwellian, with most of the neutrons having energies in milli electron volt range. The neutron flux can be in the range of 10^{13} to 10^{15} neutrons/cm²/s. A nuclear reactor of this type is a continuous source of neutrons, whose flux varies as the equilibrium energy of the reactor changes. On the other hand, a spallation source produces a pulsed neutron beam. A spallation neutron source is realized by bombarding a heavy-atom target by a high-energy charged-particle beam. For example, one proton, accelerated to energy of 600 MeV can produce 10-12 neutrons of an average energy of 2-3 MeV from a target such as tungsten or lead, and about 25 neutrons from a ^{238}U target. The average neutron production (not neutron flux) in a spallation source can be as high as 10^{16} neutrons/s. The pulse frequencies, and widths are, typically 50 Hz and a few microseconds respectively.

The simplest way to detect neutrons is by using a neutron-induced nuclear reaction. Proportional counters using BF_3 gas (enriched with ^{10}B isotope) and ^3He gas, and fission counters are among the most popular neutron detectors today. The nuclear reactions in the two former detectors are,



Thus, a typical neutron beam experiment in condensed matter physics research requires a thermal neutron source, a neutron diffractometer, or spectrometer, with appropriate instrument control

and neutron counting electronics, a neutron detector, and a PC for instrument control, data acquisition and preliminary processing.

Neutron Beam Research in India

Apsara, a low flux thermal reactor using enriched uranium as fuel, and light water as moderator and coolant, was the first research reactor to attain criticality, during mid fifties. Neutron beam research, initiated at Apsara, thus became the first such endeavor not only in India but also in Asia. This activity advanced very significantly, when Cirus, a 40 MW research reactor using natural uranium as fuel, heavy water as moderator and light water as coolant, became available at BARC during early sixties. During sixties, seventies and up to mid-eighties, many semi-automatic and automatic neutron spectrometers were built and operated at BARC. During the same period, India has helped many Asian countries, such as Philippines, South Korea, Indonesia, and other countries, in developing neutron beam facilities, and training manpower. Some of the significant research activities using neutrons during this period were, crystal structure studies on hydrogen-bonded materials, such as inorganic hydrates and amino acids, studies on magnetic materials, such as heusler alloys, mixed spinels and dilute magnetic systems and dynamics of atomic motions in various substances, such as Mg, Zn, Be and NH_4 -halides, etc.

Neutron beam research at BARC has entered its third phase with the availability of Dhruva, a medium flux research reactor operating at 100 MW power, and using natural uranium as fuel, heavy water as moderator and primary coolant, and light water as secondary coolant. More advanced instruments, fully automatic in instrument control and data acquisition modes, have been installed on various beam ports in Dhruva reactor. Table 1 lists a detailed account, including the instrument parameters, of these neutron instruments. A Neutron Guide-Tube Laboratory (GTL) has also been built, adjacent to the reactor hall. Two nickel coated neutron guides, emanating from a beam port inside the reactor hall are taken in to this laboratory. One of the guides is 21 metres long with a horizontal radius of curvature of 1916 metres, and the other, 35 metres long with a horizontal radius of curvature of 3452 metres. Details of the neutron instruments, either in

TABLE 1: Neutron Instruments in Dhruva Reactor Hall

| Instrument, Beam Location & Parameters |
|----------------------------------------------------------------------------------------------------------------------------------------------------------------------------------------------------------------------------------------------------------------------------------------------------------------------------------------------------------------------------------------------------------------------------------------------------------------------------------------------------------------------------------------------------------------------------------------------|
| Profile Analysis Powder Diffractometer-1: Located at the through-tube TT1015 Monochromator: Si(422) with take-off angle $2\theta=60^\circ$; Wavelength: 1.094 Å Scattering angle range: $5 < 2\theta < 120^\circ$; Detector: One linear He ³ PSD, covers 30° in one setting $\sin \theta/\lambda_{\max}$: 0.8 Å ⁻¹ ; Flux at sample: 5×10^5 n/cm ² /s; Resolution: ($\Delta d/d$): 1% |
| Profile Analysis Powder Diffractometer-2: Located at the tangential beam tube T1013 Monochromator: Ge (331) with take-off angle, $2\theta_M=57^\circ 27'$; Wavelength: 1.249 Å Scattering angle range: 0-130°, covered simultaneously five He ³ PSDs $\sin \theta/\lambda_{\max}$: 0.73 Å ⁻¹ ; Typical resolution ($\Delta d/d$): 0.01 |
| Single Crystal Diffractometer: Located at the tangential beam tube T1011 Monochromator: Pyrolytic Graphite (0002); Wavelength: 1.206 Å; $\Delta\lambda/\lambda$: 0.01 Scattering angle range: $0 < 2\theta < 120^\circ$; Flux at Sample: 1×10^6 n/cm ² /sec |
| Polarization Analysis Spectrometer: Located at tangential beam tube T1009 Monochromator/Polarizer: Cu ₂ MnAl (111); Wavelength: 1.205 Å Analyzer: Co _{0.92} Fe _{0.08} (200), or Cu ₂ MnAl (111); Beam polarization: > 0.98 Scattering angle range: $0 < 2\theta < 112^\circ$; Flux at Sample: 5×10^5 n/cm ² /sec Magnetic field at sample: horizontal or vertical; Low temperature: (10-300 K) with closed cycle helium cryo-cooler |
| Triple Axis Spectrometer: Located at Tangential beam tube T1007 Monochromators: Cu(111), etc.; Analyzer: Pyrolytic Graphite (0002) Range of incident neutron energy: 15-150 meV; Scattering angle: $15^\circ < 2\theta < 90^\circ$ Neutron flux at sample position: 2.5×10^6 n/cm ² /sec; Resolution: $\Delta E/E = 0.2$ |
| Quasi-Elastic Neutron Spectrometer: Located at Through-tube TT1004 Double Monochromator: Pair of pyrolytic graphite (0002) Analyzer: pyrolytic graphite (0002) in MARX mode Wavelength range: 1.3 to 4.7 Å; Energy range: $3.7 < E(\text{meV}) < 50$ Scattering angle: -80° to $+80^\circ$; Analyzer angle: -110° to $+110^\circ$ Maximum wavevector transfer: 8 Å ⁻¹ ; Maximum energy transfer: 24 meV Energy transfer range: 2.3 meV at $E = 5$ meV; Detector: One linear He ³ PSD Energy resolution: $\Delta E/E = 0.04$ |
| High-Q Diffractometer: Located at HS1019 Monochromator: Cu (111), or Cu (220) with take-off angle, $2\theta_M=35^\circ 40'$ Wavelength: 1.278 Å or 0.783 Å Range of scattering angles: $2 < 2\theta < 140^\circ$, covered simultaneously with 5 He ³ PSDs $Q (= 4\pi\sin\theta/\lambda)$ range: 0.3 – 15 Å ⁻¹ ; Resolution ($\Delta Q/Q$): 0.025 Neutron Flux at Sample Position: 2×10^6 (at $\lambda=1.278$ Å) and 3×10^5 (at $\lambda = 0.783$ Å) |
| Filter Detector Spectrometer: Located at HS1017 Monochromators: Pyrolytic Graphite (0002), etc. Analyzer: polycrystalline Be filter (replaceable with BeO) Incident neutron energy: 10-250 meV; Scattering angle: $-90^\circ < 2\theta < 120^\circ$ Typical flux at Sample: 10^6 n/cm ² /sec; Resolution: $\Delta E/E = 0.2$ |

Table 2. Instruments in Guide Tube Laboratory near Dhruva Reactor

| Instrument, Location & Parameters |
|--------------------------------------------------------------------------------------------------------------------------------------------------------------------------------------------------------------------------------------------------------------------------------------------------------------------------------------------------------------------------------------------------------------------------------------------------------------------------------------------------------------------------------------------------------------------------------------------------------------------------------------------------------------|
| Neutron Spin Echo Spectrometer: (Under development & installation at guide tube G1) Monochromator: BeO used as filter; Mean wavelength: 5.2 Å; FWHM: 20% Polarizer: Co-Ti Supermirrors; Polarization Efficiency: >0.9; Analyser: Co-Ti Supermirrors Detector: BF ₃ ; Flux at sample: ~10 ⁴ n/cm ² /s; Maximum accessible Fourier time t in F(Q,t): 1 ns Corresponding energy resolution in S(Q,E): 1 µeV |
| Double Crystal SANS Diffractometer: Located at guide tube G2-1 Monochromator: Si (111); Analyser: Si (111); Wave length (λ): 3.12 Å, Δλ/λ = 0.01 Q range: 3x10 ⁻⁴ to 1.73 x10 ⁻² Å ⁻¹ ; Resolvable real space dimension: 20000-400 Å. Flux at sample position: ~ 500 n /cm ² /s |
| Polarized Neutron Reflectometer: (Under installation & testing at guide tube G2-2) Monochromator: Si(311); Mean monochromatic wavelength: 2.4 Å; Δλ/λ: 0.01 Polarizer: Supermirror Co-Fe/Ti-Zr; Polarizing efficiency: 96%, θ _c ~12'/Å or Reflector: Ni-Mo/Ti; Reflectivity: 80%; Polarization Flipper: DC flipper Analyzer: similar to Polarizer Supermirror; Detector: linear He ³ PSD, 20 cm long 60 mm diameter Flux at sample position (estimate): 10 ⁴ n/cm ² /s ΔQ/Q: ~ 0.1 (ΔQ ~0.006 Å ⁻¹ at glancing angle of 30'); Max. Film thickness can be studied: 1500 Å |
| SANS Diffractometer: (Conventional): Located at guide tube G2-3 Monochromator: polycrystalline BeO filter at 77K; λ _{cutoff} : 4.7 Å Mean λ: 5.2Å; Δλ/λ: 0.15; Detector: linear He ³ PSD Accessible Q range: 1.8 x10 ⁻² to 3.2 x10 ⁻¹ Å ⁻¹ ; Resolvable real space dimension: 150 to 10 Å Neutron Flux at sample position: 2.2x10 ⁵ n/cm ² /s |

operation, or under development in this lab, are listed in Table 2. A layout sketch of the neutron instruments in the reactor hall and GTL is given in Fig. 1, and a view of some of the instruments inside the reactor hall is shown in Fig. 2. In addition, detector development and testing, and neutron radiography are being pursued at Apsara reactor. Neutron and x-ray detectors, developed by SSPD, not only meet all the in-house requirements of NFNBR, but also are supplied to various users within and outside BARC, others units in India and other Asian countries.

The National Facility: NFNBR

The National Facility for Neutron Beam Research (NFNBR) has been created as a part of the Solid State Physics Division (SSPD) at BARC during early nineties to cater to the needs of the

Indian scientific community in the field of neutron beam research. Scientists from BARC, other DAE units, universities and national laboratories are welcome to use these facilities through collaborative research projects with SSPD scientists, who would, not only involve themselves actively in the experiment and analysis, but also help the visiting scientist in understanding the intricacies of neutron beam research. Many of these collaborations are being supported by Inter-University Consortium for DAE Facilities (IUC-DAEF), BRNS, and other agencies. NFNBR, in collaboration with the Mumbai Centre of IUC-DAEF has been arranging annual workshops on various aspects of neutron beam research to train young scientists working in this field. Over forty collaborations, under various supporting schemes to the participating scientists from outside DAE, many of them with support from

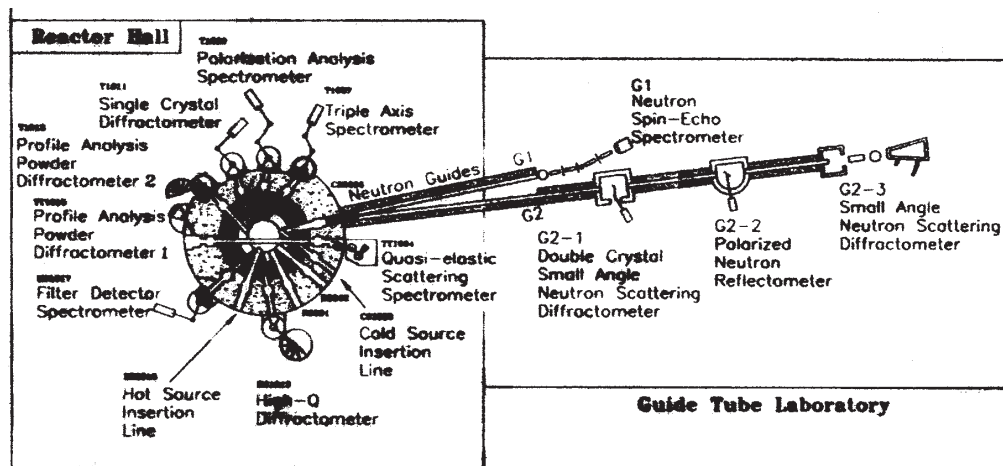


Fig. 1 Sketch showing the locations of neutron instruments inside Dhruva Reactor Hall and Guide Tube Laboratory and layout of the two neutron guides.



Fig. 2 A part view of the neutron instruments inside Dhruva Reactor Hall. Neutron instruments seen in this picture are : (from left to right) triple-axis spectrometer, polarization analysis spectrometer, 4-circle single crystal diffractometer, five 1D-PSD based profile analysis diffractometer, single-PSD based profile analysis diffractometer, and filter detector spectrometer.

IUC-DAEF, have been active during the past ten years. Articles on various neutron beam research activities are included in this issue. Further information on NFNBR can be obtained by

contacting SSPD using the modes of contact listed in Table 3.

Table 3: Contact information for NFNBR.

| | |
|-------------------|---------------------------------------------------------------------------------------------|
| Postal address: | Head, Solid State Physics Division Bhabha Atomic Research Centre Mumbai 400085, India |
| Telephone numbers | +91 22 5505224 (direct line) +91 22 5505050 (Extns: 25376 and 23754) |
| FAX Numbers | +91 22 5505151, 5519613 |
| e-mail address | sspd@magnum.barc.ernet.in |

International collaboration between neutron beam research at BARC and other countries is over four decades old. The first such agreement was the “Indian-Philippines-IAEA Agreement”, signed during sixties, under which a BARC built neutron instrument was installed at Philippines, and scientists in that country were trained by BARC scientists to use it. The more recent example is the installation of a neutron spectrometer at Bangladesh through IAEA. Scientists from countries like Philippines, Korea, Indonesia, Bangladesh, Vietnam, Malaysia and Egypt have visited BARC to work on the neutron instruments. NFNBR installed a neutron instrument on the spallation neutron source

at Rutherford Appleton Laboratory in UK. Scientists from NFNBR (SSPD) avail advanced neutron sources at UK, USA, Germany, France, Switzerland, Japan and other countries to carry out front-line research, and keep themselves up to date in this field.

Acknowledgements

On behalf of all our colleagues in NFNBR, SSPD, we thank Dr. S.K. Sikka, Director, Atomic & Condensed Matter Physics Group, BARC, Shri B. Bhattacharjee, Director, BARC, and Dr. Anil Kakodkar, Chairman AEC and Secretary, DAE, Government of India, for their active support to the development and successful operation of the neutron beam research facility, NFNBR at SSPD, BARC.

Neutron Diffraction Studies of Hydrogen Bonded Crystals



Dr. M. Ramanadham, currently the Head, Solid State Physics Division, BARC, started his research career at BARC in 1969 in the field of neutron crystallography and hydrogen bonding studies on biomolecules. He obtained Ph.D. degree in 1975 from the University of Mumbai. Subsequently, he worked on x-ray protein structures. His interests include crystallographic computing, statistical analysis of crystallographic data, hydrogen bonding and parallel computing. He served as an elected member of the Computing Commission of the International Union of Crystallography during 1993-96 and 1996-99. Presently, he is the Hon' General Secretary of the Indian Physics Association.

Dr. S.K. Sikka, presently the Director, Atomic & Condensed Matter Physics Group, BARC, started his research career at BARC in 1961. He is an internationally acclaimed scientist in the fields of neutron crystallography, hydrogen bonding and high-pressure physics. He obtained Ph.D. degree in 1969 from the University of Mumbai. His successful solving of the phase problem in neutron crystallography is the first and the only one of its kind in this field. He started high-pressure physics research group at BARC, which grew from strength to strength, and, at present ranks among the best in the world. He is currently serving as the Chairman of the National Committee for Crystallography of the Indian National Science Academy.



Dr. R. Chidambaram is presently the Principal Scientific Adviser to the Government of India, and DAE Homi Bhabha Professor. He joined BARC in 1962, after obtaining Ph.D. from the Indian Institute of Science, Bangalore, to head the Neutron Crystallography Section. During his tenure at DAE, he served as the Head, Neutron Physics Division, Director, Physics Group, Director, BARC, and Chairman, Atomic Energy Commission and Secretary, Department of Atomic Energy, Government of India. He is an internationally acclaimed scientist in the fields of neutron crystallography, hydrogen bonding, high-pressure physics, automation of experimental stations, scientific computing, and many other fields. Throughout his career, he created and sustained highly productive research groups in DAE. He served, initially as the member of the Executive Committee, and subsequently, as the Vice President of the International Union of Crystallography.

Single-crystal neutron diffraction is the method of choice to study crystal structures containing lighter atoms, such as hydrogen in the presences of other, heavier atoms. Thus, it is ideally suited for studying the structural aspects of the hydrogen-bond interaction. BARC has been on the forefront of this activity for over four decades now,

building state of the art computer-controlled neutron diffractometers, and carrying out crystal structure analyses on important hydrogen-bonded systems. Automation of instrument control and data acquisition, complex computations of the crystal structure analysis, effective utilisation of molecular graphics, and acquisition of meaningful scientific

Dr. M. Ramanadham, Solid State Physics Division, Bhabha Atomic Research Centre, Trombay, Mumbai 400 085; E-mail : ramu@magnum.barc.ernet.in; Dr. S.K. Sikka Atomic & Condensed Matter Physics Group, BARC, Trombay, Mumbai 400 085; and Dr. R. Chidambaram, Department of Atomic Energy, Mumbai

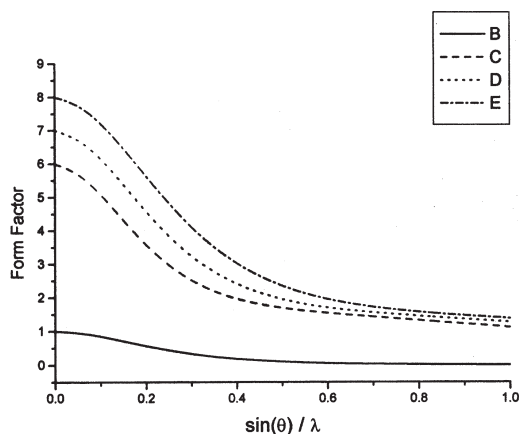


Fig. 1 Variation of x-ray form factors for, (B) hydrogen, (C) carbon, (D) nitrogen and (E) oxygen with increasing $\sin(\theta)/\lambda$.

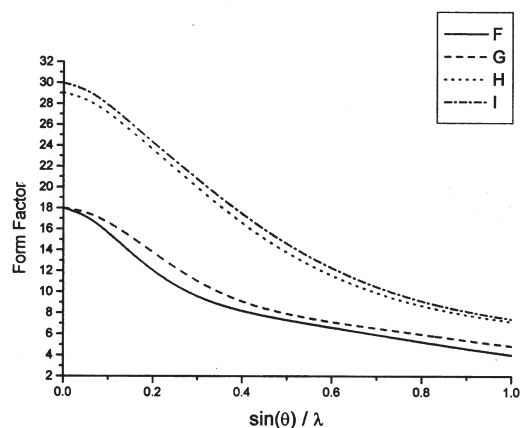


Fig. 2 Variation of x-ray form factors for, (F) Cl^- , (G) K^+ ions, and (H) Cu and (I) Zn atoms with increasing $\sin(\theta)/\lambda$.

information from the results, are among the notable achievements of this endeavour at BARC.

Symmetry and Diffraction [1]

Crystal structure analysis, though conceptually straightforward, is quite complex in practice. Only a bird's eye view of the subject matter is presented here. When a parallel monochromatic x-ray beam, or a mono-energetic thermal neutron beam, with the wavelength comparable to inter-atomic distances, is incident on a single crystal, it produces diffraction effects. Scattered intensities are confined to only a finite number of directions, defined in reciprocal space, characterised by three vectors, \mathbf{a}^* , \mathbf{b}^* and \mathbf{c}^* . The reciprocal lattice constants, the three lengths, a^* , b^* and c^* , and the inter-axial angles, α^* , β^* and γ^* , are related to the cell constants, a , b , c , α , β and γ in the crystal space. The Ewald sphere provides an elegant interpretation of the conditions for diffraction to occur, and the limiting sphere determines the reciprocal space accessible in a diffraction experiment.

X-Ray and Neutron Scattering [1,2]

X-rays are scattered by electrons, while neutrons are scattered by atomic nuclei. The neutron scattering by atomic magnetism is not considered in this article. The amplitude of the scattered x-ray beam is proportional to the electron content of the

atom. The scattering from neighbouring atoms is comparable, and, so also scattering from two ions with the same number of electrons. The atomic scattering factor decreases with increasing $(\sin\theta/\lambda)$, where, θ is the Bragg angle (2θ is scattering angle), and λ is the wavelength of x-rays. Data presented in Fig. 1 and Fig. 2 clearly bring out all these features associated with x-ray scattering. Since the size of an atomic nucleus scattering neutrons is four orders of magnitude smaller than the neutron wavelength, the scattering is isotropic, and it does not decrease with increasing scattering angle. With neutron scattering, it is possible to distinguish between neighbouring nuclei, and also between the different isotopes of the same nucleus. The neutron scattering lengths of all the nuclides fall within the same order of magnitude (See, Table 1). No nuclide dominates the scattering from the sample.

Crystal Structure Analysis [1,2]

The aim is the accurate and precise determination of all the atomic positions in the unit cell of a crystal, using the diffraction data recorded experimentally. A four-circle neutron diffractometer, operating in the normal-beam equatorial geometry, located at Dhruva reactor, BARC, is shown in Fig. 3. The diffractometer axis (2θ -axis), and the ω -axis are vertical and coincident. While the detector rotates around the 2θ -axis, always looking at the sample position, the entire

TABLE 1. Neutron coherent scattering lengths in fm (10^{-15} m) units of some nuclides for comparison with the x-ray data presented in Figures 1 and 2.

| Atomic Number | Nuclide | Scattering length (in fm) |
|---------------|-----------------|---------------------------|
| 1 | H | -3.739 |
| | ^1H | -3.7406 |
| | ^2H | 6.671 |
| 6 | C | 6.646 |
| | ^{12}C | 6.6511 |
| | ^{13}C | 6.19 |
| 7 | N | 9.36 |
| | ^{14}N | 9.37 |
| | ^{15}N | 6.44 |
| 8 | O | 5.803 |
| 17 | Cl | 9.577 |
| 19 | K | 3.67 |
| 20 | Cu | 7.718 |
| 30 | Zn | 5.680 |

crystal orientation assembly rotates around ω -axis. The crystal orienter consists of two axes, namely the χ and ϕ axes. The χ -axis is horizontal, and the spindle on which the crystal sits, rotates around this axis. The ϕ -axis is the spindle axis. It is vertical when $\chi=0$, and rotates in a vertical plane, called the χ -plane. These four axes intersect at one point on the diffraction plane, the horizontal pane containing the incident beam, the scattered beam and the scattering vector. The crystal under investigation is mounted on the spindle, such that its centre of mass coincides with this point. For recording the intensity of any Bragg reflection, it is necessary to rotate the crystal around χ and ϕ axes to bring the corresponding scattering vector (reciprocal lattice vector) into the diffraction plane. The detector is brought to the correct scattering angle position by rotating it around the diffractometer axis. Finally, rotation around the ω -axis brings the reciprocal lattice vector into a position, where it bisects the angle between the incident and scattering beam directions. Then, the profile of the Bragg reflection is recorded by step scanning across the scattering angle position, keeping the bisecting position of the scattering

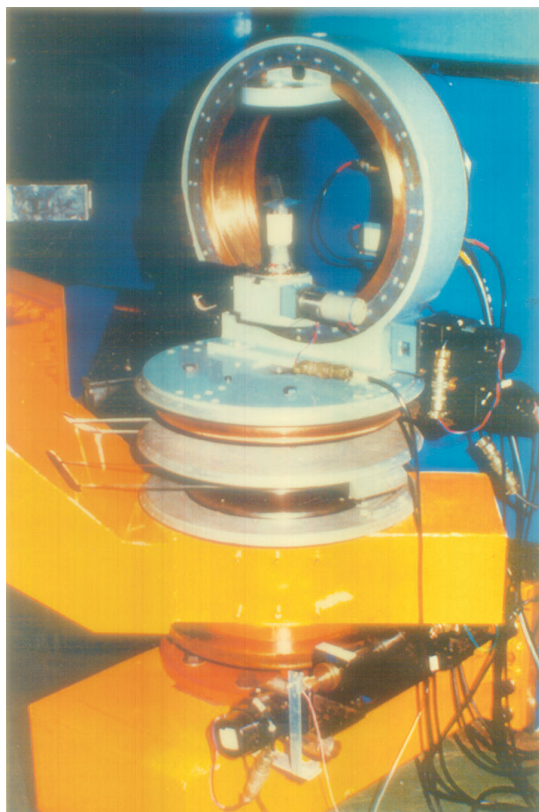


Fig. 3 Computer-controlled four-circle single-crystal neutron diffractometer inside Dhurva reactor hall at BARC

vector intact, with appropriate ω rotation. In order to do all this, it is essential to know the orientation of the crystallographic axes of the crystal with respect to the diffractometer axes. By a systematic search of the reciprocal space with the help of these rotations, three non-coplanar, and pair-wise non-parallel reciprocal lattice vectors (two are sufficient when the cell constants are known approximately from a previous experiment), in terms of the four angles, 2θ , ω , χ and ϕ for each, are located. Using these data, cell constants and the elements of orientation matrix can be computed. About 30 to 50 reflections, randomly chosen from the reciprocal space are recorded, and using these data, the cell constants and orientation matrix elements are optimised. Using the final parameters thus obtained, setting angles for all the accessible data are recomputed, and the diffraction experiment is performed, as described above. The

raw intensities, $I(hkl)$ thus obtained, are corrected for absorption, and put on the absolute scale using the Wilson method.

The electron density (for x-rays), or the neutron scattering length density (for neutrons) can be expressed as a three-dimensional Fourier series, because of the translational symmetry in crystals. Thus,

$$\rho(xyz) = \frac{1}{V} \sum_{h=-\infty}^{\infty} \sum_{k=-\infty}^{\infty} \sum_{l=-\infty}^{\infty} F(hkl) \exp[-2\pi i(hx + ky + lz)] \quad (1)$$

where, (xyz) are fractional coordinates, and V is the volume of the unit cell. The Fourier coefficients, $F(hkl)$, are structure factors, which, in general, are complex numbers. Thus,

$$F(hkl) = |F(hkl)| \exp[i\alpha(hkl)] \quad (2)$$

where, $|F|$ is the structure amplitude and $\alpha(hkl)$ is the phase angle. Scattered intensity $I(hkl)$, associated with a reciprocal lattice point (hkl) is proportional to the corresponding structure amplitude. However, the phase angle is unknown. Therefore, carrying out the Fourier summation, and interpreting it to obtain atomic positions, is not possible. This is the so-called phase problem in crystallography. As the methods of solving this problem in x-ray crystallography were considered to be inapplicable to the neutron case, neutron studies were always carried out after solving the structure with x-rays. However, Sikka has shown [3,4] that the so-called direct methods of solving the phase problem in the case of x-rays are equally applicable to neutrons. The structure of L-threonine (Fig. 4) was solved at BARC directly by neutron diffraction [5], and many crystal structures have been solved all over the world directly by neutron scattering technique during the past three decades using this method. Once the phases are obtained, they are combined with the corresponding structure amplitudes obtained from the experimentally measured intensities, and the Fourier summation (equation 1) is carried out on a fine grid in the unit cell. Approximate atomic positions are extracted from the peaks in the Fourier map. Then the structure factors based on this initial model are computed using the expression

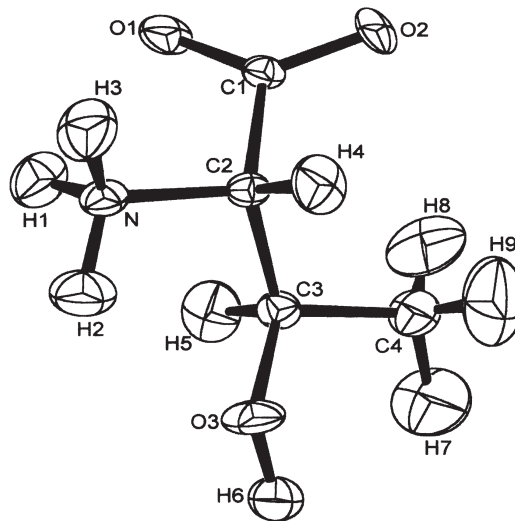


Fig. 4 Molecular structure of L-threonine, drawn using ORTEP3

$$F(hkl) = \sum_{j=1}^N b_j O_j \exp[-B_j (\sin \theta / \lambda)^2] \exp[2\pi i(hx_j + ky_j + lz_j)] \quad (3)$$

Where, the summation is over N atoms in the unit cell. The parameters b_j , O_j , B_j and (x_j, y_j, z_j) are, respectively, neutron coherent scattering length, occupancy parameter, isotropic temperature factor, and fractional coordinates of the j^{th} atom. These parameters, a scale factor, and others, such as those for extinction correction, are then subjected to a series of weighted non-linear crystallographic full-matrix least-squares refinement cycles, by minimising the quantity

$$S = \sum_K \omega_K \left(|F|_{\text{obs}}^2 - |F|_{\text{cal}}^2 \right)_K^2 \quad (4)$$

where, ω is the weight associated with the corresponding observation. The summation, k , is over all the observations. In the final stages, anisotropic temperature factors, six parameters per atom, are introduced. Convergence of refinement is monitored by the so-called R-factor, defined as

$$R(F^2) = \frac{\sum |F|_{\text{obs}}^2 - |F|_{\text{cal}}^2}{\sum |F|_{\text{obs}}^2} \quad (5)$$

Once the refinement is completed, the final structure parameters are used to interpret the properties of the crystal and molecular structure, and the structure is represented pictorially, as shown in Fig. 4.

The Hydrogen Bond Interaction [6]

Neutron studies on the structural aspects of hydrogen bonding have produced a wealth of data on this very important interaction. A covalent bond, $X-H$, where X (referred to as the proton donor) is electronegative, acquires a polar character. When this polar bond is directed towards another electronegative atom, Y (referred to as the proton acceptor) in a molecule, or crystal structure, a mild interaction, known as the hydrogen bond, is set in. The $X-H$, $H\cdots Y$ and $X\cdots Y$ distances, and the HXY angle in a H-bond are represented, respectively, by the symbols, r , d , R and θ . The strength of most of the hydrogen bonds is usually about 6 kcal/mol, or, less, but significantly more than the energy of a van der Waals interaction. It is one of the most important non-covalent interactions in nature. Base pairing in DNA, stabilising of the secondary structures, such as the α -helix and β -sheets in proteins, complementary nature of enzyme-substrate, enzyme-inhibitor, and antigen-antibody interactions are a few of many H-bond based interactions, that are vital for the sustenance of life processes. The importance of hydrogen bond lies in its ability to make and break easily at ambient temperatures, mild but significant directionality, and combined strength when many of them are formed in a structure. Water is a very important hydrogen-bonded solvent that plays a vital role in many physico-chemical and biological processes.

The strength of a H-bond interaction is best studied by spectroscopic techniques, while neutron diffraction is the method of choice to study its structural aspects. A hydrogen bond is said to have been formed when the distance between H and Y atoms is noticeably (say, by 0.2 Å) shorter than the sum of their van der Waals radii. Except in a very few strong H-bonds, and in those where symmetry considerations impose restrictions, the $H\cdots Y$ interaction is longer and weaker than that of $X-H$ interaction (asymmetry). H-bonds are generally bent (X , H and Y are non-collinear). One of the earliest

examples of a bent H-bond as a desirable feature, instead of a distorted covalent bond angle, occurs in the structure of ice-I [7].

Neutron Studies on Hydrogen Bonded Structures at BARC

Some of the earlier neutron diffraction studies at BARC focussed on the structure and lone-pair coordination of the water molecules in the crystal structures of inorganic hydrates. On the basis of the crystal structures studied at BARC and elsewhere, a classification of the lone-pair coordination of the water oxygen involved in H-bonds as an acceptor and/or in metal-ion coordination has been worked out [8]. The influence of these interactions and their directional properties on the geometry of the water molecule has been clearly brought by this analysis. A semi-empirical potential function for $O-H\cdots O$ hydrogen bonds was also developed [9].

A series of high-precision neutron studies was taken up on biomolecules, such as amino acids and small peptides (references to individual structures are listed in [10,11]), in view of the importance of hydrogen bonding in the structure and function of protein molecules. Aim of these studies was to obtain precise H-atom positions in these molecules, analyse H-bond stereochemistry, and correlate H-bond interactions involving a variety of donor and acceptor groups to the conformational and functional aspects of proteins. A detailed analysis was carried out on the results [10,11]. The extreme rotation of the amino group to optimise H-bonds (Fig. 5), non-planar distortions at the amide nitrogen of the peptide linkage to facilitate better H-bonding, clear distinction between $N-H\cdots O$ (N sp^2 hybridised) and $N^+-H\cdots O$ (N sp^3 hybridised and protonated) hydrogen bonds, development of bent H-bond potential functions for separately for these two types, etc., are some of the significant results of this analysis.

One of the most important results of this analysis is the observation that the hydrogen bonding environments of the neutral and ionised carboxyl groups are significantly different from each other. This observation was rationalised using the bond-length, bond-strength correlations, and criteria were developed to distinguish between neutral and ionised carboxyl groups in x-ray protein structures,

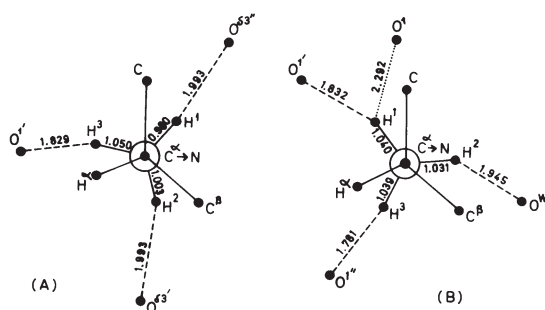


Fig. 5 Influence of hydrogen bonding on the conformation of the amino groups in the structures of (A) *L*-cysteic acid, (B) *L*-asparagine

where hydrogen atoms are not seen. It has been successfully applied to the x-ray structure of triclinic chicken lysozyme [12] to interpret the carboxyl groups in the side chains of GLU-35 and ASP-52 residues in it [13]. This result is in perfect agreement with a neutron diffraction study [14] of this protein. An interpretation of the x-ray structure [15] of an anti-tumour, antibiotic protein, neocarzinostatin (NCS), indicated that the chemical sequence at residues 48 and 51 could be wrong. Again using the hydrogen bonding criteria, the sequence was corrected. This correction immediately helped in identifying the DNA binding site on this protein, consistent with similar observations pertaining to a variety of DNA binding proteins.

Acknowledgements

Significant contributions to the BARC neutron crystallography project made by our past and present colleagues, A. Sequeira, S.N. Momin, H. Rajagopal, S.C. Gupta, R.R. Bugayong, S. Bhakey-Tamhane, P.U. Sastry, R. Chitra and R.R.-Choudhury are gratefully acknowledged.

References

1. C. Giacovazzo, H.L. Monaco, D. Viterbo, F. Scordari, G. Gilli, G. Zanotti and M. Catti, *Fundamentals of Crystallography*, C. Giacovazzo (Ed.), International Union of Crystallography, Oxford University Press, Oxford, UK, (1992).
2. G.E. Bacon, *Neutron Diffraction*, Clarendon Press, Oxford, UK, (1962).
3. S.K. Sikka, *Acta Cryst.*, **A25** (1969) 539.
4. S.K. Sikka, *Acta Cryst.*, **A26** (1970) 662.
5. M. Ramanadham, S.K. Sikka and R. Chidambaram, *Pramana*, **1** (1973) 247.
6. W.C. Hamilton and J.A. Ibers, *Hydrogen Bonding in Solids: Methods of Molecular Structure Determination*, W.H. Freeman, New York, USA, (1968).
7. R. Chidambaram, *Acta Cryst.*, **14** (1961) 467.
8. R. Chidambaram, A. Sequeira and S.K. Sikka, *J. Chem. Phys.*, **41** (1964) 3616.
9. R. Chidambaram and S.K. Sikka, *Chem. Phys. Lett.*, **2** (1968) 162.
10. M. Ramanadham and R. Chidambaram, in *Advances in Crystallography*, R. Srinivasan (Ed.), Oxford & IBH Publishing Co., New Delhi, India, (1978) pp. 81-103.
11. R. Chidambaram and M. Ramanadham, *Physica B*, **174** (1991) 300.
12. M. Ramanadham, L.C. Sieker and L.H. Jensen, *Acta Cryst.*, **B46** (1990) 63.
13. M. Ramanadham, V.S. Jakkal and R. Chidambaram, *FEBS Lett.*, **323** (1993) 203.
14. S.A. Mason, G.A. Bentley and G.J. McIntyre, in *Neutrons in Biology*, B.P. Schoenborn (Ed.), Plenum Press, New York, USA, (1984) pp. 183.
15. M. Ramanadham and L.C. Sieker, *Acta Cryst.*, **A49** (1993) C120.

Neutron Crystallographic Investigations of Ferroic and Electro-Optical Systems



Smt. Rajul Ranjan-Choudhury joined 41st Batch of BARC Training School in 1997 after obtaining post-graduate degree in physics from IIT Delhi. Subsequently she joined neutron crystallography section of Solid State Physics Division of BARC. Currently, she is working on the structural investigations of small molecular materials using x-ray and neutron diffraction.

Smt. R. Chitra obtained post-graduate degree in physics from the University of Madras in 1992. She joined 36th batch of BARC training school in 1993. Subsequently, she joined the neutron crystallography section of Solid State Physics Division, BARC. Currently, she is working in the field of diffraction of small molecules using neutrons and x-rays as probes.



Dr. P.U. Sastry obtained M.Sc in physics with first rank from central university, Hyderabad in 1986 for which he received a medal and Jawaharlal Nehru Memorial Prize. He completed 30th batch training course in physics in BARC with first rank in 1987 and received Homi Bhabha prize. Subsequently, he joined Neutron Physics Division and later, the Solid State Physics Division of BARC. He worked as a postdoctoral fellow at Los Alamos National Labs, USA for some time in 1998 and at Max-Planck-Institut für Metallforschung, Germany during 2000-2001. Currently, he is working on the investigations of structural property correlations of materials using x-ray and neutron diffraction as well as small angle x-ray scattering techniques.

Many of the technologically important properties of materials are controlled by their crystal structure. In some cases, these properties may arise as a result of transformation to a new phase (structure) at appropriate pressure and (or) temperature. If these properties are significantly anisotropic, the material is required to be in the form of a single crystal rather than in the powder form for practical applications. Hence, to prepare materials with better applications, it is essential to know the precise structural origin of these properties. In the

case of polycrystalline samples, the macroscopic properties depend significantly on the texture of the sample. Both the crystal structure of a single crystal and the bulk texture of a polycrystalline sample can be characterized using the four-circle neutron diffractometer, about which a detailed description is given in the previous chapter. Often, it is difficult to obtain a material as a pure single crystal and is available only in polycrystalline form. In that case, the structure of the sample can be refined by powder diffraction using θ , 2θ circles of the single crystal

Smt. Rajul Ranjan-Choudhury, Smt. R. Chitra and Dr. P.U. Sastry, Solid State Physics Division, Bhabha Atomic Research Centre, Trombay, Mumbai 400085; E-mail: rajul@magnum.barc.ernet.in; rchitra@apsara.barc.ernet.in; psastriy@apsara.barc.ernet.in.

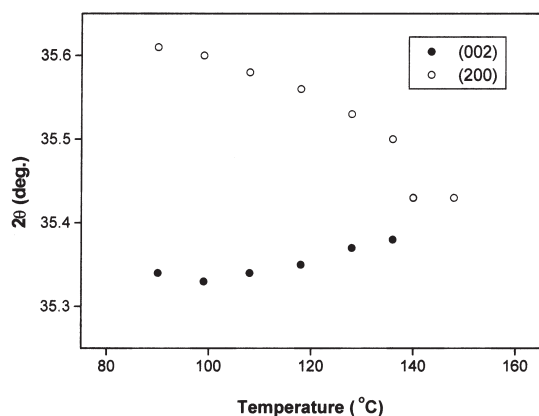


Fig. 1 Temperature dependence of profile peak positions in (Ba/Ca)TiO₃ crystal [1]

diffractometer. In this article, some examples of the structural investigations performed on the ferroic and electro-optical systems using neutron beam at Dhruva reactor are discussed.

Structural Phase Transitions in (Ba/Ca)TiO₃

Barium titanate (BaTiO₃) is a well-known ferroelectric which is widely used in variety of applications such as capacitors. Its larger dielectric response across the tetragonal to cubic transition becomes broadened over a wide range of temperature after introducing partial amount of Ca in to its lattice. In our study, the structural variations associated with this important phenomenon, called diffuse phase transition (DPT), were monitored [1] using high-temperature single crystal neutron diffraction. Set of structural parameters consisting positions, thermal parameters and site occupancies of atoms were obtained by refinements using a set of the integrated intensities of neutrons under Bragg peaks recorded at few temperatures across the tetragonal-cubic transition temperature ($T_c = 145^\circ\text{C}$) as shown in Fig. 1). At room temperature, the unit cell has tetragonal symmetry (space group P4mm) with cell constants $a = 3.982(7) \text{ \AA}$, $c = 4.025(8) \text{ \AA}$. The structure was refined with an R-factor $R(F) = 0.023$. Similar refinements were done at other temperatures across the phase transition. As the crystal was heated gradually, the Bragg intensity of each of the reflections raises between 110°C - 120°C

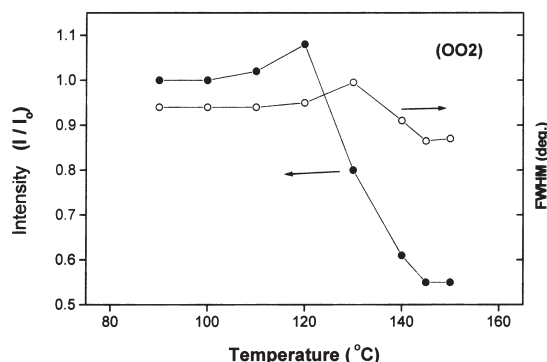


Fig. 2 Temperature variations in full-width half maximum and neutron intensity for (002) planes of (Ba/Ca)TiO₃: —, —, guides to the eye [1]

(see Fig. 2) and falls sharply above 120°C . Detailed analysis with extinction corrections showed that the observed raise in intensities is associated with reduction in domain size in the tetragonal phase and the subsequent fall in its value above 120°C is due to the nucleation and growth of large cubic domains. The maximum in the width of the diffraction profile at 130°C (below T_c) indicates the coexistence of tetragonal and cubic phases. Refinements suggested that the disorder in the Ti-ion positions observed well below T_c is responsible for DPT in (Ba/Ca)TiO₃.

Structural Phase Transitions in Ferroelastic TiNO₃

Some of the basic inorganic nitrates undergo interesting polymorphic structural transitions with variation of temperature. In our study [2], the mechanism involved in the series of transitions in TiNO₃ was investigated using neutron diffraction. It undergoes a transition from room temperature phase-III to phase-II at about 79°C and then to phase-I at 144°C . The structure of phase-III (orthorhombic, space group Pnma) was refined ($R(F) = 0.016$) based on the intensities from 230 reflections recorded using the four-circle neutron diffractometer at Dhruva. The unit cell of phase-III ($a = 12.355(5) \text{ \AA}$, $b = 8.025(3) \text{ \AA}$, $c = 6.298(3) \text{ \AA}$) contains eight molecules. Each nitrate ion is enclosed in a TI-cube with its plane oriented normal to an edge. Since the single crystal is known to

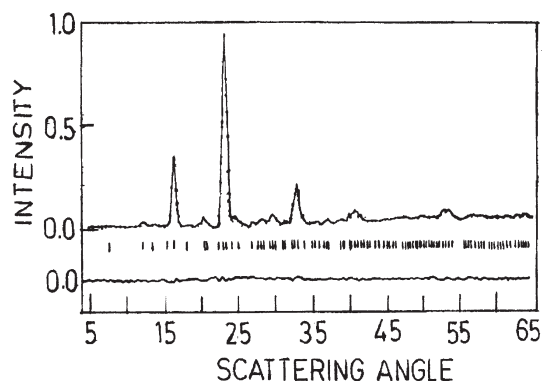


Fig. 3 Observed (...) and calculated (—) neutron diffraction pattern of phase-II ($P3_1$, $Z=9$, $a = 10.435(1) \text{ \AA}$, $c = 7.451(1) \text{ \AA}$, $R_p = 0.038$) of TiNO_3 [3]

become polycrystalline during heating and cooling cycles, structure of high-temperature phases were determined by powder diffraction method. Neutron intensity data in each of the phases were recorded using θ , 2θ circles of the four-circle neutron diffractometer and the structure of phase-II (trigonal, $P3_1$, $Z=9$) at 115°C and phase-I (cubic, $\text{pm}3\text{m}$, $Z=1$) at 170°C were refined [3] by Reitveld technique. Figure 3 shows the neutron diffraction pattern of phase-II. Results showed that, like in phase-III, nitrate ions in the high-temperature phases are oriented normal to the edges of Tl-cube. Refinements also ruled out the earlier proposed models in which the nitrates are aligned normal to the Tl-cube diagonals. Based on the crystal structures obtained for all the phases, it was demonstrated that the transition from phase-III to phase-II involves flip of a nitrate ion about an in-plane axis (Fig. 4) whereas that from phase-II to phase-I is followed by a 12-fold disorder in the orientation of nitrate ions. These results lead to detailed understanding of the phase transition behaviour in the family of nitrate compounds.

Structure and Electro-Optical Properties of Zinc(tris) Thiourea Sulphate ($\text{Zn}[\text{SC}(\text{NH}_2)_2]_3\text{SO}_4$)

($\text{Zn}[\text{SC}(\text{NH}_2)_2]_3\text{SO}_4$) (ZTS) is a semiorganic crystal which exhibits excellent nonlinear optical and electro-optical behaviour with better mechanical

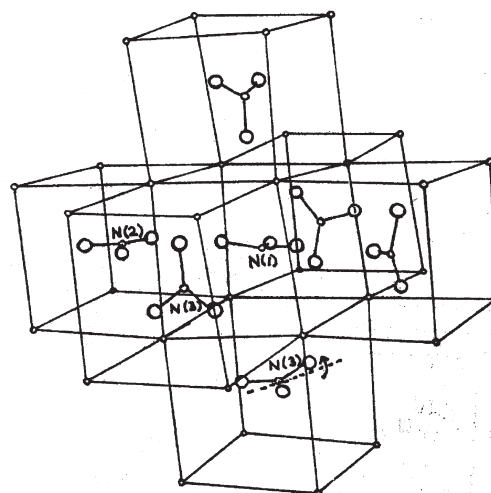


Fig. 4 A view of the structure of TiNO_3 Phase-III (orthorhombic in trigonal frame). It is equivalent to that of phase-II (trigonal) after the flip of a nitrate ion about an in-plane axis, as shown in the diagram.

properties. In our recent study, the structure of ZTS was obtained [4] by single crystal neutron diffraction technique using the crystal grown [5] at CAT, Indore. Neutron intensities were recorded in the range $(\sin\theta/\lambda) \leq 0.51$ on the four-circle neutron diffractometer at Dhruva. The data were processed to obtain the values of the square of the structure factors for 824 unique reflections. Starting from the reported [6] parameters obtained from x-ray diffraction (orthorhombic space group $\text{Pca}2_1$), structural parameters, with accurate positions for H-atoms, were obtained ($R(F^2) = 0.025$) by the method of full matrix least squared refinement. The unit cell of ZTS ($a = 11.126(5) \text{ \AA}$, $b = 7.773(4) \text{ \AA}$, $c = 15.491(5) \text{ \AA}$) consists four molecules formed by a total 148 chemical bonds (including 32 inter and intra-molecular H-bonds) which constitute three thiourea groups, Zn-tetrahedral and sulphate groups (Fig. 5). Using the structural parameters obtained from the refinement and a formalism based on bond charge theory, the bond parameters of all the bonds in the unit cell, linear optical susceptibility and electro-optical (EO) coefficients of ZTS were estimated [7]. Analysis showed (Table 1) that the covalent bonds in one of the thiourea groups (tu_2), the hydrogen bonding network and the sulphate

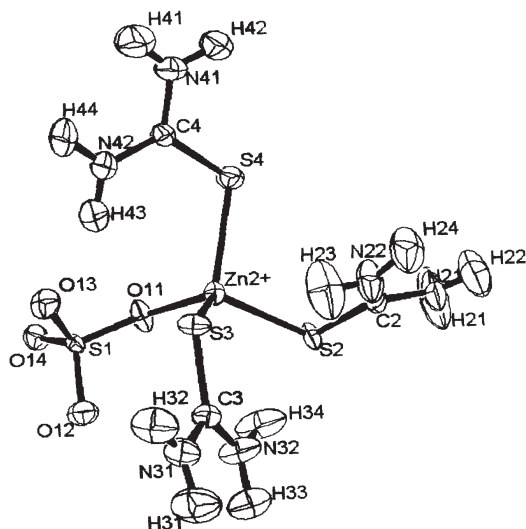


Fig. 5 Structure of zinc(tris)thiourea sulphate obtained by single crystal neutron diffraction [4]

groups are more sensitive to optical properties of ZTS.

Structural Investigations on Doped Triglycine Sulphate (TGS)

Triglycine Sulphate (TGS) is a ferroelectric [8], which is used as an infrared detector. However, the practical application as a device is limited due to depoling by which the crystal becomes multi-domained upon cooling through the ferroelectric-paraelectric transition temperature ($T_c = 49^\circ\text{C}$). One of the ways to prevent depoling effect is to introduce organic dopants like L-Alanine into TGS [9]. In order to investigate the structural changes associated with the freezing of the direction of spontaneous polarization of the unit cell due to doping, a single crystal neutron diffraction study was conducted on L-Alanine doped TGS (LATGS) crystal using four-circle single crystal neutron diffractometer at Dhurva. The measured integrated intensities were reduced to the square of the structure factors ($(F_o)^2$) for 1099 unique reflections by applying standard Lorentz and absorption corrections using the program DATARED which includes the absorption correction program ORABS as a subroutine. The cell parameters were refined to a value $a=9.444(5) \text{ \AA}$, $b=12.661(19) \text{ \AA}$, $c=5.751(3) \text{ \AA}$,

TABLE 1. Contributions from the individual structural groups to linear susceptibility (χ) and the ionic component of the linear electro-optical coefficients (r_{ij} , in pm/V) of ZTS [7]. tu_i -are the thiourea groups and Zn-T is the Zn-tetrahedral group. S represents the respective total values for the crystal.

| | χ | (r_{33}) | (r_{23}) |
|----------------------|--------|------------|------------|
| Zn-T | 0.012 | 0.52 | -0.39 |
| $(\text{SO}_4)^{2-}$ | 0.027 | -0.46 | 2.65 |
| tu1 | 0.027 | -0.61 | 0.61 |
| tu2 | 0.027 | 0.92 | -0.92 |
| tu3 | 0.028 | 0.26 | -0.62 |
| H-O | 0.040 | 0.99 | 0.44 |
| S | 0.161 | 1.62 | 1.77 |

$\beta=110.34(2)^\circ$. Starting from the reported [10] structural parameters of TGS, those of LATGS (space group $P2_1$) were refined (with an R-factor, $R(F^2)$ of 0.0439) using the program SHELXL. The modeling of L-Alanine in TGS unit cell led to the conclusion that the most likely site of Alanine substitution in TGS was GII and not GI as proposed by Keve et.al. [9]. The prevention of depoling by Alanine substitution could be explained by substitution at GII site [11]. Alanine at GII site has steric hindrances with one of the two equivalent positions of $-\text{NH}_3^+$ group of GI, which plays the most important role in polarization reversal, resulting in freezing of the polarization direction of the unit cell by forcing the $-\text{NH}_3^+$ group to occupy only one of the two equivalent sites (Fig. 6).

The symmetry of TGS is influenced by the hydrogen bond connecting Zwitterion GII with Glycinium ion GIII and the position of the nitrogen atom N1 in the $-\text{NH}_3^+$ group of Glycinium ion GI. As the deuteration has little effect on the transition temperature of TGS, it is generally believed that the mechanism of ferroelectric phase transition in TGS is the instability of nitrogen N1 in a double well potential well. The double potential well seen by N1

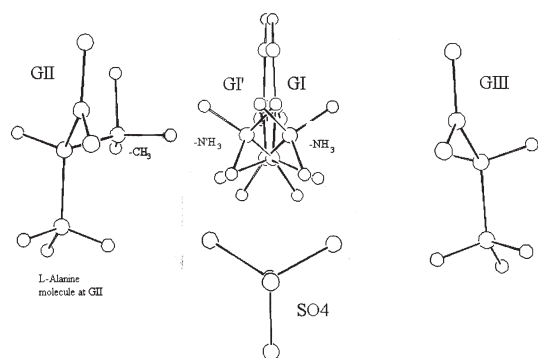


Fig. 6 A picture of L-alanine molecule at GII site having steric hindrances with GI

was successfully modeled [12] considering the hydrogen bond interactions and non-bonded interaction within an asymmetric unit, using the reported [10] TGS structural parameters. This double potential was used in the classical Hamiltonian for ferroelectrics proposed by Onodera [13] and the value of the interaction term leading to the instability of nitrogen N1 was estimated to be 0.624 kcal/mol.

Our structural investigations of LATGS has also thrown light on the long speculated correlation between the N1 motion and the motion of hydrogen (HO31) in the hydrogen bond GII—H—GIII (Fig. 7). According to Ramanadham et al. [14], the -OH oxygen in a -COOH group cannot be an acceptor of a hydrogen bond, as it has no valency left for the formation of the bond. When N1 moves to its equivalent position N1' and hydrogen bond N1'—H3'—O31 is formed, O31 which is the -OH oxygen of -COOH group becomes an acceptor of the H-bond, this is unfavorable and hence the hydrogen HO31 (bonded to oxygen O31) of the carboxyl group of GIII which made a strong H-bond O31—HO31—O21 moves along this H-bond to a new position HO31' (Fig. 7). The above-mentioned H-bond becomes O31—HO31'—O21. GIII in this case becomes the Zwitterion and GII becomes Glycinium ion. Hence the disorder of hydrogen HO31 at $T > T_c$ appears to be a result of nitrogen (N1) disorder at $T > T_c$.

This article is mainly focused on some of the examples of structural studies done by neutron diffraction using a four-circle Diffractometer. For

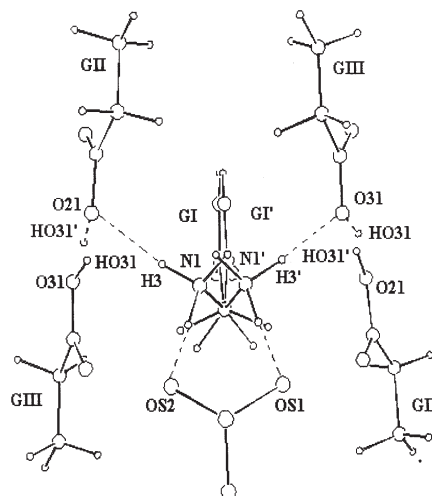


Fig. 7 Diagram showing the correlation between $-(NH_3)^+$ motion and HO31 motion

the characterization of texture in polycrystalline samples using neutrons, the reader may refer to the literature [15-17].

References

1. P.U. Sastry *et al*, J.Phys., **C8** (1996) 2905
2. P.U.Sastry, H.Rajagopal and A.Sequeira, Acta Cryst., **C50** (1994) 1854
3. P.U.Sastry and A.Sequeira, Phil. Mag., **B75** (1997) 659
4. P.U.Sastry, R.Chitra, H.Rajagopal, A.Sequeira and M.Ramanadham, XXX National Seminar on Crystallography, S.V.University, Tirupati, India, June (2000)
5. V.Venkataraman *et al*, J.Cryst.Growth, **154** (1994) 92
6. G.D. Andreetti, L.Cavalca and A.Musatti, Acta Cryst., **B24** (1968) 683
7. P.U.Sastry, Solid St. Commn., **109** (1999) 595
8. Franco Jona and G.Shirane, Ferroelectric Crystals, Chapter 2, Pergaman Press, Oxford London (1962).
9. E.T.Keve, K.L.Bye, P.W,Whipps, and A.D.Annis: Ferroelectrics, **3** (1971) 39

10. M.I.Kay and R.Kleinberg; *Ferroelectrics*, **5** (1972) 45
11. Rajul- Ranjan Choudhury, R.Chitra, M.Ramanadham, and R.Jayavel: *Applied Physics A*, (2002), in press
12. Rajul-Ranjan Choudhury, R.Chitra, and M.Ramanadham: *AsCA'01* proceedings, 19-21 November 2001
13. Yositaka Onodera, *Progress of Theoretical Physics*, **44** (1970) 1477.
14. M.Ramanadham, V.S.Jakkal and R.Chidambaram *FEBS*, **323** (1993) 203.
15. H.J.Bunge, "Texture analysis in material science" (1982), Butterworth, London
16. A.Sequeira, S.C.Gupta and R.Chidambaram, *Ann. Report of Neutron Physics*, Division No. BARC-1076 (1980) 27; BARC Internal report-UTEX-2 (1980)
17. A.Sequeira and P.U.Sastry, "Texture studies using neutrons" in the book "Neutron Scattering: Theory and Practice", unpublished.

Neutron Diffraction Study of Crystals, Liquids and Glasses



Shri P.S.R. Krishna joined BARC in the year 1988, through the 31st batch of BARC Training School. After joining Solid State Physics Division, he designed and installed the first High-Q diffractometer at Trombay and used it to delineate structures of many disordered materials. Apart from this he has designed and installed the present versions of High-Q diffractometer and Powder diffractometer at Dhruva with higher throughput.

Dr. S.M. Yusuf joined the magnetism section of Solid State Physics Division (formerly Nuclear Physics Division), BARC in 1989 after completing 32nd batch of BARC Training School. He received his M.Sc. degree in Physics from Visva Bharati University in 1987 and Post M.Sc. degree in Physics from Saha Institute of Nuclear Physics in 1988. He was intimately connected with the setting up of the neutron polarization analysis spectrometer at Dhruva reactor for magnetic scattering studies. He has also set up a low temperature laboratory for macroscopic magnetic studies. He acquired the Ph. D. (Physics) degree of the University of Mumbai in 1997 and he was a post doctoral fellow at Argonne National Laboratory, USA during 1997-1998. Dr. Yusuf has published a large number of papers in international scientific journals. He has received Best Young Physicists Award from Indian Physical Society and N.S. Sathya Murthy Award from Indian Physics Association in 1996 in recognition of his contributions to neutron scattering from magnetic materials. He is a member of American Physical Society.



Dr. Shrinivas Paranjpe joined 12th batch of Training School after completing his master's degree in Physics from University of Indore. He joined the neutron scattering group of the then Nuclear Physics Division in 1969. He worked on the magnetic structures and spin densities of alloys and compounds, for Ph.D. degree from University of Bombay. He has been actively involved in the instrumentation for beam line experiments from its inception and has been responsible for setting up many spectrometers – with special reference to position sensitive detectors. He worked in the RAL as visiting scientist for one year. Presently he is working in the International Atomic Energy Agency (IAEA) as research reactor specialist. He has been involved in the collaborative programs with University scientists under the DAE-UGC collaboration (IUC-DAEF).

Ms. Keka R. Chakraborty has got her M.Sc. in Physics from IIT Mumbai. She joined BARC, in the 34th batch Training School and has been working on magnetic neutron diffraction.



Shri P.S.R. Krishna, Dr. S.M. Yusuf, Dr. S.K. Paranjpe, Ms. K. Chakraborty and Dr. M. Ramanadham, Solid State Physics Division, Bhabha Atomic Research Centre, Mumbai 400 085; E-mail: glass@apsara.barc.ernet.in, smyusuf@apsara.barc.ernet.in, ramu@magnum.barc.ernet.in



Dr. M. Ramanadham, currently the Head, Solid State Physics Division, BARC, started his research career at BARC in 1969 in the field of neutron crystallography and hydrogen bonding studies on biomolecules. He obtained Ph.D. degree in 1975 from the University of Mumbai. Subsequently, he worked on x-ray protein structures. His interests include crystallographic computing, statistical analysis of crystallographic data, hydrogen bonding and parallel computing. He served as an elected member of the Computing Commission of the International Union of Crystallography during 1993-96 and 1996-99. Presently, he is the Hon' General Secretary of the Indian Physics Association.

Introduction

Neutron scattering is a widely used probe to study the structure as well as dynamics of both crystalline and non-crystalline substances [1]. Unlike X-ray scattering, the form factor for neutron nuclear scattering is constant irrespective of the scattering angle and is an advantage in doing structural studies on liquids and glasses. The neutron nuclear scattering length varies haphazardly with Z even different for different isotopes of the same element which again is another advantage. The knowledge of structure of a material is of prime importance as most of the physical properties are influenced by it. The structural analysis of a solid, typically consisting of 10^{23} atoms/cm³, involves determining the relative positions of each of the atoms. In crystalline materials this gigantic task is made simple by the translational and rotational symmetry present in them. In these materials one determines the structure of a unit cell (containing a few number of atoms) which represents the crystal structure. The absence of long-range order in disordered systems would imply that the concept of unit cell is not valid. Hence their structures cannot be determined in a manner analogous to the crystalline counterparts. Basic difference between the structure of the crystalline materials and the disordered materials (liquids and glasses) is that the former possesses long-range order of atomic positions and the later has short range order. However, the immediate environment in case of disordered material is not very different from that in a crystalline solid due to the presence of short-range order. Further, recent structural studies on disordered materials (e.g., network glasses like fused quartz, molten salts etc.) have shown that, while long range order in the form of perfect translational symmetry is lacking, substantial

intermediate range order may exist over and above the short range order [2]. In real substances long-range order can extend from 100 Å to 5000 Å depending on the type and quality of the crystalline substances under study, where as short and intermediate range orders have the ranges 3-4 Å and 6-10 Å respectively.

In a diffraction experiment one measures the number of neutrons scattered in the scattering plane as a function of scattering angle (2θ) of the substances under study. This data consists of sharp peaks over and above the background in the case of crystals, whereas it will have very broad diffuse peaks in the case of liquids and glasses. This data is then used for modeling the structure of crystalline materials using various techniques like Rietveld analysis [3]. In the case of liquids and glasses this data is then converted into differential cross section and then to structure factor, $S(Q)$, ($Q = 4\pi \sin \theta / \lambda$, λ = wavelength of the incident neutrons) of the substance. This structure factor is related to the pair correlation function, $g(r)$, which gives an instantaneous picture of the scattering substance. For isotropic systems like liquids and glasses, $S(Q)$ and $g(r)$ are related by Fourier transformation.

In the case of crystalline substances accurate measurement of the structure factor up to a Q -range of 10 Å^{-1} is normally used where as for disordered systems (liquids and glasses) the requirement goes to $Q \geq 15 \text{ Å}^{-1}$. In the case of liquids and glasses, $S(Q)$ should be measured with a statistical accuracy better than 1% in order to get the pair correlation function $g(r)$.

Instruments

Taking the above requirements in to consideration, a Powder diffractometer [4] for crystals and a High- Q diffractometer [5] for liquids



Fig. 1 The upgraded version of the High-Q diffractometer showing Monochromator drum, Sample table and the Detector shield assembly.

and glasses have been designed and commissioned at the beam ports TT-1015 and HS-1019 respectively at the Dhruva reactor, Trombay, Mumbai. Subsequently, upgraded versions [6] of these instruments have been commissioned at the beam ports T-1013 and HS-1019. A monochromator (usually a large single crystal) housed inside a cylindrical shield (monochromator drum) receives the polychromatic beam from the reactor and produces monochromatic neutron beam for the selected wavelength through Bragg diffraction. A photograph of the upgraded version of High-Q diffractometer is shown in Fig.1. In the case of powder diffractometer we have a Germanium monochromator giving out neutrons with a wavelength of 1.249 Å and in the case of High-Q diffractometer we have a Copper monochromator giving out neutrons with wavelengths of 1.278 Å and 0.783 Å depending on the crystal plane chosen. The total angular range for these two instruments is up to a $2\theta = 140^\circ$ in the scattering plane. This gives us Q_{\max} values of 9.4 \AA^{-1} and 15.0 \AA^{-1} respectively, for the two diffractometers. These numbers compare favourably with similar facilities existing in reactor centers elsewhere.

The neutron flux on these instruments at the sample position is about 5×10^5 neutrons/cm²/sec at the respective wavelengths of 1.249 Å on powder diffractometer and 0.783 Å on High-Q diffractometer. The neutron flux on High-Q

diffractometer at the wavelength 1.278 Å is about 2×10^6 neutrons/cm²/sec. Five position sensitive detectors (PSD) of each one metre long are housed in the detector shield. Position sensitive detectors are ideal choice for these diffractometers as they are capable of collecting data for a large angular range simultaneously. The instrumental resolution of these instruments given as $\Delta Q/Q$ is $\approx 1\%$ and $\approx 2\%$ respectively.

Electronics for the positional encoding of the PSD data by charge division method using digital electronics has been developed in the Electronics Division (BARC). The data collection is controlled by a personal computer. Data reduction and correction programs have been incorporated to get S(Q) data on an absolute scale. Reduction programs take care of the fact that the PSDs are linear and appropriate corrections are applied to the data. Correction programs take care of the corrections due to background, absorption, multiple scattering, inelasticity effects and normalization. All the programmes follow the prescription given by Egelstaff [7].

Some Results

Crystals

(i) Diffraction Studies on Ferroelectric oxides is very important due to very interesting properties of these oxides. They show a wide variety of structural phase transitions and varied physical properties associated with these structural transitions. We have studied the structural phase transitions (as a function of Ca substitution) in (Ba,Ca)TiO₃, (Pb,Ca)TiO₃, and (Sr,Ca)TiO₃ [8,9,10,11] with considerable success. In the case of (Ba,Ca)TiO₃, we found that the preparation technique of the sample changes its physical properties, viz., the nature of the ferroelectric transition. This sample with 12 atom % of Ca is prepared in the conventional dry route (D) involving calcination of BaCO₃, CaCO₃ and TiO₂ particulate mixture and also prepared in semi-wet route (SW) involving calcination of Ba_{0.88}Ca_{0.12}CO₃ and TiO₂. The D samples showed sharp ferroelectric transition whereas SW samples have shown diffuse ferroelectric transition. We have investigated the microscopic structure of these polycrystalline materials using powder neutron diffraction to understand the cause for this change in the same

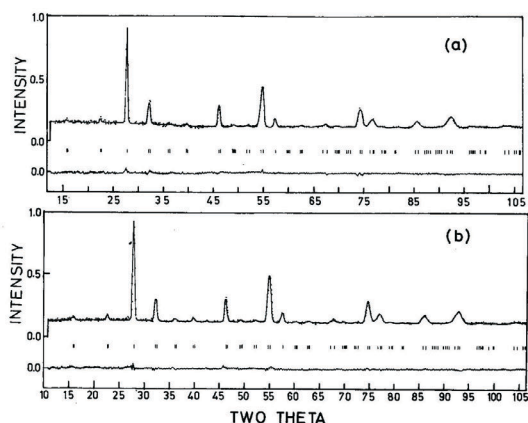


Fig. 2 Observed (dots) and calculated (solid lines) neutron diffraction patterns for the $Ba_{0.88}Ca_{0.12}TiO_3$ samples measured at room temperature. The difference between measured and calculated data is plotted below. The vertical lines indicate the position of allowed Bragg peaks.

sample prepared in two different ways. Room temperature data (Fig. 2) for both the samples were analysed using rietveld profile refinement technique using DBWS program [12]. From the site occupancies it was found that about 40% to 50% of the Ca^{2+} ions replace Ti^{4+} ions in the case of D samples where as all of the Ca^{2+} goes to Ba^{2+} site in SW samples. In these ceramics such a possibility has been suggested by Chan et. al. [13]. According to them this can happen when the atomic percentage of (Ba+Ca) is greater than that of Ti. This is not so in the present sample. However, even if the atomic percentage of (Ba+Ca) is equal to that of Ti for bulk composition, local stoichiometric variations in the conventional dry route of synthesis may lead to situations where the atomic percentage of (Ba+Ca) is greater than that of Ti. So in the samples made by this route, local stoichiometric constraints at the time of thermochemical reactions may force Ca^{2+} to the Ti^{4+} site. Such constraints are not expected if one uses $(Ba,Ca)CO_3$ solid solution precursors, prepared by chemical co-precipitation, since uniform supply of the Ba^{2+} and Ca^{2+} ions for solid state thermochemical reaction with TiO_2 can be ensured at the unit cell level. This particular aspect, namely inhomogeneities at unit cell level in the D sample

and the absence of it in SW sample, is responsible for the change in the character of the phase transition.

(ii) Fascinating properties like the colossal magnetoresistance (CMR) effect, insulator-metal transition, charge ordering phenomenon, and complicated magnetic phase transitions etc, have made $RMnO_3$, doped with divalent ion (A) at the rare earth (R) site, an attractive class of system for investigation. It is possible to control the magnetic and transport properties in these systems by an effective electron transfer probability between Mn^{3+} and Mn^{4+} which is expected to depend drastically upon the crystalline structure parameters such as bond angles between manganese ions and oxygen ions. By tuning the size mismatch of R- and A-ions in the $R_{(1-x)}A_xMnO_3$ -type perovskite, one can change structural details and thus control the magnetic and transport properties of the perovskites. Motivated by these considerations, we have performed room temperature neutron diffraction structural study in order to give the microscopic origin of the observed changes of magnetic and transport properties in the $(La_{(1-x)}Dy_x)_{0.7}Ca_{0.3}MnO_3$ system due to substitution of La^{3+} (ionic radius: 1.216Å) by Dy^{3+} (ionic radius: 1.083Å) [14]. Rietveld analysis of neutron diffraction patterns shows that for the $x = 0.243$ compound, the Mn-O1-Mn and Mn-O2-Mn bond angles are 156.5(9) deg. and 157.9(4) deg. respectively, as compared to 162(1) deg. and 159.9(6) deg., respectively, for the parent $La_{0.7}Dy_{0.3}Ca_{0.3}MnO_3$ compound. For the $x = 0.347$ perovskite, the Mn-O1-Mn and Mn-O2-Mn bond angles are 155.8(9) deg. and 157.5(8) deg., respectively. In the ideal perovskite structure, manganese has an octahedral coordination of oxygen ions. The buckling of octahedra, which increases with the increase of Dy concentration, is evident from our neutron diffraction study. The buckling of octahedra gives weaker Double Exchange (ferromagnetic) interaction as the transfer integral describing the e_g electron hopping between Mn^{3+} and Mn^{4+} decreases and explains the deterioration of the observed magnetic and transport properties.

Liquids

We have investigated strongly hydrogen bonded liquids like alcohols (methyl alcohol, t-butyl alcohol, etc.) to understand their molecular

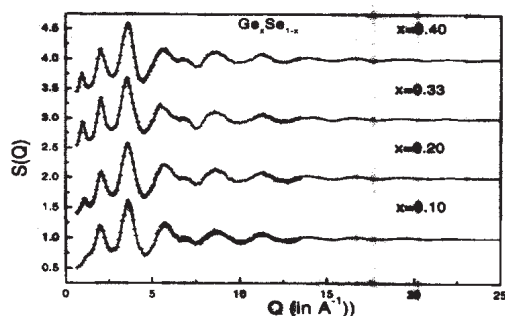


Fig. 3a $S(Q)$ vs. Q of $\text{Ge}_x\text{Se}_{1-x}$ glasses studied. Solid line: MCGR fit Dots: Experimental $S(Q)$. The data corresponding to $x=0.2, 0.33$ and 0.4 are shifted by one unit for the sake of clarity.

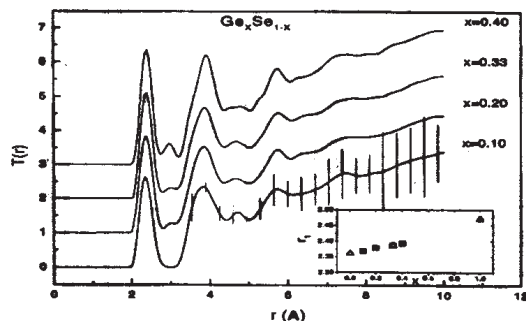


Fig. 3b $T(r)$ vs. r of $\text{Ge}_x\text{Se}_{1-x}$ glasses studied. For the sake of the clarity the curves corresponding to $x=0.2, 0.33$ and 0.4 are shifted by one unit. The vertical lines are typical error bars. Inset: Position of first peak in $T(r)$ as a function of x , which shows

structure [15,16,17] and association of these molecules via hydrogen bonding. We have observed pre-peaks in all these alcohols around a Q value of 0.7 \AA^{-1} to 0.9 \AA^{-1} . For the first time we measured this pre-peak in neutron diffraction of deuterated methyl alcohol which occurs before the main diffraction peak. When combined with the X-ray diffraction studies on these compounds, one can model the diffraction data for various types of hydrogen bonded molecular clusters that are present. We have ruled out tetramer clusters and chain like clusters in favour of hexamer clusters as the predominant clusters at room temperature in these liquids. Apart from this we have carried out the first ever neutron diffraction experiments at elevated temperatures for methyl alcohol to see changes in the liquid structure indicated by the reduction in both the main diffraction peak and prepeak size.

Glasses

We have investigated various types of glasses like semi conducting chalcogenide glasses (Ge-Se glasses) [18], Phosphate glasses (Rare earth oxide-phosphate [19], lead iron phosphate [20]) and oxide glasses. Results from one of the examples are given below.

Ge-Se Glasses

In recent years, extensive structural investigations have been carried out on

semiconducting chalcogenide glasses as there are a number of actual and potential technological applications of such materials. $\text{Ge}_x\text{Se}_{1-x}$ forms glass on melt quenching over a wide composition range. Neutron diffraction studies on these glasses for $x=0.1, 0.2, 0.33$ and 0.4 have been carried out to understand the short and intermediate range orders in this system and also to have a model which can explain the observed changes in the structure. We used Monte-Carlo $g(r)$ (MCGR) method to obtain the pair correlation function from $S(Q)$ data [21]. This method is advantageous over direct transform method as it removes the problem of spurious ripples and also gives an estimate of errors on $g(r)$. Fig. 4 gives the $S(Q)$ data obtained experimentally on the High- Q diffractometer along with the MCGR fits to the same and the generated total correlation function $T(r) (=4\pi\rho g(r))$. Salient features of the study [18] are summarized as follows:

1. The first sharp diffraction peak (FSDP) increases ($Q \approx 1 \text{ \AA}^{-1}$) in area as x increases from 0.1 to 0.33 and then goes down. Its position gets shifted to lower Q values as x increases. The width of this peak is minimum for $x=0.33$. From these observations it is concluded that intermediate range order is maximum in the glass with $x=0.33$.
2. Shortrange order is explained on the basis of chemically ordered continuous random

network model (COCRN). The co-ordination of Ge with Se is 4.1(1) for $x=0.33$ glass. This glass consists of mostly $\text{Ge}(\text{Se}_{1/2})_4$ tetrahedral units. For Ge-rich region ($x=0.4$) the basic building blocks could be $\text{Ge}_2(\text{Se}_{1/2})_6$ units. For Se rich region ($x<0.33$) $\text{Ge}(\text{Se}_{1/2})_4$ units are interlinked with $(\text{Se})_n$ links with the length of the links depending on Se content in the samples.

The peak at 3\AA in $T(r)$ grows with increasing x . This is the signature of edge shared tetrahedra in these glasses. The network connectivity in $x=0.33$ sample can be explained on the basis of 70% edge shared tetrahedra and is different from the crystal where 50% edge shared tetrahedra are present.

References

1. G.E. Bacon, Neutron Diffraction, (Clarendon Press, Oxford, 1975).
2. S.R. Elliot, Physics of amorphous materials, (John Wiley and Sons Inc., New York, 1990).
3. H.M. Rietveld, J. Appl. Crystallogr., **2** (1969) 65; S.M. Yusuf, Powder Diff., **8** (1993) 236.
4. S.K. Paranjpe, Indian J. Pure & Appl. Phys., **27P** (1989) 578; S.K. Paranjpe and S.M. Yusuf, Neutron News, Vol.13, No.3, 2002 (In press).
5. P.S.R. Krishna, R. Chakravarthy, A.B. Shinde, B.A. Dasannacharya and N.R. Rao, IAEA conference on Research reactor utilization. IAEA-SR-198/25 (1996).
6. P.S.R. Krishna and A.B. Shinde (to be published). P.S.R. Krishna, A. Das, S.K. Paranjpe, A.B. Shinde, S. Naik and M. Ramanadham (to be published)
7. P.A. Egelstaff, in: Methods of experimental physics, vol 23B, ed. D.L. Price and K. Sköld, (Academic press, San Diego, 1987).
8. P.S.R. Krishna, V.S. Tiwari, Dhananjai Pandey, R.Chakravarthy and B.A. Dasannacharya, Appl. Phys. Lett., **62** (1993) 231.
9. V.S. Tiwari, Dhananjai Pandey, P.S.R. Krishna, R.Chakravarthy and B.A. Dasannacharya, Physica, **B 174** (1991) 112.
10. Rajeev Ranjan, Neelam Singh, Dhananjai Pandey, V. Siruguri, P.S.R. Krishna, S.K. Paranjpe and Alok Banerjee, Appl. Phys. Lett., **70** (1997) 3221.
11. Rajeev Ranjan, Dhananjai Pandey, V. Siruguri, P.S.R. Krishna, S.K. Paranjpe, J. Phys. Condensed matter, **11** (1999) 2233.
12. D.B. Wiles and R.A. Young, J. Appl. Crystallogr., **14** (1981) 149.
13. H.M. Chan, M.P. Harmer, M. Lal and D.M. Smyth, Mater. Res. Soc. Symp. Proc., **31** (1988) 345.
14. S.M. Yusuf, R. Ganguly, K. Chakraborty, P.K. Mishra, S.K. Paranjpe, J.V. Yakhmi and V.C. Sahni, J. Alloys & Compounds **326**, 89 (2001).
15. A.K.Karmakar, P.S.R. Krishna and R.N. Joarder, Phys. Lett., **A 253** (1999) 207.
16. P.S.R. Krishna and R.N. Joarder, Indian J. Phys., **75A** (2001) 95.
17. Pinakpani Nath, S. Sarkar, P.S.R. Krishna and R.N. Joarder, Z. Naturforsch., **56 a** (2001) 825.
18. N.Ramesh Rao, P.S.R.Krishna, Saibal Basu, B.A.Dasannacharya, K.S.Sangunni and E.S.R. Gopal, J. Non-crystalline.Solids, **240** (1998) 221.
19. A.G. Shikerkar, J.A.E. Desa, P.S.R. Krishna and R. Chitra, J. Non-Crystalline Solids, **270** (2000) 234.
20. P.S.R. Krishna, B.A. Dasannacharya and M.S. Sonavane, Solid state physics (India), **38C** (1995) 237.
21. P.S.R. Krishna, Saibal Basu and N. Ramesh Rao, Solid State Physics Symposium, **37C** (1994) 258.

Magnetism with Neutrons



Dr. S.M. Yusuf joined the magnetism section of Solid State Physics Division (formerly Nuclear Physics Division), BARC in 1989 after completing 32nd batch of BARC Training School. He received his M.Sc. degree in Physics from Visva Bharati University in 1987 and Post M.Sc. degree in Physics from Saha Institute of Nuclear Physics in 1988. He was intimately connected with the setting up of the neutron polarization analysis spectrometer at Dhruva reactor for magnetic scattering studies. He has also set up a low temperature laboratory for macroscopic magnetic studies. He acquired the Ph. D. (Physics) degree of the University of Mumbai in 1997 and he was a post doctoral fellow at Argonne National Laboratory, USA during 1997-1998. Dr. Yusuf has published a large number of papers in international scientific journals. He has received Best Young Physicists Award from Indian Physical Society and N.S. Sathya Murthy Award from Indian Physics Association in 1996 in recognition of his contributions to neutron scattering from magnetic materials. He is a member of American Physical Society.

Ms. Keka R. Chakraborty has got her M.Sc. in Physics from IIT Mumbai. She joined BARC, in the 34th batch Training School and has been working on magnetic neutron diffraction.



Dr. S.K. Paranjpe joined 12th batch of Training School after completing his master's degree in Physics from University of Indore. He joined the neutron scattering group of the then Nuclear Physics Division in 1969. He worked on the magnetic structures and spin densities of alloys and compounds, for Ph.D. degree from University of Bombay. He has been actively involved in the instrumentation for beam line experiments from its inception and has been responsible for setting up many spectrometers – with special reference to position sensitive detectors. He worked in the RAL, UK, as visiting scientist for one year. Presently he is working in the International Atomic Energy Agency (IAEA) as research reactor specialist. He has been involved in the collaborative programs with University scientists under IUC-DAEF collaboration.

Introduction

Neutrons have a spin $\frac{1}{2}$, zero charge and a magnetic moment μ_n of -1.913 nuclear magneton. Neutrons with thermal energies between 10 and 100 meV have de Broglie wavelengths of 2.86–0.905 Å,

comparable to atomic separation in condensed matter. Thermal neutrons are therefore, useful in studying atomic positional correlations in condensed matter. Having no charge but a magnetic moment makes them a useful tool to detect atomic magnetic moments with no concomitant coulomb interaction. The award of the Nobel Prize for physics in the last

Dr. S. M. Yusuf, Ms. K. R. Chakraborty and Dr. S.K. Paranjpe, Solid State Physics Division, Bhabha Atomic Research Centre, Mumbai 400 085; E-mail: smyusuf@apsara.barc.ernet.in

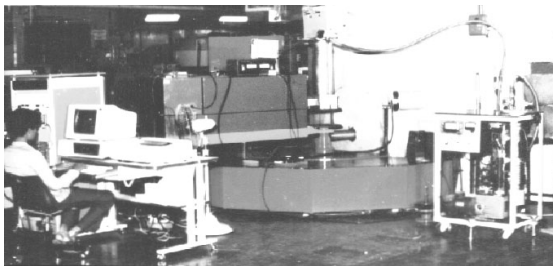


Fig. 1 Photograph of the position sensitive detector based Neutron Powder Diffractometer at Dhruva reactor, Trombay.

decade to Prof. C. G. Shull has emphasized once again the importance of magnetic neutron scattering as the most direct tool to study magnetic ordering in condensed matter on an atomic length scale.

In India, the magnetic neutron scattering activity started mainly at the CIRUS reactor. Later when Dhruva became critical in 1985, neutron instruments were also built in Dhruva. At the Dhruva reactor, the Neutron Powder Diffractometer [1] and the Neutron Polarization Analysis Spectrometer [2]) (Figs. 1 and 2) are being used extensively for magnetic studies for more than a decade. The principle of magnetic neutron scattering with a brief description of the activities at the Dhruva reactor are described in this article.

Principle of Neutron Magnetic Scattering

Neutron interacts with a nucleus via short range ($\sim 10^{-12}$ cm) nuclear force. The neutron nucleus scattering is isotropic and it is characterized by a single parameter, b , the nuclear scattering length. In magnetic materials, the magnetic scattering arises due to the electromagnetic interaction $-\mu_n \cdot \mathbf{H}(\mathbf{r}, t)$ where $\mathbf{H}(\mathbf{r}, t)$ is the magnetic field at position \mathbf{r} seen by the neutron, due to the spin and orbital moment of magnetic atom [3-5]. The interaction of μ_n with the nuclear magnetic moment (if any) is very weak as compared to the electronic $-\mu_n \cdot \mathbf{H}(\mathbf{r}, t)$ contribution. As the radial extent of the unpaired electrons (in 3d, 4f and 5f shells in transition metals, rare earths, and actinides, respectively) responsible for the atomic moment is comparable with the thermal neutron wavelength (~ 1 Å), the neutron magnetic scattering

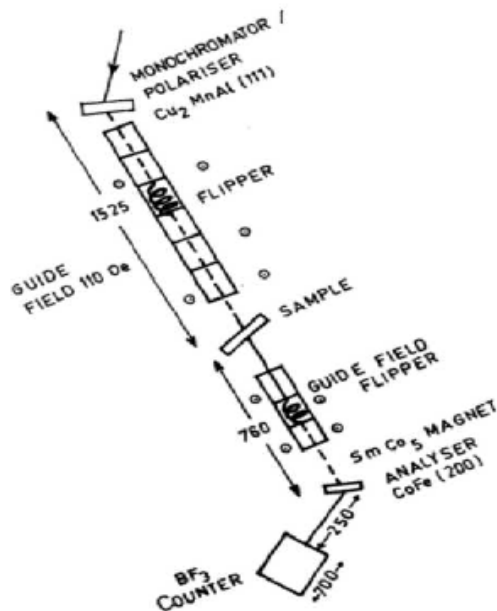
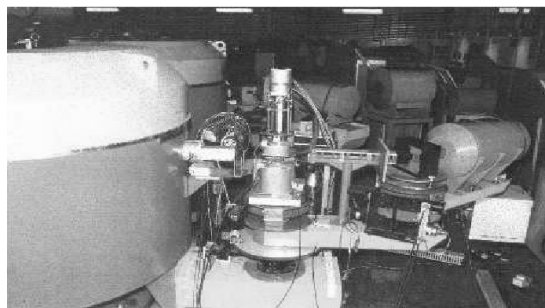


Fig. 2 Photograph and the schematic diagram of the Polarization Analysis Spectrometer located at Dhruva reactor, Trombay.

has an angular dependence and leads to a magnetic form factor $f(\mathbf{Q})$ for an atom or ion. The magnetic scattering amplitude p (in cm) is given by $0.269 \times 10^{-12} \mu f(\mathbf{Q})$. Here, μ is atomic magnetic moment in Bohr magneton due to unpaired electrons with orbital angular momentum \mathbf{L} and spin angular momentum \mathbf{S} . $\mathbf{Q} = (\mathbf{k}_0 - \mathbf{k}_f)$ is the wave-vector transfer. Here \mathbf{k}_f and \mathbf{k}_0 are the wave vector of scattered and incident neutrons, respectively. The magnetic scattering is effectively governed by the term $\mathbf{q}p$ where $\mathbf{q} = \mathbf{k}(\mathbf{k} \cdot \mathbf{K}) - \mathbf{K}$, ($\mathbf{k} = \mathbf{Q}/|\mathbf{Q}|$ is the unit scattering vector and \mathbf{K} is the unit vector in the direction of the atomic magnetic moment). Thus, for neutrons, all magnetic scattering is governed by the

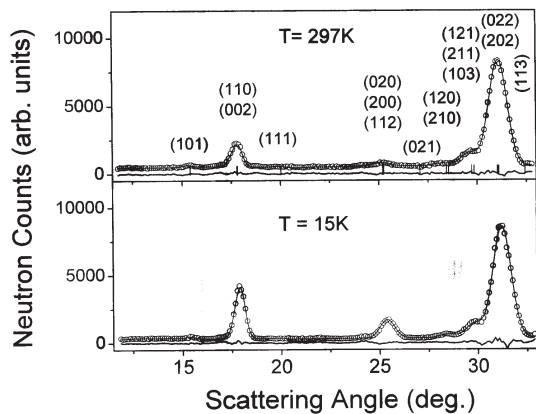


Fig. 3 Neutron diffraction patterns for $\text{La}_{0.67}\text{Ca}_{0.33}\text{MnO}_3$ perovskite at 297 K and 15 K. Open circles represent the observed data. The solid lines represent the Rietveld refined patterns. The difference pattern is also shown by solid line at the bottom. The hkl values are marked above the respective scattering angles. Enhancement of Bragg peak intensity at 15 K indicates ferromagnetic ordering [Ref. 6].

projection of the magnetic moment on the plane perpendicular to the scattering vector \mathbf{Q} . The magnetic interaction vector thus, provides information about the orientations of the atomic magnetic moments with respect to crystal axes.

Neutron Diffraction and Magnetic Structure

The magnitude and direction of the moments of magnetic atoms/ions with respect to the crystalline axes, a , b and c define the magnetic structure in a magnetically ordered material with underlying crystalline lattice. The magnetic unit cell is the building block of the magnetic crystal. Neutron diffraction has been playing a vital role in understanding the magnetic phases microscopically [3-5]. In a paramagnetic material, the atomic moments are orientationally disordered due to temperature effect and causes disordered scattering. Here, one can therefore, study the magnetic form factor $f(\mathbf{Q})$ for atoms or ions. However, below the magnetic ordering temperature of ferromagnets, ferrimagnets, antiferromagnets etc. there is a regular periodicity of moments of magnetic atoms/ions

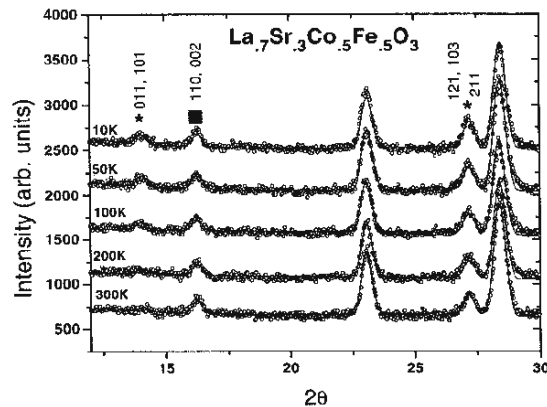


Fig. 4 Evolution of magnetic peaks with temperature for the $\text{La}_{0.7}\text{Sr}_{0.3}\text{Co}_{0.5}\text{Fe}_{0.5}\text{O}_3$ perovskite showing the coexistence of long range ferro- and antiferromagnetic ordering. * and ■ denote the rise in antiferromagnetic and ferromagnetic order, respectively [Ref. 7].

which manifests itself as magnetic Bragg peak in addition to the Bragg scattering due to regular positional arrangement of atoms/ions in crystalline solids. The knowledge of the nuclear structure is a pre-requisite for the magnetic structure determination. This is obtained either from X-ray diffraction measurements or by carrying out neutron diffraction experiments at temperatures above the magnetic ordering temperature or at higher \mathbf{Q} where magnetic scattering is very small due to its form factor dependence. In the case of ferromagnetic and ferrimagnetic materials, the magnetic unit cell is isomorphous with the chemical unit cell. This amounts to an occurrence of magnetic Bragg intensity at the same \mathbf{Q} of nuclear Bragg peak; causing an enhancement of Bragg peak intensities below the ordering temperature (Fig. 3). While in antiferromagnetic materials the magnetic unit cell can be larger than the chemical unit cell, Bragg peaks other than chemical peaks occur depending upon the symmetry of the magnetic periodicity (Fig. 4). Other types of magnetic ordering such as modulated magnetic structures also occur where magnetic satellite peaks appear at the reciprocal vector $\mathbf{Q} = \tau \pm \delta$ in neutron diffraction patterns [5]. Here τ is the reciprocal lattice vector and δ is the modulation

vector. The number of satellites observed in the diffraction pattern depends upon the magnetic symmetry.

In the case of unpolarized neutrons, the diffracted intensity for a Bragg peak with Miller indices (hkl) in a ferromagnetic or ferrimagnetic material is given by the formula [4]

$$I_{hkl}^0 = S j L (|F_N|^2 + |F_M|^2) \exp(-2W) \quad (1)$$

where S is a constant scale factor which depends on the amount of sample in the beam, neutron beam flux, detector efficiency etc., j is the multiplicity of the (hkl) plane. In a single crystal diffraction, j=1 as the intensities of different Bragg peaks are independently measured. L is the Lorentz factor (a geometrical factor to take into account the sample shape). $F_N(\mathbf{Q}) = \sum_j e^{2\pi i (hx_j + ky_j + lz_j)}$ is the nuclear

structure factor and $F_M(\mathbf{Q}) = \sum_j q_j p_j e^{2\pi i (hx_j + ky_j + lz_j)}$

is the magnetic structure factor for accounting the scattering contribution from the nuclear and magnetic unit cells, respectively. The summation over j runs for all the magnetic ions located in the magnetic unit cell. Here (x_j, y_j, z_j) are the fractional co-ordinates of the jth atom in the unit cell and exp(-2W) is the Debye-Waller factor arising from the thermal vibration of atoms.

In a single crystal diffraction, the magnetic structural parameters are obtained by least squares minimization of the difference between observed and model based calculated Bragg peak integrated intensities. In a standard powder diffraction experiment, especially for low symmetry systems there are many overlapping peaks [8] and one is forced to use profile refinement method (Rietveld refinement [9]). In this method the intensity at each observation point is calculated by summing over the contributions from all the Bragg peaks contributing at the observation point. One can apply the Rietveld profile refinement technique accounting both nuclear and magnetic structures simultaneously.

Both the Neutron Powder Diffractometer, [1] and the Polarized Analysis Spectrometer (2-axis unpolarized mode) [2], have been extensively used for carrying out powder diffraction experiments to study magnetic ordering/phase-transitions in variety

of magnetic systems [7] such as, ferrites having disordered magnetic ordering [10], manganites showing CMR behaviour [11], cobaltates showing coexistence of ferro- and antiferromagnetism [12], anisotropic $U_{1-x}Th_xCu_2Ge_2$ intermetallic compounds, and alloys of transition metals, rare-earths and actinides (UNi_2Si_2 , $ErFe_2D_x$, $TbMnFe$ etc.) showing exotic magnetic properties [13], amongst others.

Polarized Neutrons in Magnetic Scattering

Neutron is a spin half particle and the spin is $+\frac{1}{2}\hbar$ or $-\frac{1}{2}\hbar$ with respect to a reference magnetic field direction. Polarization of a neutron beam is achieved by selecting neutrons of one spin state from an unpolarized neutron beam [14, 2]. For thermal neutrons this is normally achieved by Bragg diffraction from $Co_{0.92}Fe_{0.08}(200)$ or $Cu_2MnA(111)$ single crystals under saturation magnetic field. For polarized neutrons with incident polarization parallel (+) and antiparallel (-) relative to the saturation-magnetization (aligned perpendicular to the \mathbf{Q} vector by applying a strong magnetic field), the Bragg diffracted intensities (I^\pm) are given by the above expression in Eqn. (1) with an additional cross term (interference term) $+2PDF_NF_M$ and $-2PD(2f-1)F_NF_M$ respectively, in the parenthesis. Here P (~ 0.98) is the incident neutron beam polarization, D (~ 1) is the polarization transmission through the sample, and f (~ 1) is the neutron polarization reversal efficiency of a polarization flipper. The sensitivity of polarized neutron diffraction for measurement of small magnetic moments is very high as it measures the interference between nuclear scattering and magnetic scattering [5,14]. For example, it is evident from our magnetic studies on $Co_{1.4-x}Zn_xGe_{0.4}Fe_{1.2}O_4$ spinels with x = 0.5, 0.6 and 0.7 where the tetrahedral-site (A-site) magnetic ion concentrations are 0.19(1), 0.17(1) and 0.14(1), respectively which are well below the site percolation threshold $C_p = 0.429$ [15]. The tetrahedral and octahedral site moments ($= 0.64(5) \mu_B$ and $2.54(5) \mu_B$, respectively) for the x = 0.5 sample were obtained from the unpolarized neutron diffraction data, taken at 11 K ($T_N = 255K$). However, the ordered site moments for the x = 0.6 and 0.7 samples could not be obtained from unpolarized neutron diffraction due to their low moments. These were obtained from the polarized

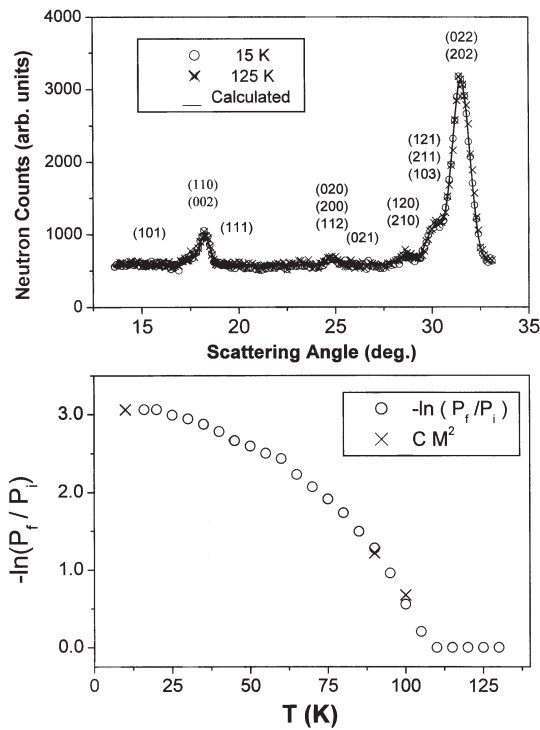


Fig. 5 Top: Neutron diffraction patterns for $\text{La}_{0.67}\text{Ca}_{0.33}\text{Mn}_{0.9}\text{Fe}_{0.1}\text{O}_3$ at 125 K and 15 K. Open circles and crosses represent the observed data. The solid lines represent the Rietveld refined pattern indicating no ordered magnetic moment down to 15 K. The hkl values are marked above the respective scattering angles [Ref. 18]. Bottom: Comparison of $-\ln(P_f(T)/P_i)$ and $C[M(T)]^2$ (C : constant scale factor, M : Magnetization at technical saturation) for the CMR perovskite $\text{La}_{0.67}\text{Ca}_{0.33}\text{Mn}_{0.9}\text{Fe}_{0.1}\text{O}_3$ [Ref. 18].

neutron diffraction study (T^+/T ratio measurements) of (220) and (222) Bragg peaks, respectively using the neutron polarization analysis spectrometer at Dhruva reactor (Fig. 4) and are found to be $0.12(6) \mu_B$ and $0.04(6) \mu_B$ for the $x = 0.5$ sample and $0.42(6) \mu_B$ and $0.14(6) \mu_B$ for the $x = 0.7$ sample, respectively. For all the three samples the B-site moments are much smaller than their free-ion

values, indicating that the octahedral site moments are non-collinear.

An accurate knowledge of magnetic structure amplitudes is essential to obtain the magnetization density distribution $\rho(\mathbf{r})$ (in $\mu_B/\text{\AA}^3$) at any point \mathbf{r} in the unit cell. The Fourier transformation of the measured magnetic structure factors gives a model independent understanding of $\rho(\mathbf{r})$ [16]. Such information helps in understanding the nature of bonding in these materials.

Transmission measurements using polarized neutrons (neutron depolarization study) are carried out to study spatial magnetic inhomogeneity in the mesoscopic length scale, say from 10 nm to several microns [14]. In an unsaturated ferromagnet, ferrimagnet or spin-cluster, the magnetic domains/clusters exert a dipolar field on the neutron polarization and depolarize the moving neutrons owing to the Larmor precession of the neutron spins in the magnetic field of domains/clusters. Neutron depolarization technique has been exploited substantially using the Neutron Polarization Analysis Spectrometer (Fig. 2) at Dhruva reactor. By using this technique some of the longstanding discrepancies regarding the nature of magnetic ordering in various magnetic systems has been resolved [2,6,17,18].

Figure 5 depicts the results of neutron diffraction and neutron depolarization for CMR perovskite $\text{La}_{0.67}\text{Ca}_{0.33}\text{Mn}_{0.9}\text{Fe}_{0.1}\text{O}_3$ [18]. The neutron diffraction study does not show any ferromagnetic Bragg contribution to the nuclear peaks at low temperatures due to low magnetic moment. However, the transmitted neutron beam polarization P_f starts decreasing right from 108 K and confirms the presence of ferromagnetic domains with low net moments below the ordering temperature (≈ 108 K). The temperature dependence of P_f is correlated with the temperature dependence of the magnetization at technical saturation, M . On theoretical considerations, this result indicates a temperature independent domain size ($\sim 2 \mu\text{m}$) [18].

The magnetic spin arrangement in a solid at finite temperature deviates from its ideal alignment expected at absolute zero temperature and the corresponding dynamics can be described in terms of spin waves. The energy transmitted by these spin

waves is quantized (magnons). Inelastic magnetic scattering plays very important role in giving information about magnon spectrum [5, 19]. In this article we are not going to talk about such scattering processes.

Conclusion

Magnetic scattering experiments using both polarized and unpolarized neutrons are being carried out quite extensively at Trombay.

References

1. S.K. Paranjpe and Y. D. Dande, *Pramana-J. Phys.*, **32** (1989) 793.
2. S. M. Yusuf and L. Madhav Rao, *Neutron News* 8, 12 (1997); S. M. Yusuf and L. Madhav Rao, *Pramana-J. Phys.*, **47** (1996) 171.
3. O. Halpern and M.H. Johnson, *Phys. Rev.*, **55** (1939) 898.
4. S. W. Lovesey, *Theory of Neutron Scattering from Condensed Matter*, (Oxford University Press, Oxford 1984).
5. *Magnetic Neutron Scattering*, Ed. Albert Furrer, (World Scientific, Singapore, 1995).
6. S.M. Yusuf *et al.*, *Appl. Phys.*, 2002 A (in press); S. M. Yusuf *et al.*, *Phys. Rev. B* 2002 (In press).
7. S.K. Paranjpe and S. M. Yusuf, *Neutron News*, Vol. **13**, No. 3, 2002 (In press).
8. S. M. Yusuf, *Powder Diff.*, **8** (1993) 236.
9. H.M. Rietveld, *J. Appl. Crystallogr.*, **2** (1969) 65.
10. R. Chakravarthy *et al.*, *Phys. Rev.*, **B 43** (1991) 6031; M. V. Subbarao *et al.*, *Pramana - J. Phys.*, **53** (1999) 341; A.K. Ghatage *et al.*, *Indian. J. Phys.*, **73A** (1999) 329.
11. S.M. Yusuf *et al.*, *J. Alloys and Compounds*, **326** (2001) 89; A. Das *et al.*, *J. Magn. Magn. Mat.* (2001) in press; P.D. Babu *et al.*, *Solid Stat. Commun.*, **118** (2001) 91; A. Das, *et al.*, *Mat. Res. Bull.*, **35** (2000) 651.
12. V.G. Sathe *et al.*, *J. Phys.- Cond. Matter*, **8** (1996) 3889; *idem, ibid* **10** (1998) 4045.
13. S. M. Yusuf *et al.*, *Phys. Rev.*, **B 53** (1996) 28; S. M. Yusuf *et al.*, *Physica*, **B223&224** (1996) 201; K. Shashikala *et al.*, *Phil. Mag.*, **B79** (1999) 1195; K. R. Chakraborty *et al.*, *Pramana- J. Phys.*, **48** (1997) 1115; S. M. Yusuf, *et al.*, *Pramana- J. Phys.*, **38** (1992) 669; S.M. Yusuf *et al.*, *Solid State Commun.*, **112** (1999) 207.
14. W.G. Williams, *Polarized Neutrons* (Oxford University Press, Oxford, 1988).
15. M.V. Subbarao *et al.*, *Pramana- J. Phys.*, **53** (1999) 341.
16. L. Madhav Rao *et al.*, *Phys. Rev.*, **B18** (1978) 6275.
17. S. M. Yusuf and L. Madhav Rao, *J. Phys.: Condens. Matter*, **7** (1995) 5891; S. M. Yusuf *et al.*, *Solid State Commun.*, **101** (1997) 145; S. M. Yusuf, *et al.*, *J. Magn. Magn. Mater.* **166**, 349 (1997).
18. S. M. Yusuf *et al.*, *Phys. Rev.*, **B 62** (2000) 1118.
19. J. W. Lynn and J. J. Rhyne, in : *Spin Waves and Magnetic Excitations*, Edited by A.S. Borovik Romanov and S. K. Sinha (North Holland, Amsterdam, 1988).

Small-Angle Neutron Scattering at Trombay



Dr. S. Mazumder joined 27th batch of BARC Training school after completing M.Sc (Chemistry) from I.I.T Kharagpur. Subsequently he joined the then Neutron Physics Division. Since then he is working in the field of small-angle neutron and x-ray scattering. He has developed a formalism for the multiple small angle scattering. Presently he is the group leader of the small angle scattering group in Solid State Physics Division, BARC. He is an IAEA expert for promotion of small-angle neutron scattering research.

Shri D. Sen obtained his post-graduate degree in physics from the University of Kalyani, West Bengal in 1994. After the completion of the BARC training school, 39th batch, he joined the Solid State Physics Division, BARC. He has been working in the field of characterization of materials, particularly, different porous media, alloys, ceramics etc. using small angle x-ray and neutron scattering.



Shri A.K. Patra, obtained his M.Sc. (Physics) from Utkal University, Bhubaneswar. He joined the Solid State Physics Division after graduating from the 30th batch of BARC training school. He has worked on the fabrication of position sensitive detectors for x-rays and neutrons. At present he is working in the field of small-angle neutron and x-ray scattering.

Dr. P.S. Goyal passed 11th batch (Physics) of training school and joined B.A.R.C. in 1968. He used neutron scattering techniques for studying structure and dynamics of a number of molecular solids and took part in development of neutron beam instrumentation. During last decade he was involved in study of mesoscopic systems using Small Angle Neutron Scattering. As an IAEA expert, he has helped neutron scattering groups in Korea, Indonesia and Bangladesh in starting SANS activity at their institutes.



Dr. V.K. Aswal obtained his post-graduate degree in physics from I.I.T. Mumbai. After completing the 36th batch of BARC Training school in Physics discipline, joined Solid State Physics Division in 1993. Ever since he is working on small-angle neutron scattering investigation on soft condensed matter particularly micellar solutions.

Dr. S. Mazumder, Shri D. Sen, Shri A.K. Patra, Dr. V.K. Aswal, Ms. E. Seth, Solid State Physics Division, Bhabha Atomic Research Centre, Trombay, Mumbai 400 085; smazu.@apsara.barc.ernet.in; Dr. P.S. Goyal, Inter University Consortium for DAE facilities, Mumbai Centre, Trombay, Mumbai 400 085; E-mail: psgoyal@magnum.barc.ernet.in



Ms. Ekta Seth completed her M.Sc. (Biochemistry) from Aligarh University in 1998. After completing the 42nd batch Training school of BARC in Biology discipline, she joined the Solid State Physics Division. At present she is working on small-angle neutron scattering investigation on biomolecules.

Small-angle neutron scattering (SANS) [1] is a powerful technique for studying structural features of the inhomogeneities (particles) or the density fluctuations in condensed matter for a length scale ranging from one nanometer up to one micron. “Structural features” include size or size distribution, shape, dimensionality, interparticle spatial correlation etc. In a unique way, SANS technique provides the door to the “nanocosmos” in almost all domains of science and technology. These include classical metallurgy (precipitate hardening), materials research (nanocomposites), soft matter (gels, colloids, polymers), chemistry (catalysis) and engineering (porous filters, structural and functional ceramics). The lower limit of the length scale resolved by SANS overlaps with the length scale of interest in crystallography while the upper limit coincides with length scale accessed by conventional microscope. SANS is a non-destructive technique that allows large specimen volumes to be analyzed without any special preparation.

SANS is an elastic scattering process, which is related to the scattering properties at small momentum transfer vector and is caused by the variation of scattering length density over a distance exceeding the normal inter-atomic distances in condensed systems. It is distinct from Bragg or diffuse scattering in the sense that it refers to scattering at that region of momentum transfer vector (q) whose magnitude is small (typically $0.001\text{--}3.0\text{ nm}^{-1}$) compared to that of the smallest reciprocal lattice vectors in crystalline substances or to that corresponding to the first maximum of the structure factor in a non crystalline materials. The consideration of scattering at low momentum transfer makes the SANS technique suitable to study gross-scale structural properties of a medium overlooking the specific details over inter-atomic distances.

In this article, a brief description of the SANS activity at the DHRUVA reactor, Bhabha Atomic Research Centre, Trombay is discussed.

SANS Diffractometers at Trombay

To probe a wide range of length scale, two SANS diffractometers have been built and commissioned at the guide tube laboratory DHRUVA. One is the double crystal-based moderate resolution (MSANS) [2] and the other is the linear position sensitive detector (PSD) based [3]. The PSD based instrument is the upgraded version of the SANS instrument which had been operating [4] at CIRUS reactor.

For MSANS (Fig.1) the accessible momentum transfer q ($= 4\pi \sin\theta / \lambda$, where 2θ is the scattering angle) range is 0.003 to 0.173 nm^{-1} . The MSANS has been calibrated with the ultra small-angle neutron scattering (USANS) instrument (S18) at the Institute of Laue and Langevin (ILL), Grenoble, France. This instrument is used to study large inhomogeneities, as commonly encountered in cements, ceramics, macromolecules, magnetic domains etc.

The another SANS diffractometer (Fig. 2) is a conventional slit collimation instrument and uses a one-meter long linear position sensitive detector. The q range of this instrument is 0.18 to 3.2 nm^{-1} . This instrument has been used to study the micellar structures and inter-micellar interactions in a variety of micellar solutions.

Some Typical Experimental Results

Pore Morphology in Sintered $\text{ZrO}_2\text{--}8\text{ mol \% Y}_2\text{O}_3$ Ceramic

The application of ceramic material depends greatly on porosity, pore morphology and pore size distribution of the compound. Recently zirconia (ZrO_2) and zirconia based ceramics like yttria

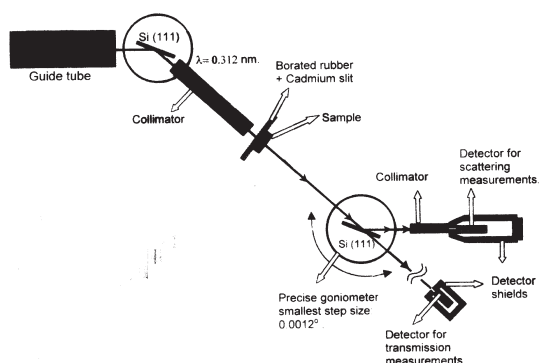


Fig. 1 Photograph and schematic layout of the double crystal based SANS instrument at the guide tube laboratory of DHRUVA.

stabilized zirconia, have attracted a great deal of attention because of their enormous technological applications.

Pore morphology and pore size distribution in yttria stabilized zirconia (ZrO_2 -8 mol % Y_2O_3) have been investigated [5] using double crystal based MSANS instrument. Fig.3, depicting the single scattering profiles (SSP) for the above-mentioned specimen, exhibits a nice shoulder. Appearance of such a shoulder [6] is indicative of the presence of two length scales in the system [5], as perceived by neutrons. In the present case, it is reasonable to assume that the larger length scale appears due to the agglomeration of the ceramic particles during compaction and heat treatments and the lower length scale is due to the pores. The estimated pore size distributions are depicted in the inset of the Fig. 3. The results unfurl that the reduction in the porosity, at 1270°C compared to that at 1200°C, occurs by the

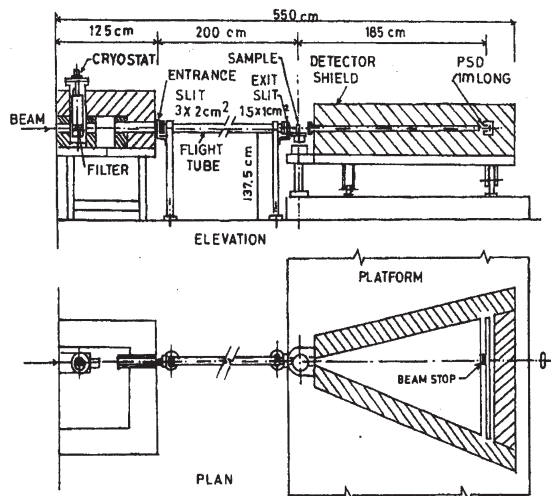


Fig. 2 Photograph and schematic layout of the PSD based SANS instrument at the guide tube laboratory of DHRUVA

elimination of the pores at the lower end tail of the pore size distribution.

Pore Surface Roughening in Rocks

Pore-matrix interface roughening in some metamorphosed sedimentary rocks, sandstones and igneous rocks, which is a subject of practical importance from the petrological point of view have been investigated [7] in the length scales of ~ 20-1000 nm using MSANS. The results reveal the fractal nature of the rock-pore interfaces. Fig. 4 represents the profiles from the three specimens of metamorphosed rocks. Power law variation for a

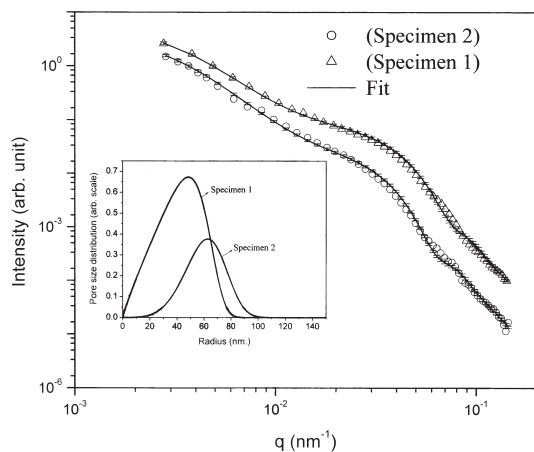


Fig. 3 Estimated single scattering profiles from the experimental profiles of 8 mol% Y_2O_3 stabilised ZrO_2 for two sintering temperatures 1200° (Specimen 1) and $1270^\circ C$ (Specimen 2). The solid line represents the fit of a model (based on the polydisperse spherical particles model along-with a fractal agglomerate at higher length scale [4]) to the data. The inset shows the estimated pore size distributions.

wide range of q , a signature of fractal system, is discernible from the figure. No signature of the upper cut-off in the accessible q range has been observed for these specimens.

However, profiles of the igneous rock and the sedimentary sandstone rock specimens (not shown here) indicated the presence of upper cut-off of the surface fractal nature. Surface fractal dimension of the metamorphosed rocks and the sandstones has been estimated to be ~ 2.8 while, that for the igneous rocks has been found to be ~ 2.3 . The relatively high surface fractal nature of the sandstones and metamorphosed rocks has been explained with the help of a computer simulation model based on the formation mechanisms (deposition and desolution mechanisms of the grains with probability P_+ and P_- respectively) of these rocks [7]. Fig. 5 depicts the results from the simulation.

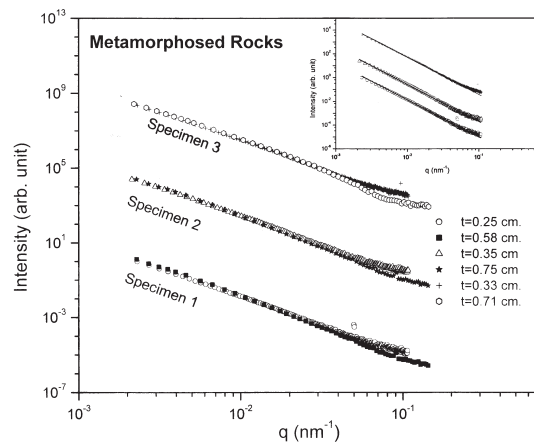


Fig. 4 SANS profiles from the metamorphosed rocks showing the power law variation for a wide range q indicates the signature of fractal. It is also evident, from the nearly identical nature of the profiles for the two thicknesses, that the power law region of the SANS profiles remain unaffected by the multiple scattering. The inset shows the fit of a model based on the framework of surface fractal [6] to the data for the thinner specimen.

Exploitation of Multiple Scattering to Investigate the Very Large inhomogeneities, which are otherwise not accessible by low resolution SANS, Instruments

The upper limit of the extractable size range of the inhomogeneities by a SANS instrument bears reciprocal relation to the minimum value of the accessible momentum transfer (q), which is limited by the finite width of the direct beam. However, as the primary feature of multiple scattering [8] is to broaden the true scattering profile, it should therefore be possible to exploit the beam-broadening feature of the multiple scattering, using suitably thick specimens, to probe very large inhomogeneities, which are otherwise not accessible. Multiple small angle scattering experiments had been performed [9], using the low-resolution SANS instrument that was operating at CIRUS, on bidisperse alumina specimens with

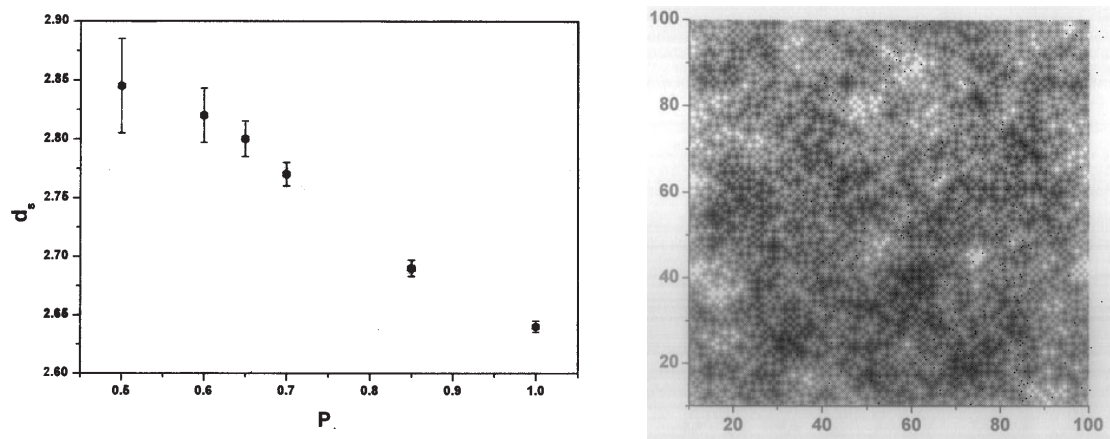


Fig. 5 The results from the computer simulation explain the high fractal dimension ($d_s \sim 2.8$) of the metamorphosed (fig. 4) and sandstone rocks. The variation of the surface fractal dimension d_s with deposition probability (P_+) from the model is depicted. A typical computed fractal surface is shown for $d_s \sim 2.8$.

particle sizes much larger than the resolution of the instrument. It is shown that the realistic structural parameters can be obtained, using the formalism of multiple scattering [8], only if the multiple scattering and the bidispersity of the specimen are accounted for.

Role of Additives on the micellar Structure by PSD based SANS Instrument

Surfactant molecules (e.g. CTAB, SDS, Triton X-100 etc.) self-aggregate into supermolecular structures when dissolved in water or oil. The simplest aggregate of these surfactant molecules is called a micelle. SANS studies have shown that micelles of ionic surfactants transform spherical to ellipsoidal or cylindrical micelles on addition of substances such as salt [10], alcohols and amines resulting an increase in viscosity of the solution. This is due to the growth of micelles in the solution, which depends on the concentration of the additives. Systematic studies on several different micellar systems show that the ionic size of the additive plays an important role in deciding the growth rate of the micelle. As an example Fig. 6, shows the results of SANS studies on 0.3 M sodium dodecyl sulphate (SDS) solutions in the presence of 0.1 M different alkali halides of the type ABr ($A = \text{Na, K, Cs}$) [11]. It is seen, that peak in the SANS distribution profiles shifts to lower q values on addition of NaBr, KBr and

CsBr and the shift is different for different salts. The peak in SANS distribution arises from a corresponding peak in the inter-particle structure factor and its position at $q_m (= 2\pi/d)$ depends on the inter-particle distance d . The growth of a micelle at a fixed surfactant concentration results in a decrease in the number of micelles or an increase in d . Thus, a larger shift in the peak position in a SANS distribution implies a larger growth of micelle.

SANS from Multi-Head Group Surfactants

The other class of experiments which were carried out, deal with the study of the role of the architecture of the surfactant molecules on the micellar structure. For example, a series of experiments have been carried out on the Gemini surfactants where the role of length, rigidity and hydrophilicity of the spacer of Gemini molecules on the micellar structure have been examined [12]. Similarly, measurements have also been made on multi-head group surfactants to examine if the surfactant molecules will form micelles when several charged head groups are incorporated on one end of a single hydrocarbon chain of the surfactant [13]. Measured SANS distributions from surfactants consisting of a single chain (same length as that of CTAB) and bearing one ($h=1$), two ($h=2$) and three ($h=3$) head groups are shown in Fig. 7. It was found that as the number of head groups in the surfactant

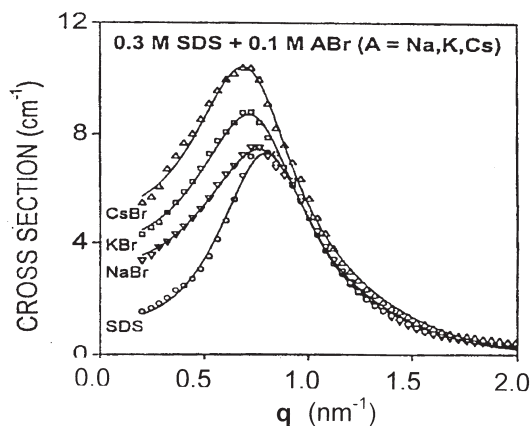


Fig. 6 SANS profiles from 0.3 M SDS micellar solution in presence of 0.1 NaBr, 0.1 KBr and 0.1 M CsBr. The shift in correlation peak for a fixed surfactant concentration is connected with the growth of the micelle. It is seen that depending on the sizes of the counterions (Na^+ , K^+ , Cs^+), the micellar growths are different.

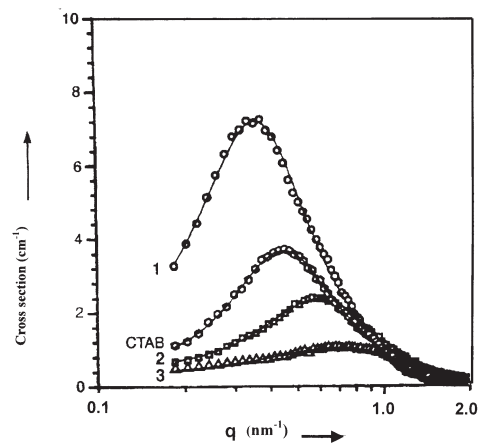


Fig. 7 SANS profiles from 0.05 M micellar solutions of CTAB and surfactants having $h=1, 2$ or 3 charged head groups attached to a single hydrophobic chain. Decrease in intensity and shift of peak to larger q values for a fixed surfactant concentration suggests that micelle size decreases with an increase in h .

molecule increases, micelle size decreases because of repulsion and steric hindrance between the adjacent head groups.

References

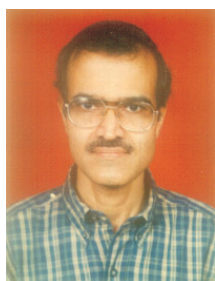
1. V. Gerold and G. Kistorz; J. Appl. Crystallogr. **11** (1978) 376; G. Kistorz in Treatise on Materials Science and Technology; Edited by G. Kistorz; (Academic Press 1979) 15, 227; W. Schmatz; T. Springer and J. Schelten and K. Ibel; J. Appl. Crystallogr., **7** (1974) 96; J.S. Higgins and R. S. Stein; J. Appl. Crystallogr. **11** (1978) 346; C.G. Windsor; J. Appl. Crystallogr. **21** (1988) 582.
2. S. Mazumder, D. Sen, T. Saravanan and P.R. Vijayraghavan; J. Neutron Res., **9** (2001) 39, S. Mazumder, D. Sen, T. Saravanan and P.R. Vijayraghavan; Current Science, **81** (2001) 257.
3. V. K. Aswal and P. S. Goyal, Current Science **80** (2001) 972.
4. J.A.E. Desa, S. Mazumder, A. Sequeira and B.A. Dasannacharya; Solid state phys. C (India), 1985, 28, 318
5. D. Sen, A.K. Patra, S. Mazumder and S. Ramanathan; J. Alloys and compounds (in press) (2002)
6. S. Mazumder, D. Sen, P.U.M. Sastry, R. Chitra, A. Sequeira and K.S. Chandrasekaran; J. Phys : Condens Matter, **10** (1998) 9969.
7. D. Sen, S. Mazumder and S. Tarafdar; J. Mater. Sci., **37** (2002) 941; D. Sen, S. Mazumder and S. Tarafdar; Applied Physics A (in press) (2002)
8. S. Mazumder and A. Sequeira; Pramana-J.Phys., **25** (1992) 221, S. Mazumder and A. Sequeira; Phys. Rev., **B 41** (1990) 6272; *ibid* **39** (1989) 6370.
9. S.Mazumder, A. Sequeira, S.K. Roy and R. Biswas; J. Appl. Cryst , **26** (1993) 357.
10. P.S. Goyal, et al., Physica, **B 158** (1989) 471.
11. V.K. Aswal and P.S. Goyal; Phys Rev., **E 61** (2000) 2947.
12. V.K.Aswal, et al., Phys Rev., **E 57**(1998) 776.
13. J.Haldar, et al.,Angewandte Chemie.Int.Ed. **40** (2001) 1228.

Inelastic Neutron Scattering for the Study of Atomic Vibrations and Magnetic Excitations



Smt. Mala N. Rao obtained her M.Sc. (Physics) from Mumbai University and joined 33rd Batch of BARC Training School in the year 1989. After training, she joined the neutron scattering group of the Solid State Physics Division. Her field of work is materials research through inelastic neutron scattering experiments and theoretical lattice dynamics model calculations.

Shri R. Mittal joined 34th Batch of BARC Training School after completing M.Sc. (Physics) from H.N.B. Garhwal University. He has been working in Solid State Physics Division, BARC since 1991. He is involved in neutron scattering experiments, X-ray diffraction experiments and lattice dynamics computations.



Dr. S.L. Chaplot joined BARC in the year 1974 through the 18th Batch of BARC Training School. He joined the then Nuclear Physics Division and has been working at the Cirus and Dhruva reactors at Trombay. His research involves the study of the structure and dynamics of various materials using neutron scattering and other experimental and theoretical techniques. He was the recipient of the DAE Homi Bhabha Award for Science and Technology for 1994, which is the highest honor bestowed by the Department of Atomic Energy, Government of India. He was a Research Associate at University of Edinburgh (1979-81), a young Associate of the Indian Academy of Sciences (1985-90), a recipient of the N.S. Satya Murthy Memorial Award of the Indian Physics Association (1989), the Alexander von Humboldt Fellowship, Germany (1992) and the Material Research Society of India Medal (2002).

Introduction

Experiments involving thermal neutron diffraction usually deal with the question of where the atoms are in solids, i.e. the time averaged atomic positions. Inelastic thermal neutron scattering, where one measures the changes in neutron energies on scattering from a sample, tells us about the motion of atoms. The dynamics of atoms in solids is the key input in understanding the thermodynamic properties of solids, such as phase transitions (e.g.

structural), specific heat, thermal expansion and thermal conductivity.

It is well known that the mean positions of the atoms in a crystal define a three-dimensional periodic array. The atoms usually oscillate about these mean positions. Small motions of the atoms about these average positions can be analyzed in terms of harmonic lattice vibrations, such that the displacements of the corresponding atoms in different unit cells are equivalent, apart from a

Smt. Mala N. Rao, Shri R. Mittal and Dr. S. L. Chaplot, Solid State Physics Division, Bhabha Atomic Research Centre, Mumbai 400 085; E-mail : mala@apsara.barc.ernet.in; rmittal@apsara.barc.ernet.in, chalpot@magnum.barc.ernet.in

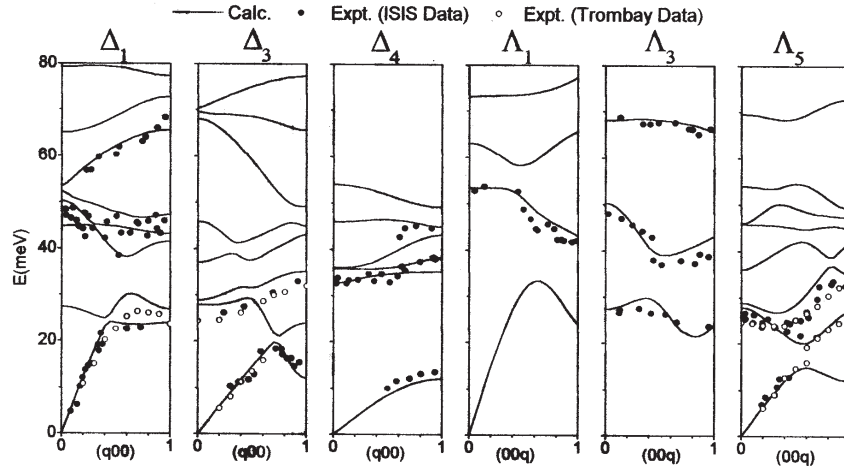


Fig. 1 Phonon dispersion curves along two directions of high symmetry $[100]$ and $[001]$ in zircon. The symbols (Δ_1 , Δ_3 , Δ_4 , Λ_1 , Λ_3 , Λ_5) on top of the figure denote the group-theoretical representations. Both the experimental data (symbols) as well as results from lattice-dynamical calculations (lines) are shown. The open and filled circles give the phonon peaks identified in the experiments at the ISIS spallation neutron source at U.K. and at Dhruva reactor, Trombay respectively.

possible phase shift. This analysis of the dynamics [1,2] of the crystal lattice leads to a description of the atomic vibrations as a superposition of travelling waves each characterized by a wave vector \mathbf{q} ($=2\pi/\lambda$, where λ is the wavelength of the wave) and angular frequency $\omega(\mathbf{q})$. The lattice vibrational energy is quantized and each quantum is called a phonon.

For a crystalline solid containing n atoms in the unit cell of the crystal lattice, there are $3n$ wave like solutions (modes) for each wave vector \mathbf{q} . It is possible to represent the frequencies ω of the $3n$ modes graphically by continuous curves as a function of \mathbf{q} . Corresponding to every direction in \mathbf{q} -space, there are $3n$ curves. Such curves comprise the phonon dispersion relation (PDR). A typical PDR is shown in Fig. 1. The form of the phonon dispersion curves depends on the crystal structure and on the nature of the interatomic forces. Single crystals are needed to measure the PDR.

Another quantity of interest is the frequency distribution function or phonon density of states, $g(\omega)$. It is a measure of the number of modes of vibrations per unit energy interval. The phonon density of states (PDOS) is thus an average over all

the phonons along all directions in the wave vector space. PDOS at different momentum transfers can be measured using polycrystalline samples.

The experimental study of lattice vibrations is through the interaction of phonons with radiation – basically by the techniques of Brillouin scattering, Raman scattering, infrared absorption and inelastic neutron scattering (INS). It may be noted here that Brillouin scattering, Raman scattering and infrared absorption probe the phonons close to $\mathbf{q}=0$ (refer to Fig. 1) only, because of the large wavelength of light. Also, not all phonons of $\mathbf{q}=0$ are observable by optical experiments. On the other hand, inelastic neutron scattering can be employed to probe the entire phonon spectrum throughout the \mathbf{q} -space.

Further, neutron with its magnetic moment (-1.913 nuclear magnetons) provides us with a magnetic probe to investigate magnetic properties. Neutron diffraction experiments help in determining magnetic moment values whereas inelastic neutron scattering elucidates energy level structures. In magnetically ordered systems, similar to lattice waves, we have spin waves; the energy of these spin waves is quantized in units of magnons. Dispersion relations of magnons may be determined using

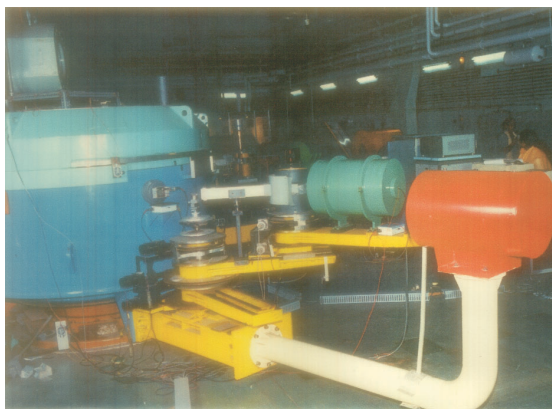


Fig. 2 A photograph of the Triple Axis Spectrometer at Dhruva reactor, Trombay.

single crystals of magnetic materials in their ordered states. Neutrons can also probe the behaviour of magnetic ion in the crystalline electric field (CEF) from neighbouring non-magnetic ions. For rare earth group, CEF gives sublevels within each J state separated by 1 meV to 100 meV and this splitting can be measured by inelastic neutron scattering. Information about symmetry and strength of crystalline electric field can also be derived.

Inelastic Neutron Scattering Experiments

INS experiments are invariably carried out using thermal neutron beams from reactors, which provide intense neutrons of energy 5-200 meV and corresponding wave vectors $\sim 10^8 \text{ cm}^{-1}$ ($\sim 1 \text{ \AA}^{-1}$). The ranges available are ideally suited for phonon investigations, since they overlap with the ranges of typical phonon energies and wave vectors. During the process of scattering of neutrons from the sample, the total energy and momentum are conserved. Neutrons may create or destroy phonons and thus lose or gain energy and momentum. Energy of a phonon is $E(\mathbf{q}) = \hbar\omega(\mathbf{q})$ and its momentum is $\mathbf{p} = \hbar\mathbf{q}$. In INS, by observing the change in energy and momentum of a neutron, the wave vector \mathbf{q} (or momentum transfer) and the frequency $\omega(\mathbf{q})$ (and hence energy of the phonon) can be determined simultaneously. By repeating the experiment under varied conditions, the dispersion relation (or the phonon density of states) may be mapped.

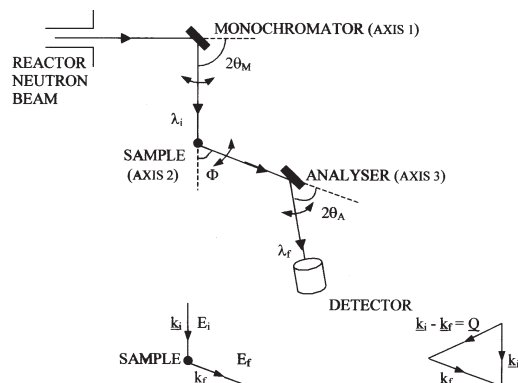


Fig. 3 Schematic diagram of the Triple Axis Spectrometer at Dhruva reactor, Trombay.

In a typical experiment [3], a monochromatic beam of neutrons is incident on the sample and the scattered neutrons at different momentum transfers are analyzed with respect to their energy. At thermal neutron reactors, such experiments are usually carried out using a 'Triple Axis Spectrometer' (TAS). Figs. 2 & 3 show a photograph and a schematic diagram of the TAS at Dhruva reactor, Trombay, respectively. This spectrometer has three axes of rotation – the monochromator axis, the sample axis and the analyzer axis. The monochromator and analyzer are single crystals (usually of copper, Pyrolytic Graphite or silicon) which help in monochromatizing the polychromatic neutron beam emerging from the reactor, and in analyzing the scattered beam from the sample, respectively. Both monochromatizing and analyzing are carried out through an application of Bragg's law of diffraction. The wave vectors are decided by suitably aligning the sample with respect to the incident and scattered neutron beams. The spectrometer is fully automated with data collection and movements of the various arms are controlled through a computer.

There are alternative techniques, such as measuring neutron energies by the neutron time of flight, which is usually a preferred method on pulsed spallation neutron sources. Neutron energy changes can also be measured by the neutron spin-echo technique, which makes use of the precession of the neutron spin in a magnetic field. We shall not refer to these methods in more detail here.

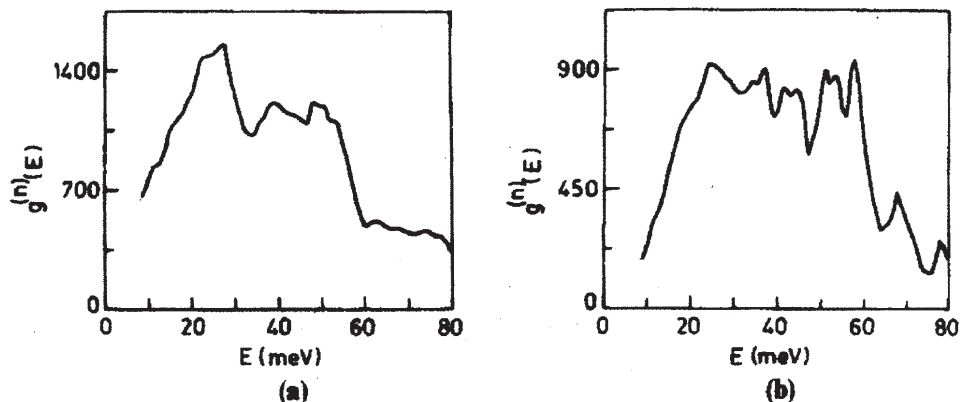


Fig. 4 Neutron-weighted phonon density of states $g^{(n)}(E)$ of two high T_c superconductors (a) $Tl_2CaBa_2Cu_2O_8$, and (b) $YBa_2Cu_3O_7$.

Some Results

Here we describe some important examples of inelastic neutron scattering studies carried out at Dhruva reactor at Trombay.

High Temperature Superconductors

Lattice dynamical investigations are of importance in understanding the interatomic interactions and the role of phonons in superconductivity. We had compared the phonon spectra (Fig. 4) in $Tl_2CaBa_2Cu_2O_8$ (Tl-2122, $T_c=107$ K) and $YBa_2Cu_3O_7$ (Y-123, $T_c=92$ K), obtained through coherent inelastic neutron scattering [4]. The data in Tl-2122 represent the first reported phonon spectra in this material. The density of phonon states in Tl-2122 is enhanced at low energies of 6-17 meV and reduced at 40-70 meV as compared to that in Y-123.

Hydrogen in Metals

Intermetallic hydrides are interesting because of the possibility of using these materials as hydrogen storage media. The intermetallic compound Zr_2Ni can absorb a large amount of hydrogen. The structure of Zr_2Ni permits four types of tetrahedral interstitial sites for H-atom occupancy. Two of the sites have four Zr atoms at the vertices of the tetrahedron, one site has three Zr and one Ni while the remaining one site has two Zr and two Ni atoms at the tetrahedral vertices. Hydrogen at each site should be characterized by a distinct

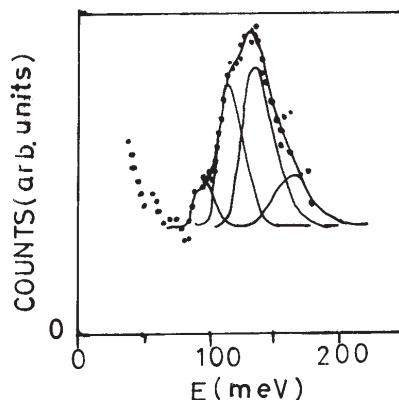


Fig. 5 A plot of neutron counts against energy transfer E for $Zr_2NiH_{4.6}$. The neutron-weighted phonon density of states is derived from this data. This allows us to get information about the local environment of the hydrogen atoms in this intermetallic system.

vibrational spectrum. We performed inelastic neutron scattering studies on $Zr_2NiH_{4.6}$ [5] to determine the vibrational frequencies and hydrogen site occupancies. The phonon spectrum in the energy range 35 to 175 meV consists of a broad structure (Fig. 5), which could be fitted to four Gaussians centred at 95, 112, 134, and 161 meV, respectively. Since hydrogen is most tightly bound in the sites having four Zr atoms at the vertices, the frequency of 161 meV has been assigned to hydrogen in this site. The other three frequencies have been attributed to H

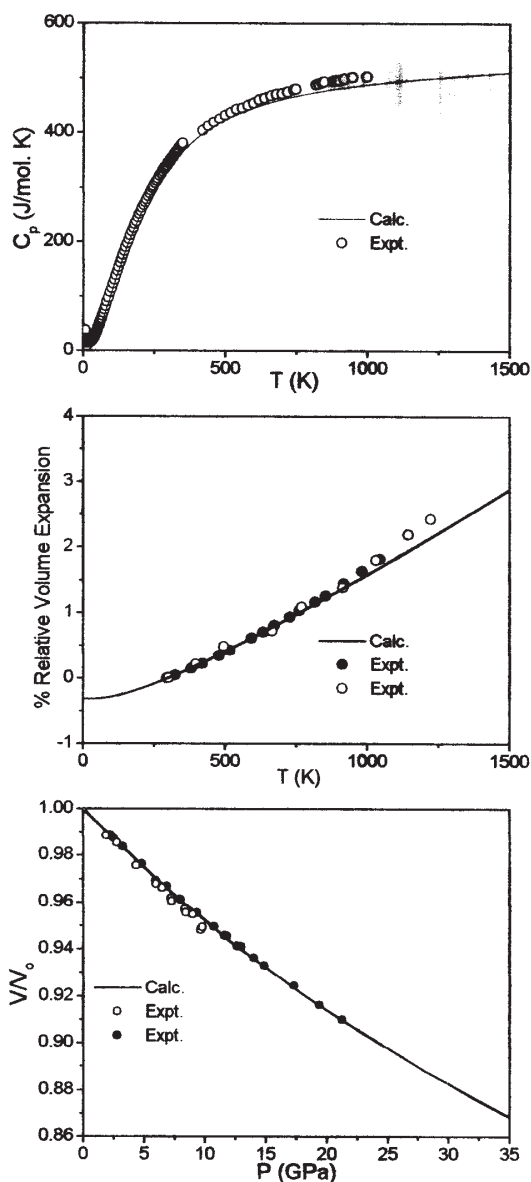


Fig. 6 Comparison of the calculated (full line) specific heat, thermal expansion and equation of state of the garnet mineral almandine $\text{Fe}_3\text{Al}_2\text{Si}_3\text{O}_{12}$ with available experimental data (symbols). The references for the experimental data are available in Ref. [8].

in the site with three Zr and one Ni at the vertices. The frequencies at 112 and 134 meV can be understood to arise from vibrations parallel to the plane containing three Zr and that at 95 meV due to vibration in a perpendicular plane. Similar studies on hydrogen in solids give an idea of the environment of hydrogen atoms in the solid.

Minerals

A study of the thermodynamic properties of geophysically important minerals that form part of the earth is essential to give an insight into many aspects of the evolution of our planet. Such a study would consist of experiments at very high temperatures and pressure, which are feasible in very few laboratories. In such cases, theoretical predictions of these properties are very invaluable. We have employed a combination of experimental neutron scattering studies at Dhruva and elsewhere, and theoretical lattice dynamical calculations to understand the vibrational and thermodynamic properties of a number of silicate minerals [6] like forsterite (Mg_2SiO_4), fayalite (Fe_2SiO_4), enstatite ($\text{Mg}_2\text{Si}_2\text{O}_6$) polymorphs, silicate perovskite (MgSiO_3), Al_2SiO_5 polymorphs [7], garnets ($\text{M}_3\text{Al}_2\text{Si}_3\text{O}_{12}$) [8] and zircon (ZrSiO_4) [9]. As examples, we present some of our results on zircon and the garnet mineral almandine ($\text{M}=\text{Fe}$).

In zircon, the phonon dispersion relation was first measured at Dhruva reactor at energies below 32 meV and then at higher energies up to 70 meV at the ISIS pulsed neutron source [9]. The phonon dispersion relation data on zircon (Fig. 1) may be seen as a rare example of extensive measurements up to such high energies on minerals of geophysical interest.

In Fig. 6, we show the thermodynamic properties of almandine. The calculations reproduce the features in the experimental data very well. Almandine is known to exhibit antiferromagnetic ordering below $T_N=8.7$ K; the measured low-temperature specific heat shows a corresponding anomaly.

Magnetic Materials

In Kondo lattice compounds containing cerium, the two competing processes of interatomic RKKY interaction and single site Kondo interaction

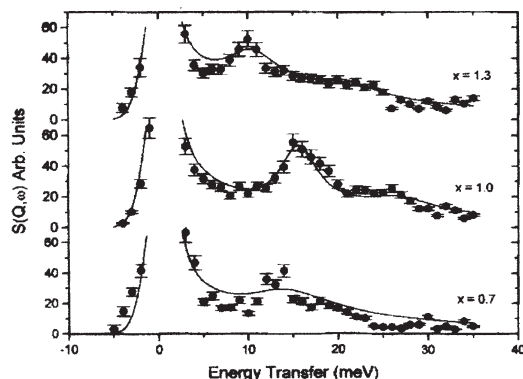


Fig. 7 Magnetic spectral response of $\text{CeSi}_{2-x}\text{Ga}_x$. The solid curves show the least squares fit to the data. The inelastic peaks are a direct measure of the crystalline electric field levels in these compounds.

exist. Dominance of one over the other leads to either magnetically ordered or a non-magnetic ground state. Over the years, many cerium systems have been studied to understand the competition and various types of ground states these materials exhibit. In addition to this competition, for nearly all cerium Kondo systems, the crystalline electric field (CEF) plays an important role in determining the ground state of the system. Inelastic neutron scattering is the most direct method of determining the CEF splitting of the ground state in such systems.

We studied [10] polycrystalline samples of $\text{CeSi}_{2-x}\text{Ga}_x$ ($0.7 \leq x \leq 1.3$), using inelastic neutron scattering. Fig. 7 shows the magnetic spectral response of the three compounds at 12 K obtained after correction for the contributions from phonons. Also, from the thermal evolution of the quasielastic linewidth, the characteristic temperatures T_K and T_{RKKY} as well as the coupling constants (characterizing the hybridization strength between the conduction electrons and the Ce 4f electrons) have been estimated. We have seen that the coupling constant increases with increasing Ga concentration and the $x=0.7$ compound is a magnetic 4f metal whereas the other two compounds are magnetic concentrated Kondo systems.

Conclusions

Inelastic neutron scattering can be employed to determine phonon dispersion relations in single crystal specimens. On the other hand, polycrystalline samples may be used to obtain the neutron weighted phonon density of states. Presence of magnetic ions entails magnetic contributions to the spectrum, either in the form of spin waves or as crystalline electric field levels. For inelastic neutron scattering experiments, thermal neutron reactors as well as accelerator based pulsed neutron sources are used. The planning of INS experiments and the analysis of the results from such experiments are extremely facilitated if model lattice dynamics calculations are available. Recently, inelastic X-ray scattering has been carried out using synchrotrons to measure PDRs of some materials [11], though the energy resolution achieved is not as good as with neutrons.

References

1. M. Born and K. Huang, Dynamical theory of crystal lattices (Clarendon, Oxford), 1954.
2. G. Venkataraman, L. Feldkamp and V.C. Sahni, Dynamics of perfect crystals, (MIT press, Boston), 1975.
3. P. A. Egelstaff (ed.), Thermal Neutron scattering, (Academic Press, New York), 1965.
4. S.L. Chaplot *et al.*, Bull. Mat. Sci., **14** (1991) 603; Physica, **B 174** (1991) 378; Phys. Rev., **B45** (1992) 4885.
5. R. Mittal *et al.*, Solid State Physics (India), **38C** (1995) 92
6. K.R. Rao *et al.*, Science, **236** (1987) 64; S.L. Chaplot *et al.*, Euro. J. Miner., **14** (2002) 291
7. Mala N. Rao *et al.*, Sol. State Comm., **121** (2002) 333.
8. R. Mittal *et al.*, Phys. Rev., **B.64** (2001) 94302-1-9.
9. R. Mittal *et al.*, Phys. Rev., **B. 62** (2000) 12089.
10. K.R. Priolkar *et al.*, J. Magn. Magn. Mat., **185** (1998) 375.
11. R. Lubbers *et al.*, Science, **287** (2000) 1250.

Neutron Quasi-elastic Scattering in Material Science



Shri S. Mitra joined Solid State Physics Division, BARC in 1994 after completing his M.Sc. from University of North Bengal. Since joining, he is working in neutron scattering group and is involved in neutron scattering instrumentation at DHRUVA. His field of research includes the study of molecular motions in condensed matter using quasielastic neutron scattering technique.

Dr. Ramaprosad Mukhopadhyay joined 23rd batch of BARC Training School in 1979 after completing his M.Sc. (Physics) from Kalyani University. Since joining he is associated with neutron scattering group of Solid State Physics Division. Topic of his Ph.D. thesis was "Phase Transitions and Rotational Dynamics in Molecular Solids". He has worked as visiting scientist at ISIS facility, Rutherford Appleton Laboratory, UK during 1990-91, visiting professor at Depto de Fisica de Materiales, Universidad del Pais Vasco, Spain during 1996-97 and at KENS, KEK, Japan in 2000. He has about 55 papers to his credit in international journals and about 70 papers in International and national conferences.



Neutron scattering is a powerful experimental tool for studying the translational and rotational motions of atoms and molecules in condensed matter [1,2]. It is particularly well suited for studying the dynamics of hydrogenous system because of its large scattering cross section with hydrogen. Inelastic neutron scattering experiments where a finite energy is exchanged between neutron and the system are used either for studying the periodic motions like molecular vibrations or for studying the thermally activated stochastic molecular motions which show up as broadened elastic line. In an inelastic neutron scattering experiment, the scattered intensity is analysed as a function of both the energy transfer $\hbar\omega$ and wave-vector transfer $Q = \left(\frac{4\pi \sin \theta}{\lambda} \right)$.

2θ is the scattering angle. This is illustrated in Fig. 1 where intensity is plotted against energy transfer, $\hbar\omega$ at a suitable Q value. In the case of an ideal simple harmonic oscillator, one can expect an elastic line

(delta function) at zero energy transfer and an inelastic peak (delta function) at $\omega = \omega_0$. However, in a real neutron scattering experiment, these lines will be broadened due to finite instrumental resolution. Moreover, in systems where there are stochastic motions, elastic line will be further broadened due to the random nature of the molecular motions and this broadening is known as quasielastic broadening. Quasi-elastic neutron scattering (QENS) technique

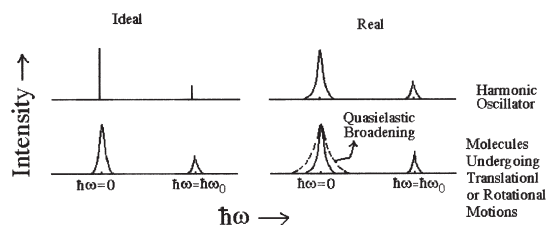


Fig. 1 Scattering from different type of materials.

Shri S. Mitra and Dr. R. Mukhopadhyay, Solid State Physics Division, Bhabha Atomic Research Centre, Trombay, Mumbai 400 085,
Email: smitra@apsara.barc.ernet.in, mukhop@apsara.barc.ernet.in



Fig. 2(a) Photograph of the QENS spectrometer installed at beam tube TT1004 at DHRUVA

thus involves the measurement of spectra within a small energy transfer range (≤ 2 meV) centered at zero energy transfer. The time-scale of the dynamical motion ($\sim 10^{-9}$ - 10^{-13} sec), its geometry as well as the nature of the hindering potential can all be obtained from QENS experiments. Such experiments are carried out using either a triple axis or a time-of-flight spectrometer [1]. The quasielastic spectrometer at DHRUVA designed by modifying the conventional triple axis spectrometer facilitates higher throughput. The scattered neutrons are energy selected by a large analyser crystal and detected by a position sensitive detector. Thus, an energy scale is set up along the detector and the spectrometer provides energy spectrum for one instrumental configuration. This type of spectrometer is known as MARX (Multi Angle Reflecting X-tal) spectrometer, first built in Risö, Denmark [3]. MARX spectrometer is a well-suited instrument for neutron quasielastic scattering experiments [4,5] in a medium flux reactor. Photograph of the QENS spectrometer located at DHRUVA is shown in Fig. 2(a). The schematic diagram of the spectrometer is given in Fig. 2(b). Details on this spectrometer are given in Ref. 6. The instrumental resolution is obtained from the measured FWHM of the spectrum of a vanadium sample. In the present configuration, the instrument has an energy resolution of 200 μ eV for neutrons of incident energy 5 meV and the wave-vector transfer (Q) range covered by this

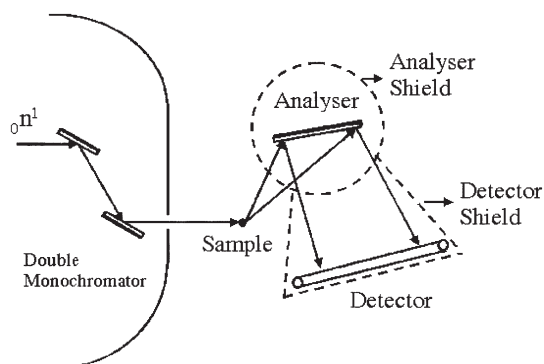


Fig. 2(b) Schematic of the QENS spectrometer in MARX mode

spectrometer is 0.67 - 1.8 \AA^{-1} . Some basic principles of QENS technique will be discussed below.

Principles

In an inelastic neutron scattering experiment, the quantity measured is the double differential scattering cross section which represents the probability that a neutron is scattered with energy change $\hbar\omega$ into the solid angle $d\Omega$ [1]. For hydrogenous systems, it is proportional to $\frac{k}{k_0} [\sigma_{\text{inc}} S_{\text{inc}}(Q, \omega)]$. $S(Q, \omega)$ is known as the scattering law and the subscripts inc denotes the incoherent scattering components. \mathbf{k} and \mathbf{k}_0 are the final and initial wave-vectors. $\mathbf{Q} = \mathbf{k} - \mathbf{k}_0$ is the wave-vector transfer and $\hbar\omega = E - E_0$ is the energy transfer. Incoherent scattering involves the same nucleus at two successive times, so there is no interference effects between the amplitudes scattered by different nuclei. Whereas in coherent scattering, the total observed intensity results from the sum of the different intensities scattered from the individual nuclei. For quasielastic events, the incoherent scattering law for rotational motion of a molecule can be approximated as addition of an elastic and a quasielastic components. Quasielastic part is a Lorentzian function, where the half width at half-maximum (HWHM) of the Lorentzian function is inversely proportional to the time scale of the rotational motion. It is convenient to analyse the data in terms of elastic incoherent structure factor (EISF)

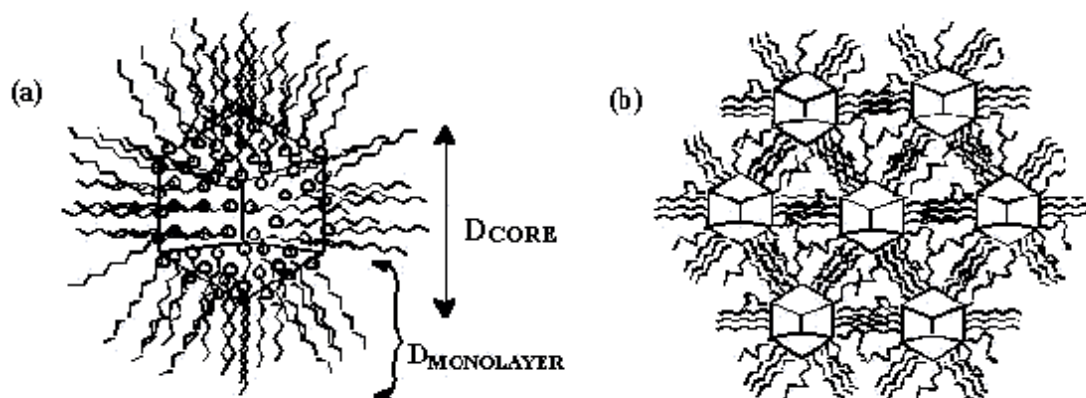


Fig. 3 (a) Schematic of a monolayer protected cluster (MPC) (b) Schematic of the superlattice assembly of MPCs.

which can be defined [1] as the fraction of elastic intensity out of the total intensity in $S(Q, \omega)$ and provides information about the geometry of the molecular motions.

In the case of translational motion, incoherent scattering law, $S_{inc}^T(Q, \omega)$, consists only a Lorentzian [1]. In a system, where both translation and rotational motion exist simultaneously, total scattering law can be written as $S_{inc}^{Tot}(Q, \omega) = S_{inc}^T(Q, \omega) \otimes S_{inc}^R(Q, \omega)$. Here \otimes represents the convolution product. However, to compare with the experimental spectrum, the theoretical scattering law has to be convoluted with the instrumental resolution function.

Rotational Motions

We shall give only one example of jump rotational motions among N equivalent sites on a circle that are studied using the QENS spectrometer. Other examples of rotational motions studied using the same spectrometer can be found in Ref. 7. In jump rotational model among N equivalent sites on a circle, it is assumed that the motion is specified by jumps of certain angle and a residence time τ , taken by the particle at a particular site. It is also assumed that the jump time is very much shorter than the time τ i.e., jumps are instantaneous. For a particle, which is allowed to perform a random walk among N

equivalent sites on a circle, in which jumps are restricted to neighboring sites only, the expression of the scattering law for a powder sample is a combination of an elastic component and a series of Lorentzians. HWHMs of the Lorentzians will be inversely proportional to the residence time τ [8].

Akyl Chain Dynamics in Monolayer Protected Clusters (MPCs)

Monolayer protected metal clusters (MPCs) are the monolayers of surfactants formed spontaneously by self assembly of the long-chain alkyl thiol molecules on a nano-sized metal-core. Fig. 3 represents the (a) schematic of a MPC and (b) superlattice assembly of MPCs. Dynamics of alkyl chains in an isolated MPC, $Au_{C_{18}}$ ($C_n = n$ carbon n -alkanethiolate), and a superlattice of Ag_{C_8} MPC have been investigated for the first time by QENS technique in the temperature range of 300-400 K [9]. The results have been compared with a layered silver thiolate, $Ag_{C_{12}}$, chosen to represent a planar two-dimensional monolayer. In the cluster superlattice, QENS broadening was observed even at room temperature and below the chain melting temperature ($T_{cm}=333K$) whereas for the isolated cluster it was seen only above T_{cm} . In the layered silver thiolate, it was observed above the melting point. The experimentally extracted EISF at different temperatures are shown in Fig. 4 (a) for

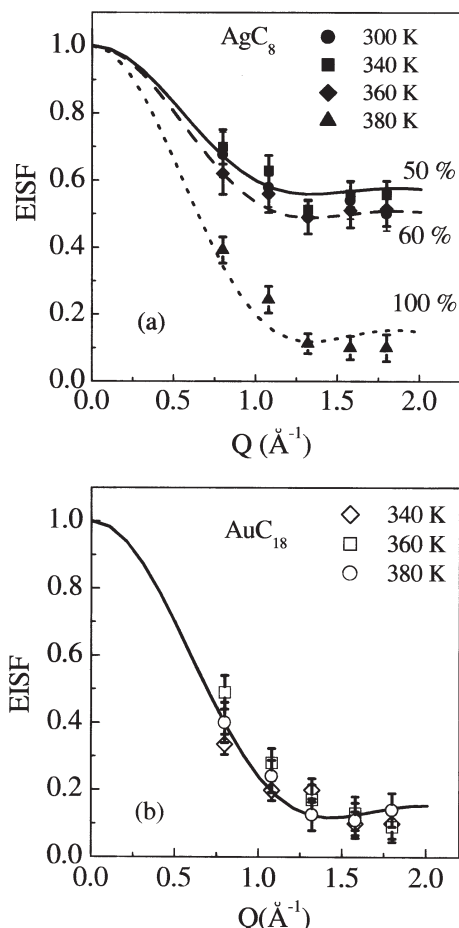


Fig. 4 (a) Variation of EISF with Q for Ag-OT at different temperatures. The solid lines correspond to uniaxial rotational diffusion about the chain axis (b) Variation of EISF with Q for Au-ODT at different temperatures. The solid line corresponds to the uniaxial rotational diffusion about the chain axis

AgC_8 . Solid lines in Fig. 4 (a) are the fitted ones with proportion of alkyl chains participating in the dynamics taken as a parameter with a 6-fold jump diffusion model. AgC_8 forms a superlattice structure and this is by virtue of the chain interdigitation among the neighboring clusters. The fact that 50% of the protons participating in the dynamics in the temperature range 300–360 K is in accordance with the structural conformation. However at 380 K, data

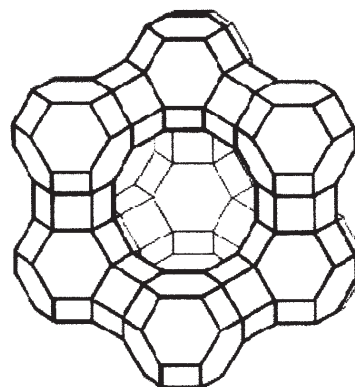


Fig. 5 Schematic of Na-Y zeolite.

show that almost all the chains are contributing to the dynamics. This being closer to the melting point, the chains, which were earlier held fixed due to interdigitation, now have enough energy to be dynamic.

In Fig. 4(b), variation of EISF is shown at different temperatures for AuC_{18} . It can be seen that above chain melting temperature all the chains are participating in the dynamics which is in contrast with the findings on superlattice AgC_8 . In case of layered thiolate AgC_{12} , data also can be described with a 6-fold jump diffusion model with 100% dynamic chains.

Translational Motions

We shall give one example where translational diffusion of a molecule is studied using the QENS spectrometer at DHRUVA.

Propane in Na-Y Zeolite

Na-Y zeolite structure is made up of a network of tetrahedrally connected pores (α -cages) of diameter ~ 11.8 Å. The pores are interconnected through windows of diameter ~ 8 Å. Schematic of Na-Y zeolite is shown in Fig. 5. Propane ('size' ~ 6 Å) coverage of 4.5 molecules per zeolitic supercage was used for the experiment. In this case, only translational motion of propane molecule is observed to contribute to the present experiment. The analysis of the experimental data was attempted using several available models of the dynamics and it is found that a model of $S(Q, \omega)$ proposed by Hall and

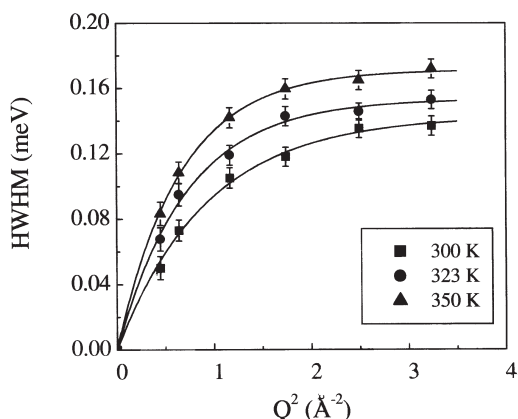


Fig. 6 Variation of HWHM of the quasielastic component with Q for propane in Na-Y zeolite. Solid lines are the fit to the data assuming Hall & Ross model (see text)

Ross is adequate and consistent with the experimental data. In this model, Hall and Ross [10] assumed that for a residence time τ , an atom remains on a given site, vibrating about a center of equilibrium, building up a thermal cloud. After this time, the atom moves rapidly to another site, in a negligible jump time. It was also assumed that the jump lengths are not fixed but are Gaussian distributed. Scattering law in this case is a Lorentzian with HWHM

$$\Gamma(Q) = \frac{1}{\tau} \left[1 - \exp \left(-\frac{Q^2 \langle \ell^2 \rangle}{6} \right) \right] \quad (1)$$

here, τ is the residence time and $\langle \ell^2 \rangle^{0.5}$ is the root mean square jump length. Diffusion constant, D can be calculated from Einstein's relation. Fig. 6 shows the variation of HWHM of the quasielastic line with Q^2 . Solid lines are the fit with Hall-Ross Model (Eq. 1). Residence time τ , root mean square jump length, $\langle \ell^2 \rangle^{0.5}$ and diffusion constant, D , are obtained at various temperatures in the range 300-350 K [11].

To conclude, quasielastic spectrometer in DHRUVA, Trombay has been operating successfully for last several years. The spectrometer

is in use at present to study molecular dynamics in different systems, e.g., dynamics of different hydrocarbons in cages like zeolite, molecular reorientations of alkyl chains in monolayer protected clusters (MPC), molecular reorientations in various organic and inorganic salts in different solid state environments, etc.

Acknowledgement

We are thankful to all our collaborators for their active help in pursuing the various studies reported here. We would also like to thank Dr. M. Ramanadham and Dr. S.K. Sikka for their constant support and encouragement.

References

1. M. Bée, Quasielastic Neutron Scattering (Adam-Hilger, Bristol, 1988).
2. W. Press, Single Particle Rotations in Molecular Crystals (Springer, Berlin, 1981).
3. J.K. Kjems and P.A. Reynolds, Inel. Scatt. Neut., (IAEA, Vienna, 1972) p. 733.
4. R. Mukhopadhyay, S. Mitra, I. Tsukushi and S. Ikeda, Chem. Phys. Lett., **341** (2001) 45.
5. S. Mitra, R. Mukhopadhyay, I. Tsukushi and S. Ikeda, J. Phys.: Condens. Matter, **13** (2001) 8455.
6. R. Mukhopadhyay, S. Mitra, S.K. Paranjpe and B.A. Dasannacharya, Nucl. Inst. Meth., **A 474** (2001) 55.
7. A.K. Tripathi, A. Sahasrabudhe, S. Mitra, R. Mukhopadhyay, N.M. Gupta and V.B. Kartha, Phys. Chem. Chem. Phys., **3** (2001) 4449; S. Mitra, R. Mukhopadhyay, A.K. Tripathy and N.M. Gupta, Appl. Phys. A (in press).
8. J.D. Barnes, J. Chem. Phys., **58** (1973) 5193.
9. S. Mitra, Binoj Nair, T. Pradeep, P.S. Goyal and R. Mukhopadhyay, J. Phys. Chem. **B**, **106** (2002) 3960.
10. P.L. Hall and D.K. Ross, Mol. Phys., **42** (1981) 673.
11. S. Mitra, A. Sayeed, R. Mukhopadhyay, S. Yashonath and S.L. Chaplot, Appl. Phys. A (in press).

Neutron Reflectometry: An Ideal Tool for Thin Film Characterization



Dr. Saibal Basu received his M.Sc degree in Solid State Physics from IIT Kharagpur. He joined one year orientation course in physics in BARC training school during 1982-83 and topped the list of physics trainees. On completion of the training he joined the neutron scattering group of Solid State Physics Division (then Nuclear Physics Division). He has been intimately involved with neutron instrumentation program at Dhruva. He carried out experiments on Neutron Reflectometry as a part of his Ph.D. thesis. During the year 2001 he worked as a technical officer in International Atomic Energy Agency in Vienna, taking care of research reactor utilization programs in the Member States of the Agency. At the moment he is commissioning a neutron reflectometer in Dhruva guide tube laboratory.

Introduction

All of us are familiar with the reflection of light from various surfaces surrounding us. Reflection of light from a surface depends on the refractive index of the medium with respect to air. It is also our daily experience that the image, thus formed, bears signature of the quality of the surface that reflects the light. These observations underpin the fact that by observing reflection of waves from a surface we can study properties of the surface. Optical waves have wavelengths in the range of 3000 Å to 7000 Å, which dictates the resolution in length scale, over which the surface properties may be determined. Thermal and subthermal neutrons have wavelengths in the range of several Å (typical energy ~ few meV to 100 meV) and by measuring reflectivity of thermal neutrons from thin film surfaces, we can obtain various structural information about the surface and interfaces of the film with resolution in the range of Å. As early as 1946, Fermi and Zinn [1] observed the refraction of neutron waves at air- film interface. This phenomenon was extensively used by them to evaluate coherent scattering length of materials for thermal neutrons. Coherent scattering length is the nuclear spin and isotope averaged scattering length of an element. The technique of neutron reflectometry for characterizing thin films and multilayers was reinvented in 1980's as a surface characterization tool. Since then there have been

rapid development in the technique and presently all the major neutron sources in the world possess at least one neutron reflectometer. It is the simplicity of the experimental technique and the rich information content regarding structure of thin films, that has made neutron reflectometry an important and popular tool [2,3]. The neutron is a spin $\frac{1}{2}$ particle and it possesses a magnetic moment of -1.913 nuclear magnetons. Polarized neutron reflectometry is ideally suited for determining structure of magnetic thin films. The contrast in coherent scattering lengths of hydrogen and deuterium makes neutron reflectometry an ideal tool for studying polymer films and Langmuir-Blodgett films. Popularity of this technique also has its roots in the development of precision thin film fabrication techniques. In the present article, thin films of typical thickness of few thousand Å will be discussed. Such films are usually fabricated on a substrate by means of some deposition technique.

Thin films have started playing very important role in many areas of advanced technology. The wide range of applications include semiconductor superlattices in device applications, thin magnetic films for magnetic and magneto-optic recording devices, Langmuir-Blodgett films, liquid crystals and liquid surfaces. Knowledge of the structure of thin films is essential towards understanding their

Dr. Saibal Basu, Solid State Physics Division, Bhabha Atomic Research Centre, Mumbai 400 085
E-mail: sbasu@apsara.barc.ernet.in

physical properties. The perfection of thin film deposition systems have gone up drastically in the last two decades. Today it is possible to grow films at atomic resolution, using molecular beam epitaxy. Characterization of these films also requires probes with similar resolutions. There are several probes to study surfaces of thin films. Scanning Tunneling Microscopy and Atom Force Microscopy are two such widely used probes. Whereas these probes have the advantage of providing direct picture of the surface, they suffer from the inadequacy of not being able to probe deep inside the sample. Also the information available with such microscopes represents a small area of the sample surface (\sim micrometres). On the contrary, neutron reflectivity measurement is a non-destructive technique, reaching down to deeply buried interfaces and also provides information with accuracy in the range of \AA . The information is averaged over the sample surface area of about few cms, thus bridging two wide-apart length-scales. These advantages make neutron reflectometry an ideal probe for characterizing thin films and multilayers.

Experimental Technique

The refractive index 'n' of a material for neutrons can be calculated from the optical theory of refraction, which gives $n = 1 - \delta$ [4]. The parameter δ is proportional to the density of the refracting medium, its coherent scattering length for neutrons and square of the wavelength λ of the incident neutrons. The value of $\delta \sim 10^{-5}$ for most of the materials. Since the refractive indices of neutrons for most of the materials are smaller than unity, it indicates that there will be total external reflection at an air-medium interface (light coming from a denser media undergoes total internal reflection at the interface, e.g. light coming from water to air). Also due to the fact that refractive index for neutrons is marginally smaller than unity, total reflection of thermal or sub-thermal neutrons ($\lambda \sim 2 \text{ \AA}$) takes place at near grazing incidence on the surface, typically in the range of half of a degree. Neutron reflectivity experiments are carried out in the angular range of 0-2 degrees and in this sense can be compared with Small Angle Neutron Scattering (see the article by Mazumder et. al. in this issue). We measure the reflected intensity as a function of momentum transfer $Q = (4\pi/\lambda)\sin \theta$, θ is the angle of incidence

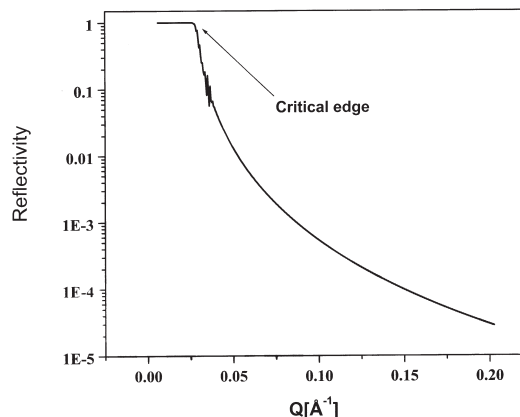


Fig. 1 Reflectivity of an ideally flat nickel surface

on the surface]. The reflectivity of neutrons of wavelength 4 \AA as a function of Q for an ideal nickel film of infinite thickness is shown in Fig. 1. One can see that the reflectivity is unity below a critical wavevector (angle) and it is sharply falling beyond the critical edge ($\propto 1/Q^4$). The rapid fall in intensity beyond the critical edge makes neutron reflectivity extremely dependent on neutron flux and adds to the difficulty of the experiment.

The scan in Q space can be accomplished in several ways, depending on the type of the neutron source. Usually in a reactor we tend to use monochromatic neutron beams in angle dispersive mode. For reflectometry experiments one needs to prepare a monochromatic neutron beam of very small angular divergence (few arcminutes). This highly collimated beam of neutrons is reflected from the sample surface at grazing incidence. The sample and the detector rotate in θ - 2θ coupled mode respectively, to collect data in a range of Q values typically from 0.003 \AA^{-1} to 0.2 \AA^{-1} . Fig. 2 shows the schematic of such a set up, which we used in Dhruva, Trombay, to measure reflectivity profile of thin films. Now-a-days intense pulsed neutron sources are available at several research centres in the world. For a pulsed beam one records the Q scan by reflecting a polychromatic neutron beam from a sample kept at a fixed angle with respect to the incident beam. This amounts to varying λ in the expression for Q for a fixed θ . Because of pulsed nature of the source, the wavelength is analyzed by Time-of-Flight technique (TOF) in such a set up.

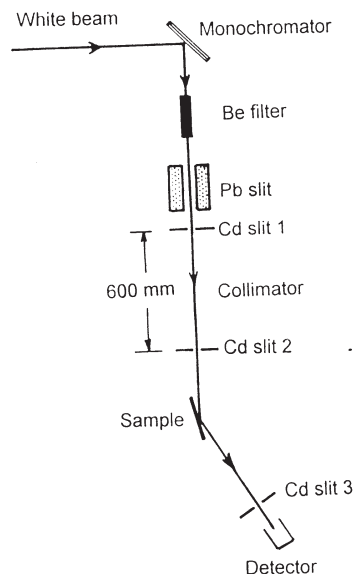


Fig. 2 Schematic of the neutron reflectometer set up used in Dhruva

There are two possible choices for the sample geometry. In case of a vertical sample geometry, the plane of reflection is horizontal. In this case only solid surfaces and interfaces can be studied. In a recently installed reflectometer in Dhruva, Trombay we will be able to study samples in vertical geometry using a position sensitive neutron detector. In the case of horizontal sample surface, the plane of reflection is a vertical plane. Horizontal sample geometry facilitates study of liquid surfaces. For horizontal samples, in case of angle dispersive scan, the beam has to be tipped down onto the sample and the sample needs to be moved vertically for the scan, along with the detector rotating in the vertical plane. This requires high precision coupled movement of several components that adds to mechanical complexity of the system. Alternatively by using a polychromatic beam one can scan the Q space in a fixed sample geometry. The CRISP reflectometer in the pulsed, spallation neutron source ISIS at Rutherford Appleton Laboratory, UK allows one to study horizontal samples in TOF mode [5].

The Structural Information

The reflectivity pattern from a thin film or a multilayer is sensitive to several structural

parameters of the thin film that we try to extract from a reflectivity pattern. The critical edge (angle/ Q) of a reflectivity pattern strongly depends on the product of density of the medium and the coherent scattering length. The absorption coefficient of the medium tends to round off intensity at the critical edge. Specular reflectivity of unpolarized neutrons from a thin film is routinely used to obtain chemical density profile as a function of depth. For an angle of incidence above the critical angle, the neutron beam will strongly penetrate the film. In case of a film of finite thickness there will be reflection at the air-film interface and at the film-substrate interface. The interference between these reflected beams causes oscillations in intensity beyond the critical angle, known as Kiessig fringes. One can see these oscillations in the reflectivity patterns from Ni films of thicknesses 200 Å and 210 Å as shown in curves (a) and (b) respectively in Fig. 3. The change in the period of oscillation between the reflectivity curves (a) and (b) is due to a small change of 10 in thickness of the film. From the periodicity of these oscillations in Q space, one can calculate back the thickness of the film. Interface roughness causes damping of these Kiessig oscillations. To extract the structural parameters like density, thickness, interface roughness, of the thin film we start with a structural model of the film with these parameters as variables. For a film with a given set of structural parameters, one can generate the reflectivity pattern in Q space, using several formalisms. The model is improved through χ^2 minimization, till we achieve reasonable fit between the generated pattern and the experimentally measured reflectivity pattern. To demonstrate the sensitivity of a reflectivity pattern upon the physical parameters, we show in Fig. 4 a generated reflectivity pattern from 20 bilayers of nickel and copper, each bilayer consisting of 20 Å Ni and 22 Å Cu. The Kiessig fringes give the total thickness of the film and the Bragg peak at 0.15 Å^{-1} gives the bilayer thickness of 42 Å. Curve (a) is for zero interfacial roughness and curve (b) is for average interfacial roughness of 1 Å. A large change in the pattern occurs due to the introduction of an interfacial roughness as small as 1 Å! One can obtain all the above parameters of this multilayer film with accuracies in the range of a few to fractions of an Å, by measuring reflectivity pattern from such a film. This example demonstrates that since neutrons

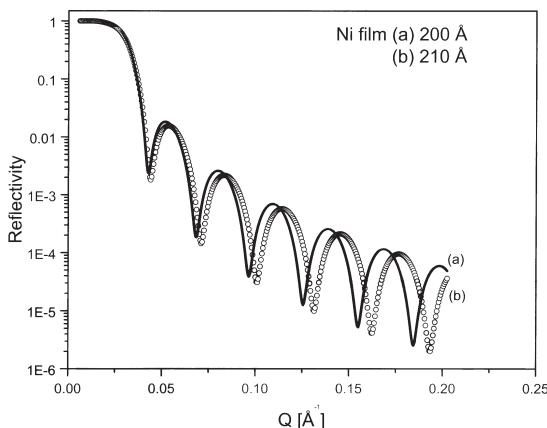


Fig. 3 Reflectivity of 200 and 210 thick nickel films

penetrate strongly in any medium the neutron reflectivity pattern is sensitive to buried layers and interfaces. Also it may be mentioned here that the bilayer pairs in the above example, Cu and Ni have almost no contrast for X-rays, but the strength of the Bragg peak in the neutron reflectivity pattern, shows that they have sufficient contrast for neutrons. We have successfully used this technique for microscopic characterization of several thin film samples in our set up at Dhruva. We could estimate the level of alloying at the Ni/Cu interface in Ni/Cu multilayer film [6]. We could also study the level of oxidation in a Ni-Ti multilayer film [7] and surface oxide layer on Si wafer surface.

Refractive index of polarized neutrons depend on the magnetization density and its direction for magnetic thin films. By observing reflectivity pattern of polarized neutron beam from a magnetic sample, magnetized along an axis, one can generate magnetization density profile as a function of depth with a resolution of few Å. This information is of paramount interest for understanding properties of magnetic films of technical and fundamental interest.

Conclusion

In this short article an attempt has been made to show the importance of neutron reflectometry as a non-destructive tool for characterizing structure of thin films. With the aid of a few examples it has been demonstrated that the technique is almost

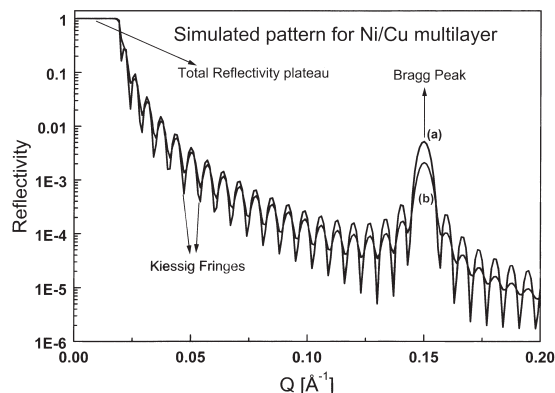


Fig. 4 Reflectivity profile of 20 bilayers of nickel and copper with 20 Ni and 22 Cu in each bilayer

unmatched for obtaining structural parameters with resolution in the range of Å. This technique is of special significance for obtaining structural information of magnetic and polymer thin films. The deep penetrability of neutrons in most of the materials also makes neutron reflectometry a unique tool for obtaining structural information of buried interfaces and layers.

References

1. E.Fermi and W.Zinn, Phys. Rev., **70** (1946) 103.
2. Springer Proceedings in Physics, Surface x-ray and neutron scattering 61, Eds. H. Zabel and I.K.Robinson (1992).
3. Proceedings of the fourth International Conference on Surface x-ray and neutron scattering (Lake Geneva, 1995), Physics B 221, 1996, Eds. G.P.Felcher and H.You.
4. J Lekner in Theory of Reflection of Electromagnetic and Particle Waves, (Martinus Nijhoff Publishers, 1987).
5. ISIS user guide, Experimental Facilities, Ed. Brian Boland and Sarah Whapham (1992).
6. Mahesh Vedpathak, Saibal Basu and S.K.Kulkarni, Appl. Surf. Sci., **115** (1997) 311.
7. Mahesh Vedpathak, Saibal Basu, Shubha Gokhale and S.K.Kulkarni, Thin Solid Films, **335** (1998) 13.

Neutron Interferometry and Optics



Dr. A.G. Wagh joined BARC in 1972 after topping the 15th batch of Physics Trainees in the BARC Training School. He was awarded the International Atomic Energy Agency's Fellowship for the period 1976-78 in University of Aarhus, Denmark. He acquired the Ph.D. (Physics) degree of the University of Mumbai in 1983. Dr. Wagh has published a large number of papers, invited review articles and an invited book review in international scientific journals. He serves as a referee for papers submitted to prestigious international journals. A few of his scientific achievements have been touched upon in this overview.

Dr. Veer Chand Rakhecha is at Solid State Physics Division (formerly Nuclear Physics Division) after training in physics from the 11th Batch of BARC Training School (1967-68). He did his M.Sc. in Physics (1965) from Rajasthan University and Ph.D. (1978) from Mumbai University. He is engaged in neutron beam based research and has worked on both experimental and theoretical problems. Till mid 1980's he investigated microscopic structure and dynamics of magnetic systems by magnetic neutron scattering techniques. He worked as Research Associate for 2 years (1979-81) at Argonne National Laboratory, USA, where he worked on magnetic neutron scattering problems involving very low temperatures and high magnetic fields. After the post-doctoral stint his research interests have gradually shifted to neutron interferometry and optics. He is a referee for prestigious international physics journals in his area of research. Currently, he is Facility Correspondent from India for the Journal Neutron News published by Taylor & Francis Inc.



Prologue

That's me and me

I am a young chap¹ born milliseconds before
In a nuclear big bang at the reactor core
Winding my way out I became a moderate
Bouncing off chaps nearly twice my weight
I fly about gleefully with no driving licence
Cruising kilometres in a matter of seconds
I get scattered in matter yet keep my cool
And never ever violate a conservation rule
Some people fancy my particulate nature
Others rave about my wavy signature
Here I shall perform a magical feat

Which, to say the least, is a bit off-beat
A trick straight out of the science fiction shelf
I am gonna interfere with Myself!
I shall split into two and later recombine
Carrying a phase angle different from mine
Crazy it sounds till you see the oscillation
Bringing you a package of quantum information

Neutron Interferometry

A study of interference between two coherent waves affords determination of their relative phase. The neutron, due to its zero electrical charge, large mass, spin 1/2 and associated magnetic moment, constitutes a fascinating quantum wave packet.

¹This chap had just emerged from the heavy water moderated reactor CIRUS at Bhabha Atomic Research Centre.

Dr. Apoorva G. Wagh and Dr. Veer Chand Rakhecha, Solid State Physics Division, Bhabha Atomic Research Centre, Mumbai 400085; E-mail: nintsspd@magnum.barc.ernet.in

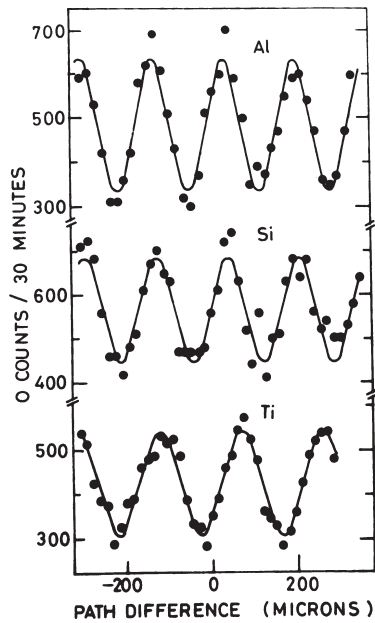


Fig. 1 O-detector intensity oscillations [1] recorded as a function of the path difference introduced between the two neutron subbeams with Si, Al and Ti phase shifter plates at the CIRUS interferometry setup.

Neutron interferometry [1,2] therefore is the ideal probe of quantum mechanical ideas. Several quantum mechanical concepts, which could previously be dealt with only in thought experiments, have been explicitly verified in the laboratory using neutron interferometry. A number of counterintuitive phenomena, e.g., the change in the sign of the wavefunction when a spin 1/2 is rotated through 360° and a superposition of up and down spin states yielding a transverse spin state, have thus been directly confirmed.

Bragg diffraction at perfect crystal silicon slabs, precision carved on a single ingot, is employed to split and recombine monochromatic neutron beams coherently. Micron level mechanical vibrations and temperature gradients of a few mK/cm within the silicon crystal can completely wash out neutron interference oscillations. Neutron interferometry is hence an extremely difficult experimental proposition. Only a handful of neutron interferometers operate in the world. Fig.1 shows

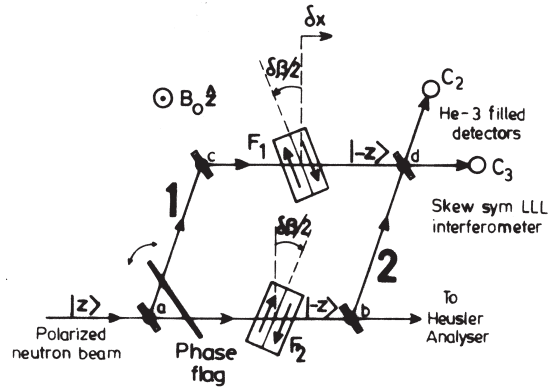


Fig. 2 Schematic diagram of the interferometric experiment [3]. Identical dual flippers F_1 and F_2 on paths 1 and 2 take the incident $+z$ spin to $-z$. A current reversal in a flipper coil enables direct verification of Pauli anticommutation. Geometric and dynamical phases get clearly separated by getting associated with distinct physical operations, viz. relative rotations and translations respectively between F_1 and F_2 .

interferograms recorded with Si, Al and Ti phase shifters at the CIRUS setup in BARC. Direct verification of Pauli anticommutation, separation of geometric and dynamical phases and observation of noncyclic amplitudes and phases, have been implemented in BARC experiments.

Fig.2 depicts the scheme of the interferometry experiment [3]. Identical spin flippers F_1 and F_2 on paths 1 and 2 of the interferometer take the $+z$ -polarized incident neutron beam to the $-z$ state. Each flipper performs an operation $-\sigma_I\sigma_{II}$, in terms of the Pauli spin operator components along mutually perpendicular axes I and II, say. A reversal of current in the coils of a flipper effects the operation $-\sigma_{II}\sigma_I$. Pauli anticommutation implies that these two operations differ by just a sign, i.e. a 180° phase. Fig. 3 shows a direct interferometric verification of this effect, implemented with a mere flick of a switch.

A relative rotation $\delta\beta$ between the flippers F_1 and F_2 generates a pure geometric phase equal to $\delta\beta$.

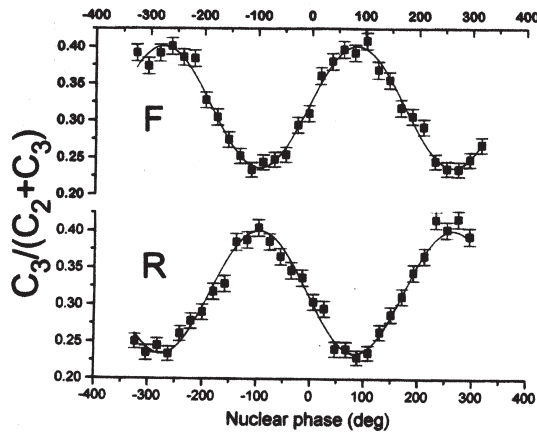


Fig. 3 Pauli anticommutation stands directly verified [3]. The interferogram has shifted by 180.5 ± 3.0 degree on switching the current in the flipper from forward (F) to the reverse (R) sense.

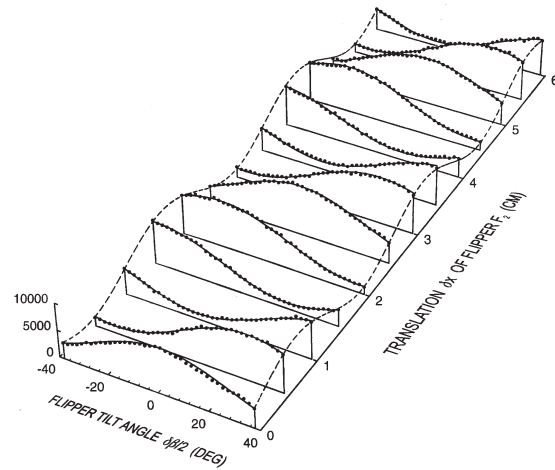


Fig. 5 Interference intensity variation [4] with geometrical and dynamical phases produced by flipper rotations and translations respectively.

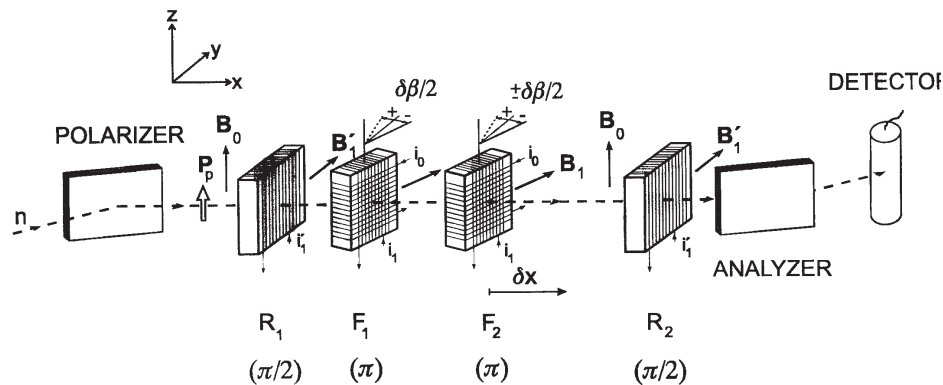


Fig. 4 Polarimetric experiment [4] to observe well demarcated geometric and dynamical phases (schematic), for the z-state arising from relative rotations and translations respectively between identical single flippers F_1 and F_2 .

A relative translation δx on the other hand, produces a proportionate pure dynamical phase due to the guide field B_0 . We have effected this clear separation of the two phases in interferometric [3] as well as polarimetric [4] experiments. Fig. 4 is a schematic sketch of the polarimetric experiment. Here the spin rotation of a coherent superposition of two orthogonal states, each cyclic under the same hamiltonian, is observed to infer the equal and opposite spinor phases of these states. Fig. 5 displays

the observed oscillations due to the geometric and dynamical phases introduced by $\delta\beta$ and δx respectively. The geometric and dynamical phases extracted from the data are plotted in Figs. 6 and 7. The geometric phases were also measured in another experiment, with a B_0 -free environment, to eliminate the dynamical phase contamination. As expected, a null geometric phase was observed when the flippers were rotated together ($\delta\beta=0$).

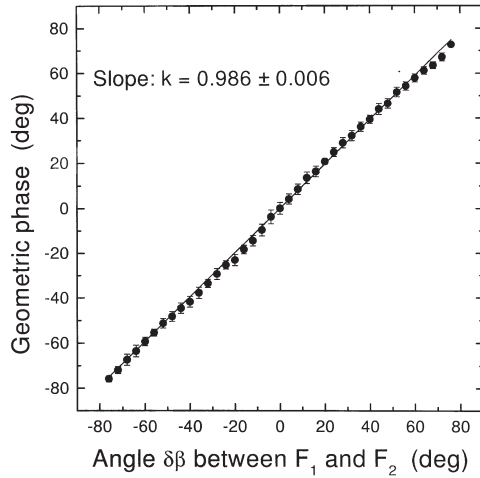


Fig. 6 Pure geometric phase variation [4] with the angle between F_1 and F_2 .

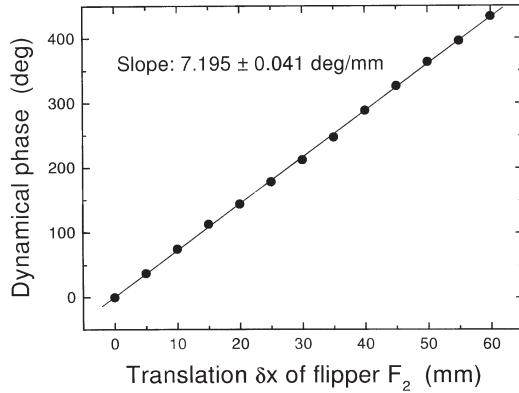


Fig. 7 Pure dynamical phase [4] as a function of F_2 translation

For a noncyclic evolution, one in which the initial and final states are distinct, the definition of phase is nontrivial. Pancharatnam connection [5-6] specifies an interference amplitude (less than unity) in addition to the phase for a noncyclic evolution. When a neutron spin precessing about the z -axis at an angle θ , performs a fractional revolution, the initial and final spin directions differ and the spinor evolution is noncyclic, unless $\theta=0^\circ$ or 180° . We have measured the interference phases and amplitudes simultaneously for such noncyclic evolutions in an interferometric experiment [7]. Fig. 8 presents phase

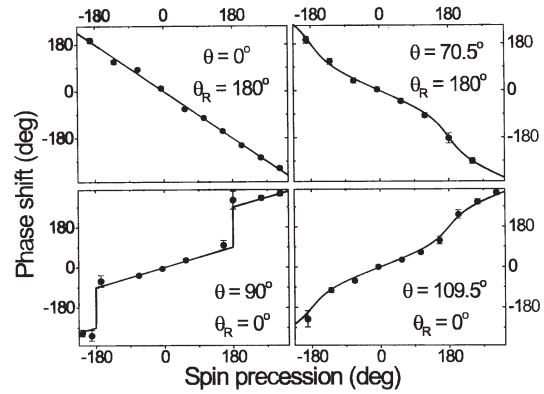


Fig. 8 Phase shifts [7] between incident states with spin angles θ and θ_R as a function of the spin precession.

shifts measured for obtuse θ states with $\theta_R=0^\circ$ as the reference state and for acute θ states with $\theta_R=180^\circ$ as the reference state. The interference amplitudes for the various θ states are shown in Fig. 9 as a function of the precession angle. The product of the amplitude with the cosine of the corresponding phase is state-independent (Fig. 10), as expected for SU(2) evolutions [6].

Neutron Optics

The refractive index of most materials for thermal neutrons is extremely close to unity. It is hence impossible to use conventional optical elements like prisms, lenses and mirrors in neutron beam optics. However, Bragg diffraction can deflect neutrons through large angles. With perfect crystals, it produces sharp angular profiles, only a few arcseconds wide, of diffracted neutrons. Bonse and Hart [8] proposed that a number of successive identical Bragg reflections of X-rays from two slabs of a channel-cut monolithic single crystal would yield a highly collimated beam with a top-hat (nearly rectangular) angular profile. However, experimental angular profiles thus obtained for X-ray and neutron beams the world over for the past 36 years exhibited tail intensities a few orders of magnitude higher than expected. These were conjectured to stem from thermal diffuse scattering within the crystal slabs. We showed that dynamical diffraction effects within the perfect crystal [9] can lead to stray beams that

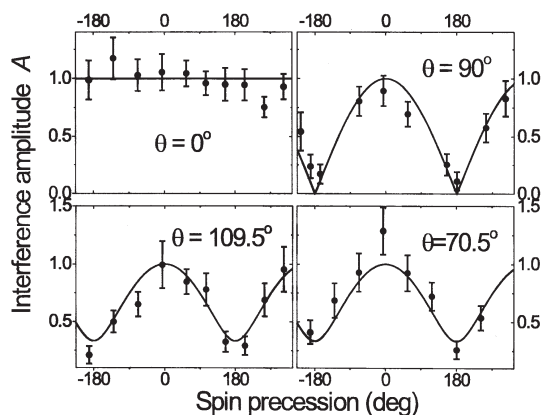


Fig. 9 Interference amplitudes [7] for incident spin angles θ . Points: data, Curves: theory.

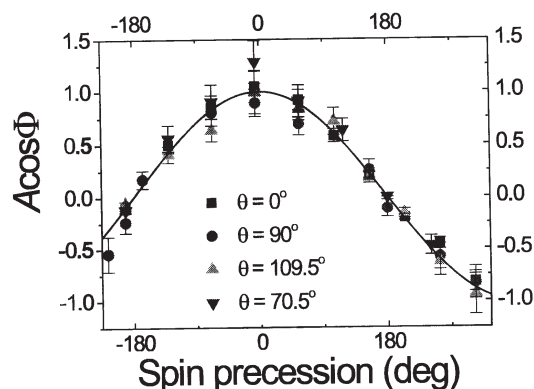


Fig. 10 Product of the observed interference amplitudes and cosines of the corresponding phases for 4 incident angles θ , all lie close to a single curve [7], as expected.

would contaminate the genuine multiply reflected beam and produce the observed excessive tails. Based on these considerations, we arrived at an optimal design for the channel-cut crystals that would eliminate the tails. A typical rocking curve recorded between two such optimal triple symmetric Bragg reflectors [10] is displayed in Fig. 11. The data (circles) agree with the theoretical curve (triangles) over an intensity range spanning 5 orders of magnitude. This constitutes the first realization of the Bonse-Hart proposal in its totality. The best

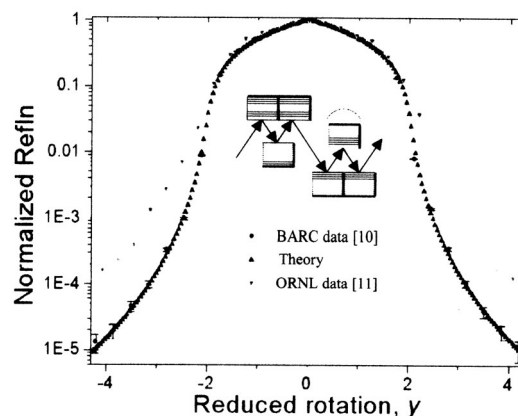


Fig. 11 Rocking curve between two optimal triple symmetric $\{111\}$ Bragg reflections from channel-cut silicon single crystals [10]. Circles: our experimental data. Triangles: calculated triple-triple Darwin profile. Inverted triangles: ORNL quadruple-triple Bragg reflection profile [11].

previous Bonse-Hart profile [11] recorded for quadruple-triple symmetric Bragg reflections at Oak Ridge National Laboratory in USA, is also shown (inverted triangles) in the figure. Our results thus mark well over an order of magnitude improvement over all Bonse-Hart multiple Bragg reflection profiles reported previously. We have thus produced a monochromatic neutron beam with the sharpest angular profile in the world. This work opens up new possibilities for SUSANS (Super Ultra-Small Angle Neutron Scattering) studies enabling characterization of samples containing micron-size agglomerates.

Epilogue

Mirrored to Perfection

Reflecting on the monolith monochroma
The Duo conceived a sharp-featured Angstroma
‘Mirror, mirror on the (channel) wall
Shall make her the shapeliest of all!’
Gallant men, some heroic, some frantic
On both sides of the Pacific and Atlantic
Wooded her, alas, with little success
‘Thanks to her Guardian Demon TDS’
The real spoilsports worked behind the scene
In the Dynamical Trojan horse from deep within
Well, make no Bonse about it

When the Hart of the matter is hit
 She appears, lo and behold, in just a top hat
 Revealing vital statistics SANS all fat
 May we present, Ladies and Gentlemen
 The Beauty of Research Reactor Utilisation?

References

1. A.G. Wagh and V.C. Rakhecha, Prog. Part. Nucl. Phys., **37** (1996) 485.
2. Neutron Interferometry: Lessons in Experimental Quantum Mechanics by H. Rauch and S.A. Werner (Oxford Univ. Press, UK, 2000).
3. A.G. Wagh, V.C. Rakhecha, J. Summhammer, G. Badurek, H. Weinfurter, B.E. Allman, H. Kaiser, K. Hamacher, D.L. Jacobson and S.A. Werner, Phys. Rev. Lett., **78** (1997) 755; J. Phys. Soc. Jpn. **65** Suppl. A, **73** (1996); Phys. Rev. A **56** (1997) 4420.
4. A.G. Wagh, G. Badurek, V.C. Rakhecha, R.J. Buchelt and A. Schricker, Phys. Lett., A **268** (2000) 209.
5. S. Pancharatnam, Proc. Indian Acad. Sci., **A44** (1956) 247.
6. A.G. Wagh and V.C. Rakhecha, Phys. Lett., A **197** (1995) 107 & 112.
7. A.G. Wagh, V.C. Rakhecha, P. Fischer and A. Ioffe, Phys. Rev. Lett., **81** (1998) 1992; Phys. Rev. Lett., **83** (1999) 2090.
8. U. Bonse and M. Hart, Appl. Phys. Lett., **7** (1965) 238.
9. A.G. Wagh, Phys. Lett., A **121** (1987) 45; A **123** (1987) 499.
10. A.G. Wagh, V.C. Rakhecha and W. Treimer, Phys. Rev. Lett., **87** (2001) 125504; Appl. Phys. A (2002), in press.
11. M. Agamalian, D.K. Christen, A.R. Drews, C. J. Glinka, H. Matsuoka and G.D. Wignall, J. Appl. Cryst., **31** (1998) 235.

Neutron Activation Analysis



Dr. A.V.R. Reddy obtained his M.Sc. (Chemistry) in 1974 from Sri Venkateswara University, Tirupati and graduated from BARC Training School in 1967-77. He joined Nuclear Chemistry Section, Radiochemistry Division in 1977 and at present is the Head of the Section. His main areas of research are nuclear fission, nuclear reactions, radiochemical separations and neutron activation analysis. He has more than 100 publications to his credit and co-author of three books. He has worked as a visiting scientist for an year on the extension of periodic table in Institut für Kernchemie, Mainz, Germany. He is a member of IUPAC's Commission on Radiochemistry and Nuclear Techniques. During 1999-2000, he served as Technical Officer in the Division of Physical and Chemical Sciences, IAEA, Vienna.

Dr. R. Acharya obtained M.Sc. In Chemistry from Utkal University in 1992. After graduating from BARC Training School in 1993-94, he joined Radiochemistry Division. Since then he is engaged in research and development work on conventional, k_0 and prompt gamma-ray neutron activation analysis. The other areas of interest are trace element speciation and positron annihilation studies. He obtained his Ph.D. Degree from University of Mumbai in 2000 and has about 50 publications to his credit. Recently, he has pursued his postdoctoral studies at Dalhousie University, Canada.



Dr. A.G.C. Nair joined Radiochemistry Division of BARC in 1969. Since then he is actively engaged in the development of radiochemical separation procedures of fission products and trace element determination using conventional, k_0 , and prompt gamma-ray neutron activation analysis. He obtained his Ph.D. Degree from Bombay University in 1989 and has about 100 publications to his credit.

Neutron Activation Analysis is essentially a nondestructive nuclear analytical method, capable of simultaneous multielement analysis [1]. It is one of the major applications of a research reactor as reactor is a huge source of neutrons. Neutron activation analysis is carried out by (i) on-line measurements using a neutron beam [Prompt gamma ray neutron activation analysis (PGNAA)] and (ii) off-line measurements after irradiating the sample (NAA). In PGNAA, intensities of gamma rays emitted by the compound nucleus are measured to arrive at the concentration of the measurand while

in conventional NAA γ -rays from the radioisotopes produced are measured with or without chemical separations. NAA is being used extensively as an analytical tool due to its selectivity, detection limit, absence of analytical blank and relative freedom from matrix.

Neutron being non-charged particle interacts with the nuclei of isotopes of all elements in the periodic table resulting in nuclear reactions. The product formed in such a nuclear reaction might be a radioisotope. By measuring the radioactivity formed, concentration of the isotope that underwent

Dr. A.V.R. Reddy, Dr. R. Acharya and Dr. A.G.C. Nair, Radiochemistry Division, Bhabha Atomic Research Centre, Trombay, Mumbai 400 085; E-mail: avreddy@magnum.barc.ernet.in, raghu@magnum.barc.ernet.in and chitrac@vsnl.net

nuclear reaction is measured. Using the isotopic abundance, elemental concentration is calculated. Multi element analysis is carried out by measuring gamma rays corresponding to different radioisotopes (elements).

Detection Limits

In NAA, about 70 elements can be measured with a detection limit better than 10^{-7} g. For elements like In, Eu and Dy, achievable detection limit is about 10^{-12} g where as for Mn it is 10^{-11} g. Detection limit is between 10^{-8} g and 10^{-7} g for elements like K, Sc, Rb and Cd. These calculations are based on the assumption that the neutron flux is of the order of 10^{12} n.cm⁻².s⁻¹ and 100 Bq is the lower limit for activity measurement. Neutron fluxes of the order of 10^{13} - 10^{14} cm⁻².s⁻¹ available in reactor like Dhruva would accordingly improve the detection limits.

Chemical Separations in NAA

When certain elements like Na, K and Br are present as major constituents of the sample, the gamma rays from activation products formed would complicate the measurements [1]. Additionally, if the sample contains uranium, it undergoes nuclear fission and the products formed would be between Z=35 and 70 and therefore, estimation of a elements like La, Ce, Eu, Zr and Mo would be erroneous. In such situations, it is essential to either preconcentrate and/or remove elements like U prior to neutron irradiation. This procedure is known as Chemical Neutron Activation Analysis (CNAA). In Radiochemical NAA (RNAA), the sample is irradiated and the higher abundant matrix elements are removed by chemical methods. In CNAA, gamma ray spectrum becomes simpler because matrix elements are removed before irradiation resulting in minimum radiation exposure and improved detection limit, since a higher amount of sample can be used. However, reagent blank correction is often required. On the other hand, in RNAA gamma spectrum becomes simpler and blank correction for reagents is not needed. In this approach radioactive samples have to be handled.

Methods of NAA

Elemental concentrations in a sample can be determined by absolute, relative and k_0 method,

although in practice absolute method, for obvious reasons, is not preferred.

Relative Method

In the relative method, a chemical standard with a known mass of the element is co-irradiated with the sample of a known mass and radioactivity in both are measured, in the same geometrical arrangements with respect to the detector, so that the absolute detection efficiency of the detector need not be determined. When short-lived radionuclides are employed both the standard and sample are irradiated separately in the same conditions with a monitor of the neutron flux. The ratio of activities of an isotope in the sample and standard is related to the concentration of that isotope and hence the element. Though the relative method is simple and precise, prior knowledge of the elements present in the sample is necessary and standards for all the elements in similar matrices to be analysed are difficult to prepare.

k_0 Method (Single Comparator Method)

The concept of the k_0 -standardization in NAA is based on coirradiation of the sample and a neutron flux monitor instead of multielement standard, and on using a composite nuclear constant k_0 [2-5]. In k_0 -method, the analysis results are linked to the k_0 -factors, absolute detection efficiency and neutron spectrum characteristics. The k_0 -factor is a ratio of four nuclear constants of element of interest to the comparator element and these four constants are average atomic mass, isotopic abundance, thermal neutron capture cross section and gamma ray abundance [2].

Applications of NAA

Neutron activation analysis finds application in a large number of areas of research like biology, geology, agriculture, anthropology, chemistry, engineering & industry, fisheries, forestry, medicine, oceanography, pharmacy and forensics. A judicious combination of k_0 NAA and relative method, and with and without chemical separations are being used for multi element determinations in a variety of matrices in the Radiochemistry Division, BARC for the last 8 years. Apsara reactor (10^{11} to 10^{12} n.cm⁻².s⁻¹), Cirus reactor (10^{13} n.cm⁻².s⁻¹) and Dhruva reactor (10^{13} to 10^{14} n.cm⁻².s⁻¹) are used for

neutron irradiation. The areas of R&D include standardization of k_0 NAA, determination k_0 factors, validation of k_0 NAA [6] and measurement of elemental concentrations in ruby samples [5], emeralds and associated rocks [7], serpentines and host rocks [8], ferromanganese encrustations [9], sediments [10], medicinal and edible leaves [11], cereals and pulses [12]. In addition, chemical methods for the determination of gold and platinum group elements (PGEs) in ores [13], REEs in minerals, derivative neutron activation analysis for the determination of phosphorous [14] and elemental concentrations in large samples have been developed [15]. In this article standardization of k_0 NAA, a few applications and development of prompt gamma ray neutron activation analysis method are briefly presented.

Standardisation and Validation of k_0 NAA

The k_0 NAA has been standardized by calibrating irradiation sites at Apsara and pneumatic irradiation facility of Cirus reactors by determining two important parameters; epithermal neutron flux shape factor (α) and thermal to epithermal neutron flux ratio (f) and redetermining the k_0 -factors for 35 elements [4,5]. This methodology has been applied to obtain multi element profiles in a variety of matrices. Since there is a large variation in the nature of the samples and the concentration of the elements present, it is essential to validate this analytical technique. A variety of the (standard / certified) reference materials (RMs) were analysed. Some of the RMs analysed by this technique are USGS AGV-1, W-1, and NOD-A-1, IAEA CRM-SOIL-7 and NIST SRM-1571. A good agreement between the measured values and the reported data was obtained. Percentage deviation of the measured and certified values are plotted in Fig. 1 [6]. The over all % deviation from certified values is between 2 to 10%. In our studies, an appropriate reference material was analysed, as a control, along with the samples in each set of experiments.

Emeralds and Associated Rocks

Multielement analysis was carried out in natural emeralds, their associated rocks (host and trapped rocks) and one sample of beryl from Tikki area, Rajasthan with an aim to understand the process of formation of emeralds. The concentrations of 21

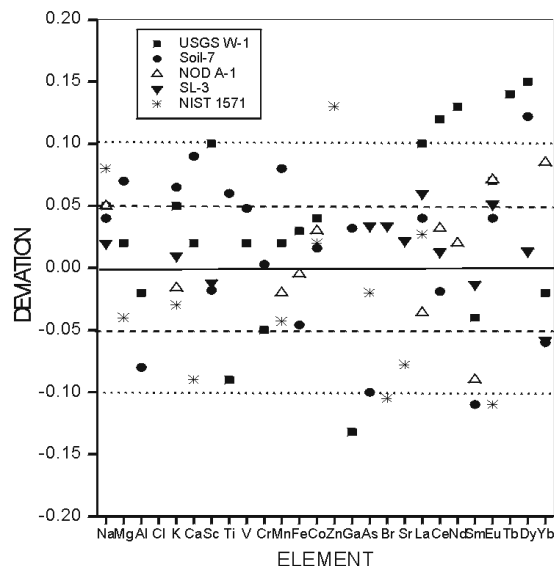


Fig. 1 Comparison of measured and certified elemental concentrations in five reference materials

elements were determined by k_0 -INAA method. These four sets of samples were analysed to understand the segregation of elements from associated rocks to mineral beryl forming the gemstones. The comparative concentration profiles are given in Figs. 2 and 3 respectively for major and minor constituents [7]. The following observations were made: (i) the concentrations of aluminium in emerald and beryl are found to be 10.02 and 10.03 %, respectively which agree well with expected concentration of aluminium in emerald and beryl (~10%) and is in good agreement with the formula for beryl, beryllium aluminium silicate $[\text{Be}_3\text{Al}_2(\text{SiO}_3)_6]$, (ii) emerald contains higher concentrations of V, Cr, Sc, Cs and Rb compared to associated rocks, (iii) the chromium content of the emerald is the highest and decreases in the following order, emerald, trapped rock, host rock, indicating depletion of Cr from associated rock to emerald, (iv) potassium was found to be absent and Na was present in varying concentrations in emerald and associated rocks, (v) Our studies showed the presence of Mg as a major and Co as a trace constituent in emerald and the absence of expected elements such as K, Ga and Ca compared to some results of PIXE/PIGE. The enrichment of some trace

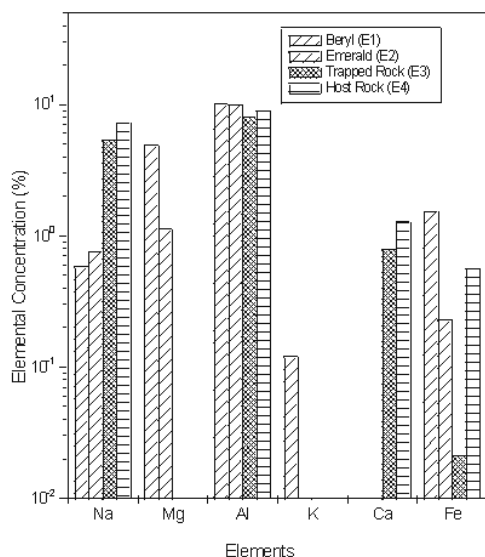


Fig. 2 Concentration profile of major elements of E1, E2, E3, E4

and other elements in emerald compared to associated rocks may be due to the following reasons: (i) in the formation of gemstones, these elements might have segregated and/or (ii) these elements might have weathered away from rocks over the time after formation of the gemstones.

Ferromanganese Encrustations from Indian Ocean

Ferromanganese oxide encrustations are common depositional features on exposed rock outcrops in the deep sea. They are mostly found on mid-oceanic ridges, seamounts and raised areas of sea floors of the oceans and significantly differ in their composition and mineralogy. Multielemental analysis together with a varying Mn/Fe ratio is relevant in understanding their distribution in Mn and Fe phases. Three sets of ferromanganese crusts from different locations of the Indian Ocean and another crust from the Lau basin of the Pacific Ocean were analysed by k_0 NAA method for studying the influence of different oceanic conditions on the trace element distributions in ferromanganese crusts [9].

Edible and Medicinal Leaves, Pulses and Cereals

The role played by micro nutrients and trace elements in the biochemical functions of human life

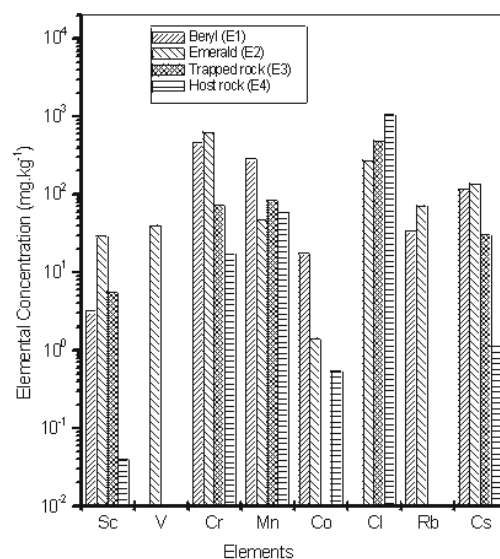


Fig. 3 Concentration profile of some of the minor and trace elements of E1, E2, E3, E4

and their impact on human life are important. These are supplied through food chain. Additionally carbohydrates, proteins and minerals are provided through food items like cereals, pulses and leaves. Concentrations of 17 elements in a few varieties of leaves, which are used either as a natural ingredient in ayurvedic medicine preparations or as items for human diet, were determined by k_0 NAA method (11). Elemental concentrations of a few varieties of cereals and pulses, which are main dietary items for supplying trace elements and nutrients, were determined (12). We have compared the Recommended Dietary Allowance (RDA) for some of the known major essential elements with that of the values obtained from this work based in an intake of 100 g cereal or pulses per day.

Palladium and Gold Determination by CNAA

Measurement of trace elements in the presence of large amounts of Fe, Cu and U by NAA is very difficult due to the spectral interferences and also becomes complicated due to the fission product contribution from nuclear fission of uranium. In such cases, it becomes imperative to preconcentrate elements of interest and decontaminate from the major elements. A Chemical Neutron Activation Analysis (CNAA) method was developed to measure the trace amounts of Au and Pd present in

matrices that may contain uranium, copper and iron [13]. Pd and Au were preconcentrated on Dowex 1X8 (100-200 mesh) in Cl⁻ form. Concentrations were evaluated by comparison method of NAA. Under the ideal interference free conditions, an absolute detection limit of 0.12 ng for Pd and 0.05 ng for Au were achieved. This is being used routinely to measure trace amounts of Au and Pd in different matrices.

Enhanced Sensitivities of Elements using PCF at Dhruva reactor

The pneumatic carrier facility (PCF) at irradiation facilities is used for determining the elements via their short-lived (seconds to minutes) isotopes. We have used PCF at Dhruva for the determination of elements such as Al, V, Ti, Ca, Mg, Br and Cl using short-lived activation products, along with other elements of medium lived isotopes. The elemental sensitivities (counts.μg⁻¹) obtained using a neutron flux of 2×10^{13} n.cm⁻².s⁻¹ are 10-100 times higher than those obtained using Apsara reactor and also the detection limits for many elements are better by several orders [16].

Prompt Gamma ray Neutron Activation Analysis (PGNAA)

Prompt Gamma ray Neutron Activation Analysis (PGNAA) is a complementary technique to conventional Neutron Activation Analysis (NAA) and is characterised by its capability both for nondestructive multielement analysis and by its ability for analyzing, in principle, all elements including light elements like H, B, C, N, P, Si and S which are difficult to analyse by Instrumental Neutron Activation Analysis (INAA). Neutrons from a thermal or cold neutron guided beam are commonly used for prompt gamma ray measurement.

For the first time in BARC, a PGAA facility was set up using thermal guided beam in GT lab of Dhruva reactor. The γ-ray detector surrounded by 30 cm thick lead shielding was located at about 40 cm distance from the sample and was placed at 90° with respect to the beam direction. Neutron flux at the sample irradiation position was determined using gold and indium as flux monitors and was 2×10^7 n.cm⁻².s⁻¹ and the thermal component was found to be

more than 99.99%. The MCA was calibrated using the delayed gamma-rays from ¹⁵²Eu, and prompt gamma-rays from ³⁶Cl. The absolute full energy peak efficiencies were determined for low energy region (i.e., up to 1500 keV) using gamma ray spectrum of ¹⁵²Eu and the relative efficiency plot for the energy region from 0.5 to 8.5 MeV was obtained from the prompt gamma ray spectra of ³⁶Cl and ⁴⁹Ti. The relative efficiency was converted to absolute efficiency values using the values obtained with ¹⁵²Eu [17]. The efficiency of the PGNAA system is shown in Fig. 4.

For standardisation of k₀-method in PGNAA, prompt k₀-factors for elements like H, B, K, Co, Cu, Ca, Ti, Cr, Cd, Ba, Hg and Gd with respect to 1951 keV gamma line of ³⁶Cl have been determined [18]. About 100-500 mg of elements in the form of chloride compounds or stoichiometric compounds of the elements mixed with NH₄Cl were wrapped in thin Teflon tape and exposed to neutron beam.

In view of the potential of ⁶⁰Co [⁵⁹Co (n,γ)] both as a comparator for k₀ standardisation as well as a γ-ray standard for efficiency calibration in prompt γ-ray measurement (150-7500 keV), the absolute prompt gamma ray abundances per 100 neutron capture of 49 gamma lines of ⁶⁰Co were determined [17]. Analytical sensitivities for elements like Hg, B, Sm, and Cd were determined. It is planned to develop a dedicated neutron beam facility for PGNAA in Dhruva reactor hall and work has been initiated.

Conclusion

Neutron activation analysis is being used for multielement analysis in a variety of matrices belonging to various areas of research and developments. For most of the our work, Apsara reactor has been used. With the commissioning of PCF at Dhruva, with a flux of $\sim 5 \times 10^{13}$ n.cm⁻².s⁻¹, not only detection limits have improved but also scope for studying short-lived isotopes is enhanced. PGNAA using thermal neutron beam at Dhruva reactor has provided an avenue for the on-line analysis of various materials. A dedicated beam line for PGNAA is being developed. This along with PCF would improve the scope for activation analysis as well as basic studies like nuclear spectroscopy.

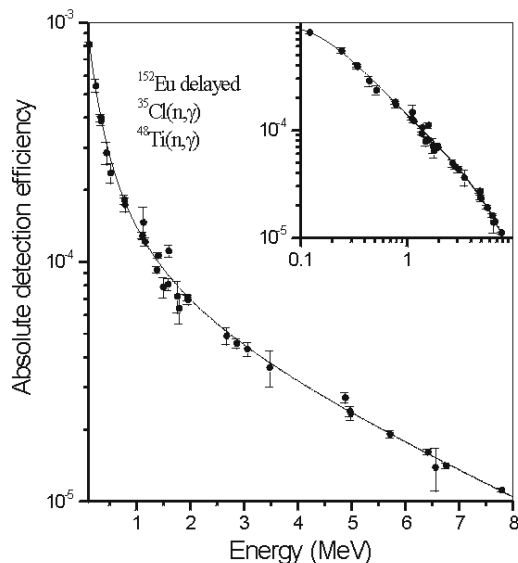


Fig. 4 Absolute efficiency of the PGNA system (inset shows the log-log plot of absolute efficiency)

Acknowledgments

We thank all our colleagues and collaborators, who have contributed to the activation analysis program, particularly Dr. S.B. Manohar, Dr. A. Goswami, Mr. P.P. Burte, Mr. K. Sudarshan, Mr. T. Newton Nathaniel and Mr. Y.M. Scindia. We are grateful to Dr. M. Ramanadham, Dr. S. Basu, Dr. V.K. Aswal and other colleagues of SSPD for their cooperation in PGNA work. We are also thankful to the operation crew of Apsara, Cirus and Dhruval reactor facilities.

References

1. D. Desoete, R. Gijbels and J. Horte, Neutron Activation Analysis, John Wiley & Sons, NY, 1972.
2. A. Simonits, F. De Corte and J. Hoste, J. Radioanal. Chem., **24** (1975) 31.
3. F. De Corte, A. Simonits, A. De Wispelaere and A. Elek, J. Radioanal. Nucl. Chem., **133** (1989) 43.
4. R. Acharya, Ph.D Thesis, University of Mumbai, Mumbai (2000).
5. R.N. Acharya, P.P. Burte, A.G.C. Nair, A.V.R. Reddy and S.B. Manohar, J. Radioanal. Nucl. Chem., **220**(2) (1997) 223.
6. R.N. Acharya, A.G.C. Nair, A.V.R. Reddy and S.B. Manohar, Appl. Radiat. Isot. 2002 (in Press).
7. R.N. Acharya, R.K. Mondal, P.P. Burte, A.G.C. Nair, N.B.Y. Reddy, L.K. Reddy, A.V.R. Reddy, S.B. Manohar, Appl. Radiat. Isot., **53** (2000) 981.
8. R.N. Acharya, A.G.C. Nair, L.K. Reddy, N.B.Y. Reddy, A.V.R. Reddy and S.B. Manohar, (in preparation).
9. R.K. Dutta, R.N. Acharya, V. Chakraborty, A.G.C. Nair, A.V.R. Reddy, S.N. Chintalapudi and S.B. Manohar, J. Radioanal. Nucl. Chem., **237** (1998) 91.
10. S.K. Jha, R.N. Acharya, A.V.R. Reddy, S.B. Manohar, A.G.C. Nair, S.B. Chavan and S. Sadasivan, J. Environ. Monit., **4** (2002) 131.
11. T. Balaji, R.N. Acharya, A.G.C. Nair, P.P. Burte, G.R.K. Naidu, A.V.R. Reddy and S.B. Manohar, J. Radioanal. Nucl. Chem., **243** (2000) 783.
12. T. Balaji, R.N. Acharya, A.G.C. Nair, A.V.R. Reddy, K.S. Rao, G.R.K. Naidu, and S.B. Manohar, The Science of Total Environment, **253** (2000) 75.
13. A.G.C. Nair, A.V.R. Reddy, R.N. Acharya, P.P. Burte and S.B. Manohar, J. Radioanal. Nucl. Chem., **240** (1999) 877.
14. Y.M. Scindia, A.G.C. Nair, A.V.R. Reddy and S.B. Manohar, J. Radioanal. Nucl. Chem. (in press)
15. K. Sudarshan, A.G.C. Nair and A. Goswami, J. Radioanal. Nucl. Chem. (communicated).
16. A.V.R. Reddy, T.N. Nathaniel, A.G.C. Nair, Y.M. Scindia, R.N. Acharya, S. Duraiswamy, D.K. Lahiri and S.B. Manohar, Proc. NUCAR 2001, P. 513.
17. K. Sudarshan, *et al.*, Nucl. Instr. Meth., **A47** (2001) 180.
18. R.N. Acharya, *et al.*, J. Radioanal. Nucl. Chem., **250** (2001) 303.

Neutron Detection Techniques in Neutron Scattering and Radiography Experiments



Dr. A.M. Shaikh joined BARC in 1992. His areas of specialization are neutron detectors, neutron radiography, high temperature X-ray crystallography and instrumentation. A Ph.D. from IISc, Bangalore, he was post doctoral fellow at University of Washington Seattle, USA and has worked as faculty member at IISc, Bangalore and University of Kuwait. Dr. Shaikh has been associated with IAEA in programmes related to Neutron Radiography and worked as expert in this field. He has about 60 research papers in national and international journals to his credit.

Introduction

Charged particles and electromagnetic radiations are detected by their interactions with matter, leading to either a prompt electrical signal (ionization devices), a light photon (scintillators) or a latent track (photographic emulsions). The lack of charge and the weak absorption of neutrons in most materials make their detection by these direct methods difficult. Also, the intensity of neutron sources is weak compared to conventional laser and X-ray sources. Experiments therefore, run for fairly long time. To make best use of expensive neutrons, rugged, high efficiency neutron detectors operating reliably for long duration of time are of prime necessity. The present article describes various thermal neutron detection techniques used in neutron scattering and radiography experiments.

Detection of Thermal Neutrons

Neutron detection is a two-step process. Neutrons first have to undergo nuclear reactions, which result in energetic charge particles such as protons, alphas and fission fragments [1]. These charged particles are then detected through coulombic interactions. Every type of neutron detector involves combination of a target material to carry out this conversion and one of the conventional techniques to detect the particles liberated. Nuclear reactions on which most of the neutron detection methods are based are listed in Table 1. All the nuclear reactions are sufficiently exothermic.

The total detector efficiency (ϵ) is convolution of the efficiency of capture by the converter and that of the subsequent detection of the particles emitted and can be expressed as $\epsilon = \xi(1 - e^{-N\sigma t})$, where N is the number of converter nuclei per unit volume, σ is the absorption cross section for the process and t is the thickness of the detector. ξ , the subsequent detection efficiency depends on the detector geometry, other competing capture processes for the charged particles or the efficiency of conversion.

Of the converter materials listed in Table 1, ^{10}B (in the form of BF_3) and ^3He are widely used in making neutron detectors in which charged particles liberated are detected via gas ionization. Natural boron contains 19.8% of ^{10}B , the high capture isotope. BF_3 gas with ^{10}B enrichment up to 96% is commercially available. ^3He is in more use because of its higher capture cross section, though it is an expensive gas. ^6Li is used mostly in making detectors, which are neutron scintillators. One of the commonly used scintillator (NE426) has a chemical composition of LiF (96% ^6Li -enriched) + $\text{ZnS}(\text{Ag})$. The neutron scintillator converts neutrons in to light which can be detected by either a light sensitive film or camera. Neutron scintillators find wide applications in neutron diffraction topography and neutron radiography.

If the neutron converter is in the form of a foil, then the charged particles created by neutron capture or fission escape from the converter and can be detected by a gas detector or a photographic plate.

Dr. A.M. Shaikh, Solid State Physics Division, Bhabha Atomic Research Centre, Trombay. Mumbai 400 085
E-mail : detsspd@magnum.barc.ernet.in

TABLE 1. Some nuclear reactions used for neutron detection

| Reaction | Cross-section for thermal neutrons (barns) | Energy liberated Q (MeV) | Detected particles and their K.E. (MeV) |
|----------------------------------------|--------------------------------------------|--------------------------|-----------------------------------------|
| $^{10}\text{B} (n,\alpha) ^7\text{Li}$ | 3840 | 2.78 | α 1.47 and ^7Li 0.84 |
| $^3\text{He} (n,p) ^3\text{H}$ | 5330 | 0.765 | ^3H 0.19 and p 0.57 |
| $^6\text{Li} (n,\alpha) ^3\text{H}$ | 940 | 4.78 | α 2.05 and ^3H 2.74 |
| ^{235}U fission | 320 | ~ 200 | Fission fragments 80 |
| ^{239}Pu fission | 410 | ~ 200 | |
| $^{157}\text{Gd} (n,\gamma)$ | 74000 | 0.07 - 0.182 | Conversion |
| $\text{Gd} (n,\gamma)$ | 17000 | 0.07 - 0.182 | Electrons |

All the converters mentioned in the Table 1 can be used for this method except ^3He , which is gas. However the efficiency of the foil detectors made of ^{10}B , ^6Li , ^{235}U and ^{239}Pu is very low. Gd foils are commonly used in the neutron radiography work. Image plates based on storage phosphor and containing gadolinium are now commercially available for neutron detection.

Gas-filled Neutron Detectors

The most common method of detecting a charged particle is through ionization produced when it passes through a gas. The ion pairs have natural tendency to recombine to form neutral atoms but it is prevented in the detector by the application of electric field, which causes the electrons and positive ions to drift towards their respective electrodes. Proportional counters function on the phenomenon of ionization multiplication that can amplify the initial ionization charge produced, by a few orders of magnitude. The high electric field necessary to produce this multiplication is easily achieved by using a fine anode wire (10 μm -50 μm) positioned along the axis of a large cylindrical cathode. The value of ξ for gas ionization detector is nearly unity. Since the capture cross section of both $^{10}\text{BF}_3$ and ^3He vary as $1/v$ in the thermal region their efficiencies can be shown as a function of X, where $X = \text{gas pressure(atm)} \times \text{thickness (cm)} \times \text{wavelength (\AA)}$. The dependence of efficiency on X is shown in Fig. 1. An 80% efficient detectors would require $X = 21 \text{ atm.cm.}\AA$ for ^3He or $30 \text{ atm.cm.}\AA$ for $^{10}\text{BF}_3$. Gas

detector of good efficiency are therefore either large or operate at high pressure.

A typical pulse height distribution of a BF_3 -filled proportional counter designed and fabricated in BARC is shown in Fig. 2. The main peaks at 2.31 MeV (94%) and 2.78 MeV (6%) as well as the wall effect¹ steps at 1.47 MeV and 0.84MeV, are clearly seen. BF_3 -filled counters are conventionally used as 'end-on' counters to detect scattered neutrons, because of the greater detection efficiency in long column of the gas. Counters in 'broadside-on' position are used as low-efficiency monitors and in time-of-flight experiments to define the flight-path of neutrons precisely. BF_3 counters can discriminate gamma rays and neutrons. High pressure of ^3He together with a high stopping power gas like Ar, Kr, Xe or CF_4 reduces the range of the released particles to a few mm and improves the efficiency and spectral shape. A common composition is 4 bar $^3\text{He} + 2 \text{ bar Kr}$. A typical pulse height spectrum from ^3He - detector made in BARC is shown in Fig. 3.

Position Sensitive Detectors

In a typical scattering experiment, one or more detectors are used to scan the scattering space and obtain the angular distribution of scattered intensities. Since scattered intensities are generally low, it takes long time to record them. A more economical way of using expensive neutrons is to measure intensities simultaneously over the full or a large fraction of scattering space. Position sensitive

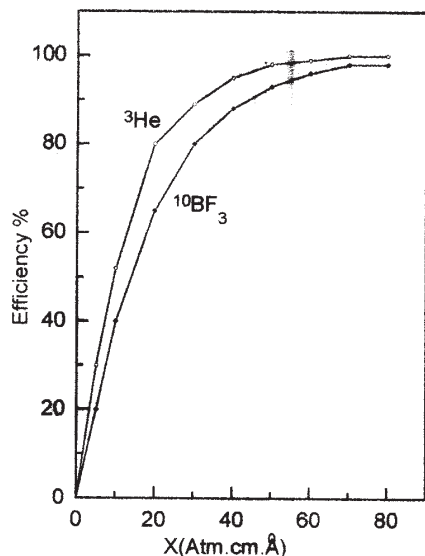


Fig. 1 Detection efficiency of ^3He and BF_3 gases

detectors (PSDs) are used for this purpose. PSDs are capable of not only detecting but also sensing the position of detection. PSDs are of two types: 1-Dimensional or linear PSDs and 2-D PSDs or area detectors. Different types of PSDs such as gas proportional chambers, scintillators, imaging plates, and solid state detectors have been used for a wide range of problems. Gas filled PSDs are more commonly used because they can be built in large size, have relatively good energy and position resolution, high efficiency, good uniformity over the sensitive volume and show no radiation damage as compared to the solid state and scintillation detectors.

1-D Position Sensitive neutron Detectors

A gas proportional counter can be modified to operate as a PSD by using a resistive anode wire and monitoring the signal from both the ends [2]. When a neutron is captured and an avalanche produced on anode wire at a distance X from one end A, the charge Q released divides itself in the inverse proportion of the resistances of the two segments and flows towards the ends. Depending up on the position X , the amplitude, rise time and the time of

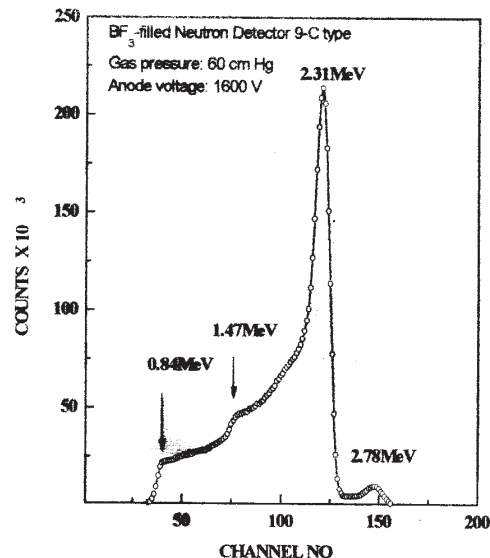


Fig. 2 Typical pulse-height distribution of a BF_3 -filled detector

arrival of the two signals differ from each other. The position can be inferred by measuring the difference in these parameters. The method of charge division based on variation of amplitude with X is shown in Fig. 4. One or more PSDs are placed across the scattering space to collect all the reflections simultaneously, thereby reducing data collection time. The 1-D PSD developed at BARC are of the dimensions (i) 38 mm ϕ , 850 mm sensitive length and (ii) 25mm ϕ and 450 mm sensitive length and filled with 4bar ^3He + 2 bar Kr, giving an efficiency of around 60% for 1.08 Å neutrons and an intrinsic resolution of about 6 mm (FWHM). Both PSDs make use of 10 μm NiCr wire with $\rho = 9\Omega/\text{mm}$ as anode. An excellent position linearity and uniformity of response over 90% of the sensitive length is obtained (Fig. 5). Several of such PSDs are now being used on the profile analysis, High-Q, Quasi-elastic and small angle scattering spectrometers at Dhruva reactor.

2-D Position Sensitive Detector

A 2-D PSD is essentially an extension of the 1-D PSD in two orthogonal directions to generate the X , Y coordinates of the detected particle. A

¹Wall effect arises when range of one of the charge particles produced exceeds the detector dimension and full energy of the reaction is not deposited in the gas.

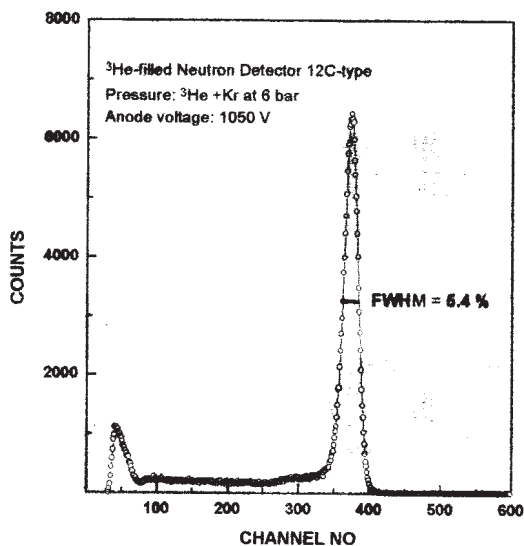


Fig. 3 Typical pulse-height distribution of a high pressure ^3He -detector

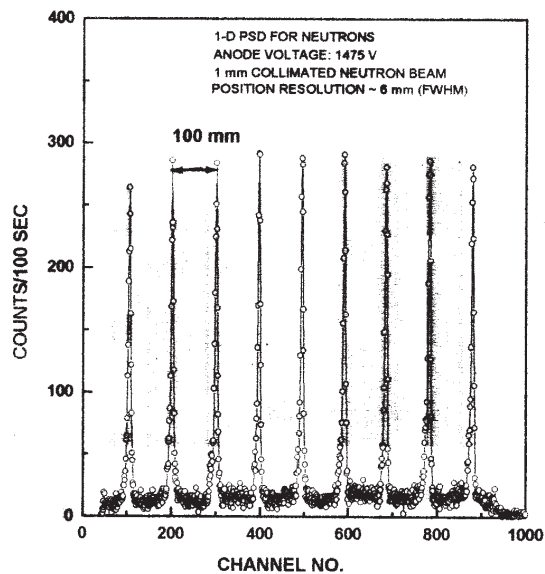


Fig. 5 Position spectrum of a 1-D PSD recorded with 1 mm collimated neutron beam of Apsara

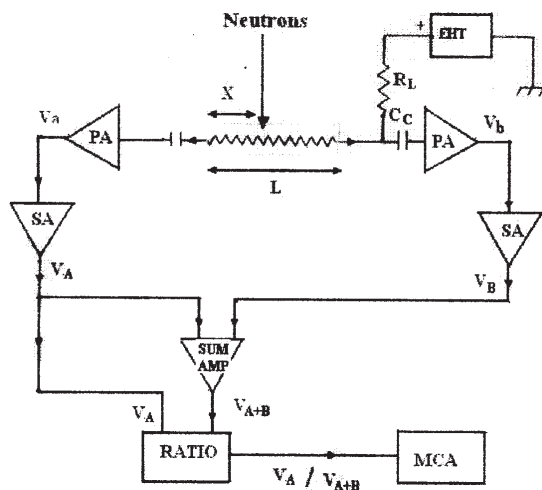


Fig. 4 Schematic diagram of resistive anode, 1-D PSD and charge division method for position encoding. The Position X is $\propto V_A/V_{A+B}$

multiwire proportional chamber (MWPC) proposed by Charpak [4] has been the most popular design for the 2-D PSD (Fig. 6). The anode consists of plane of wires, all connected in parallel and held at high voltage. Each anode wire acts like an independent anode of a proportional counter. Position information can be gained from this device by placing planes of cathode wires, at lower potential than the anodes, on either side of the plane of anode wires. If the cathode wire planes are orthogonal then 2D information on the interaction can be obtained by looking at the signal induced on the two cathode planes. At BARC a 2-D MWPC has been developed for the SANS instrument [5]. The detector has an active area of 345mm x 345mm with a pixel size of 5mm x 5mm. The position resolution perpendicular to the wire depends on the wire spacing which practically cannot be made smaller than 1 mm. The second disadvantage is the low counting rate which arises due to build up of cloud of positive charge around the anode.

Microstrip Proportional Counters

Microstrip Detector (Fig. 7) was introduced by A. Oed in 1988 [6]. The wires of the MWPC are

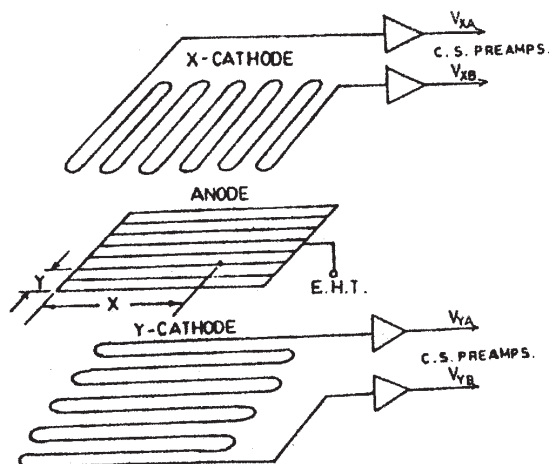


Fig. 6 Principle of operation of a MWPC

replaced by alternating anode (8-10 μm) and cathode (100-200 μm) strips deposited on a suitable insulating substrate using photolithographic technique. The anode pitch is typically 200-400 μm . The microstrip plate operates as gas amplifier just like a proportional counter. The ion cloud produced in avalanche does not have to drift towards the detector cathode, but only to neighbouring cathode strips. Since the structure is made in micrometer dimensions, the position resolution should be comparable. An energy resolution of 1.3% (FWHM) and position resolution of 2.2 mm (FWHM) for thermal neutrons have been reported. The MS plate can be converted in to a 2-D PSD by adding an array of thin metallic strips on the rear side of the plate, orthogonal to the microstrip structure. At BARC microstrip detector with anode: 12 μm , Cathode: 300 μm , anode-cathode gap: 150 μm and an active area of 25mm x 25mm has been developed in collaboration with IISc, Bangalore.

Detection Techniques in Neutron Radiography

Neutron radiography is a non-destructive testing technique that is widely used in the nuclear and aerospace industries. It is similar to X-radiography insofar as both techniques use beams of penetrating radiation to interrogate an object, and generate an image that allows visualization of areas that attenuate the beam differently than neighbouring areas (Fig. 8). However, neutrons are

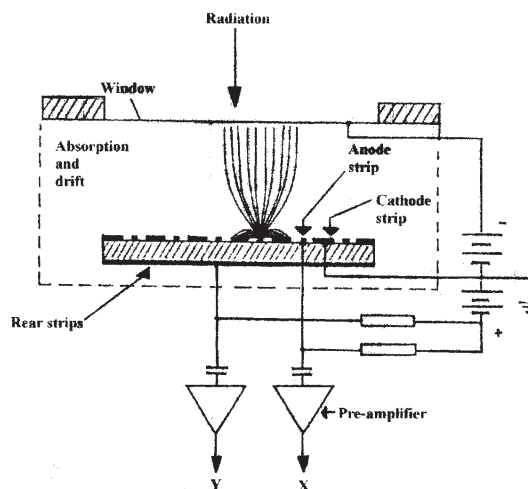


Fig. 7 Schematic cross-sectional view of Microstrip Gas Counter (MSGC)

attenuated very differently than X-rays, and therein lie the differences. Creation of images from the attenuated neutron beam can be accomplished in a variety of ways. X-ray film and a suitable conversion screen are frequently used [7].

Direct Method

In this method, X-ray film is placed on the source side of a converter screen and exposed to neutron beam that emerge out of the object. The film is exposed by the prompt electron emission from the converter screen upon neutron capture. Since the film is exposed to the beam and to the sample, this method is not suitable for radioactive materials. A commonly used conversion screen is a thin foil of Gd metal.

Indirect or Transfer Method

When radioactive materials are being inspected, thin foils of either Dy or In are generally used. These become radioactive in the neutron beam. After sufficient exposure, the foils are removed from the beam and placed in close contact with an X-ray film. The radioactive decay of the foil causes darkening of the X-ray film. Subsequent development of the film yields a radiograph. Since the film is never exposed to the beam itself, this method yields pure neutron radiographs.

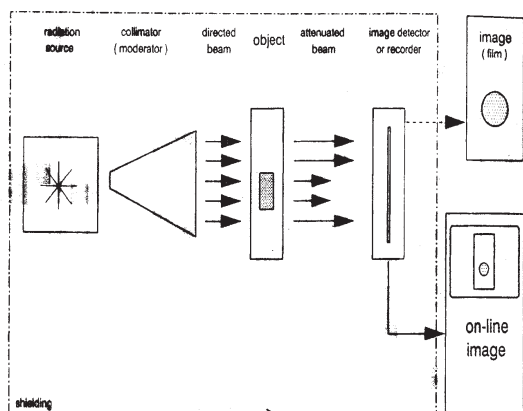


Fig. 8 Basic principle of Neutron Radiography

Track-Etch Imaging

If a plastic film in close contact with a material that yields heavy ions upon neutron absorption is exposed to a neutron beam, then the generated heavy ions will produce damage in the plastic film. These damaged areas will be more easily dissolved than other areas. Thus, etching of the plastic with a suitable reagent (e.g. 6N NaOH) will yield damage pits. Under suitable lighting these pits will be rendered visible. The film based imaging provides a resolution of $\sim 30\mu\text{m}$. Neutron radiographs of some of the objects taken with direct and indirect methods using Apsara NR facility are shown in Fig. 9.

Electronic Imaging Method

This method produces neutron images on a video monitor. It is especially attractive for the high-throughput inspection of parts requiring instant feedback of information. At BARC, an electronic imaging system based on NE-426 neutron scintillator, image intensifier and a CCD camera has been developed for static and dynamic radiography and tomography [8]. The most useful source of information related to NR methods, imaging technologies and applications are the proceedings of

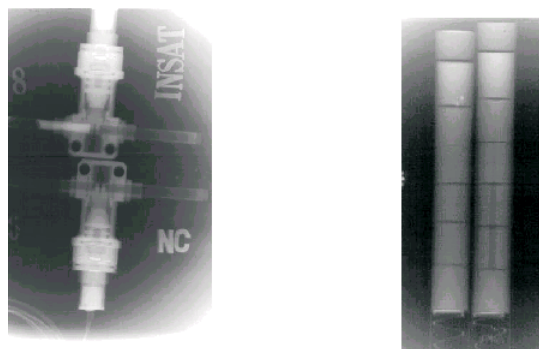


Fig. 9 Radiographs of INSAT provalve and PHWR fuel pins recorded with NR facility at Apsara

the six World Conferences on Neutron Radiography held 1981 in San Diego, 1986 in Paris, 1989 in Osaka, 1992 in San Francisco, 1995 in Munich and 1999 in Osaka.

References

1. G.F. Knoll, Radiation Detection and Measurement, II edition, John Wiley & Sons, 1989.
2. G.L. Miller et al., Nucl. Instr. and Meth., **91** (1971) 389.
3. Position-Sensitive Detection of Thermal Neutrons, edited by P. Convert and J.B. Forsyth, Academic Press, London, 1983, p20.
4. G. Charpak, R. Bouclier, T. Bressani, J. Favier and C. Zupancic, Nucl. Instr. and Meth., **62** (1968) 235 and **65** (1968) 217.
5. A.M. Shaikh, A.K. Patra, J.N. Joshi and N.D. Kalikar, Solid State Physics (India), **39C** (1996) 422.
6. A. Oed, Nucl. Instr. and Meth., **A263** (1988) 351.
7. H. Berger, Neutron Radiography, Elsevier Publication, Amsterdam, 1965.
8. A. Sinha, A.M. Shaikh and A. Shyam, Nucl. Instr. and Meth., **B142** (1998) 425.

Large Scale Radioisotope Production



Shri M. Ananthakrishnan joined the Atomic Energy Establishment in 1966 after doing his post-graduation in Chemistry from Madras University. He has vast experience in handling large levels of radioactivity and has incorporated various techniques for the processing of a number of radiochemicals. He is responsible for the processing and supply of a number of reactor produced radioisotopes which find extensive applications in medicine, industry, agriculture and research. He has the expertise in handling radioactive gases in vacuum system. He is presently Head, Radiochemicals Section, RPhD, BARC.

Shri S.V.Thakare, joined 30th batch of BARC training School after obtaining his M.Sc degree from Nagpur University, Nagpur. He joined the Isotope Division in 1987. He is looking after the irradiation of various targets in different reactors.



Shri K.V.S.Sastry obtained his M.Sc degree from Osmania University, Hyderabad. He has graduated from 21st batch of BARC training school in Physics. He has worked initially in the preparation and characterization of Tritium targets. From 1989 he has been working in BRIT. At present he is the Senior Manager in SS & R, BRIT looking after the production of sealed sources

Large volume radioisotope production has been an ongoing activity in India since the sixties to meet the ever increasing demand for the use of radiation and radioisotope in industry, agriculture, healthcare and research. Research reactors in Trombay, Apsara, Cirus and Dhruva- are utilized for the production of these isotopes and nuclear reactions such as $X(n,\gamma)Y$, $X(n,\gamma)Y \rightarrow Z$ or $A(n,p)B$ are employed. The radiochemical processing involves simple dissolution, solvent extraction, ion-exchange or oxidation-reduction and presently over 10 kCi of various radioisotopes are handled

every month. About 4000 consignments are being supplied every month to more than 1900 user institutions in India and abroad.

Production of Radioisotopes in a research reactor

Radioisotopes are produced in a nuclear reactor by exposing appropriate target material to the neutrons in the reactor. The factors which decide the type of nuclear reaction that takes place and the rate of production of the product are:

1. The energy of the neutrons and neutron flux

Shri M. Ananthakrishnan, Shri S.V. Thakare, Radiopharmaceuticals Division, Bhabha Atomic Research Centre, Mumbai 400 085
Shri K.V.S. Sastry, Board of Radiation and Isotope Technology, Mumbai; E-mail : svt@apsara.barc.ernet.in

TABLE 1. Nuclear reactions for the production of major radioisotopes

| Isotope | T _{1/2} | Nuclear reaction | Absorption cross section(σ) | Period of irradiation | No. of cans in reactor | Area of applications |
|-------------------|------------------|----------------------------------------------------------------------------------|--------------------------------------|-----------------------|------------------------|----------------------------------------------------|
| ¹³¹ I | 8 d | ¹³⁰ Te(n, γ) ¹³¹ Te \rightarrow ¹³¹ I | 67 mb | 3 weeks | 4x3 cans | Medical - thyroid disorder |
| ⁹⁹ Mo | 67 h | ⁹⁸ Mo(n, γ) ⁹⁹ Mo | 0.13b | 1 week | 9 cans | Source of ^{99m} Tc -Medical diagnostic |
| ³² P | 14 d | ³² S(n,p) ³² P | 165mb | 6-8 weeks | 3x12 cans | Medical, agriculture. Nucleotide labelling |
| ⁵¹ Cr | 27 d | ⁵⁰ Cr(n, γ) ⁵¹ Cr (Szilard-chalmers) | 0.69b | 1 week | 3 cans | Medical; Biochemical research |
| ¹⁵³ Sm | 47 hr | ¹⁵² Sm(n, γ) ¹⁵³ Sm (enriched target) | 206b | 1 week | 1 can | Medical Therapy |
| ¹⁹² Ir | 74d | ¹⁹¹ Ir(n, γ) ¹⁹² Ir | 370b | 3 months | 12 cans | Industrial radiography and brachytherapy |
| ⁸² Br | 35.4 h | ⁸¹ Br(n, γ) ⁸² Br | 1.6b | 4-7d | On request | Industrial tracer |
| ⁴⁶ Sc | 84 d | ⁴⁵ Sc(n, γ) ⁴⁶ Sc | 22b | 7d | On request | Industrial tracer |
| ²⁰³ Hg | 47 d | ²⁰² Hg(n, γ) ²⁰³ Hg | 1.13b | 2-3 months | On request | Industrial tracer |

2. The characteristics and quantity of the target material
3. The activation cross-section for the desired reaction

Energy of neutrons in the pile ranges from a few meV to a few MeV. Depending on neutron energy neutrons are called thermal neutrons (0.025eV), epithermal neutrons (keV range) and fast neutrons (with energy above 1 MeV) and the distribution of energy of neutrons in the reactor varies from point to point. The neutron interaction with the nucleus of the target material can be expressed quantitatively in terms of nuclear cross section. It is a measure of the probability that a given nuclear reaction takes place. The unit of cross-section is 'barn' (10⁻²⁴ cm²). The value of the cross section varies with the energy of the neutrons and from nucleus to nucleus. The maximum value of cross section is for thermal neutrons and are the most important component of neutrons spectrum for large scale radioisotope production.

The term neutron flux refers to the product of neutron density and the average speed and is expressed as n/cm²/sec.

Table 1. lists the major radioisotopes that are in regular production and their areas of application.

Facilities in Research Reactors for Radioisotope Production

Various irradiation facilities like self serve, tray rod, slug rod and pneumatic facilities are available in these reactors, for the isotope production. The target material can be irradiated in these facilities from a few seconds to several years. Of these, self-serve and tray rod positions are regularly used for radioisotope production normally. Both on-power or off-power unloading of target from the tray rod is resorted to depending upon the requirement.

Self Serve

This facility is used for short half life isotopes which require irradiation times from a few hours to

days. This facility is housed at the periphery of the reactor core. There are about thirty self serve positions in Cirus where the flux varies from $1.7 \times 10^{12} \text{ n/cm}^2/\text{sec}$ to $1.4 \times 10^{13} \text{ n/cm}^2/\text{sec}$. Cooling air is passed through the self serve units to maintain the temperature of the samples within the permissible limits.

Tray Rod

High specific activity radioisotopes are produced by irradiating target materials in specially designed tray-rod where neutron flux is high. The time of irradiation varies from a few days to months and years depending upon the isotope to be produced. Tray-rod consists of various trays into which the samples are housed. The entire assembly with suitable shielding on top is called the tray rod assembly. Tray rod assembly is normally cooled with air or water to minimise the temperature of the structural material and that of the containers. The target material is enclosed in standard aluminum cans having dimension of 22mm diameter and 46 mm height. This sealed aluminium can is then housed in the tray rod. A single tray rod in CIRUS can hold 30 aluminium cans while DHRUVA tray rod can hold 90 aluminium cans. The flux in Cirus tray rod varies from $1.4 \times 10^{13} \text{ n/cm}^2/\text{sec}$ to $6.7 \times 10^{13} \text{ n/cm}^2/\text{sec}$, while in Dhruva reactor the flux in tray rod varies from $1.44 \times 10^{13} \text{ n/cm}^2/\text{sec}$ to $1.8 \times 10^{14} \text{ n/cm}^2/\text{sec}$ at full power.

Target Container

Target material to be irradiated for production of radioisotopes is sealed in an aluminium container of a standard size and an identification number is punched for all subsequent handling. High purity aluminium is chosen for container material because of its low neutron absorption cross section, good thermal conductivity and ease of fabrication of capsules.

Choosing the Target Material

1. Substances which are explosive, pyrophoric, volatile etc. are not permitted to be irradiated in reactor.
2. Targets should be stable under irradiation conditions.

3. Isotopically pure target gives high specific activity radioisotopes.
4. The physical form of the target should be such that the neutron flux depression is minimum.
5. The target should be in a suitable chemical form for post irradiation processing. Usually target in metallic form or oxides is preferred.
6. If the target is hygroscopic, it is preferable to preheat the target prior to encapsulation.

Irradiation Procedure

Irradiation of target material in a reactor and its subsequent handling involves

1. Radioisotope sample request form with details of target material, quantity, irradiation time and isotope required.
2. Evaluation of reactivity load, cooling required and shielding by the Reactor Physics group.
3. Testing and loading of aluminium cans in appropriate irradiation position
4. Unloading the sample after the completion of irradiation. Extraction and loading into a suitable lead flask and
5. Safe transportation to Radiological Labs for further processing and shipment to different users

Irradiation of Target in Different Research Reactors for Isotope Production

Generally, targets are irradiated for two half-lives of the activation product of interest. In practice, the achievable activity level in any target can be quite different from the theoretically calculated value. Self-shielding factor becomes appreciable in the case of thick targets with high absorption cross section. Target burn-up factor becomes important when the irradiation is extended over a long period in a high neutron flux. The effect of these factors on activity build-up can be estimated theoretically and ascertained experimentally. Power variation in the reactor, flux depression due to adjacent targets and depletion of the product nucleus due to subsequent neutron capture also contribute to this effect. In certain cases, contribution from epithermal neutrons leads to an enhancement in the

activity produced as compared to the theoretical calculation e.g. in the case of ^{99}Mo , ^{153}Sm etc..

The ratio of the activity actually developed in the target to the activity calculated using basic activation equation is referred to as the irradiation efficiency. The value of irradiation efficiency depends on the cumulative effect of all factors mentioned earlier and is experimentally determined by trial irradiation.

APSARA

Apsara is swimming pool type reactor with enriched uranium as fuel. The maximum flux obtainable in this reactor is around $1 \times 10^{13} \text{ n/cm}^2/\text{sec}$, and the maximum thermal power of the reactor is 1MW. Because the reactor is water cooled, the targets are not heated to any appreciable temperature, and hence encapsulation procedures are simple. Introduction of targets for irradiation and removal after irradiation could be carried out easily using simple gadgets. Apsara is ideally suited for the production of short lived radioisotopes. However, it is not useful for production of high specific activity radioisotopes nor for large quantity.

CIRUS

Cirus is natural uranium fuelled, heavy water moderated and light water cooled reactor with a maximum thermal power of 40MW. In Cirus, target materials are irradiated in different irradiation facilities such as tray rod, self-serve, adjuster rod and pneumatic carrier facilities for routine irradiations. The maximum neutron flux available (at full power) in tray rod is $6 \times 10^{13} \text{ n/cm}^2/\text{sec}$ and approximately $1.5 \times 10^{13} \text{ n/cm}^2/\text{sec}$ in self-serve position. The targets are enclosed in standard cold aluminium capsules of 22mm ϕ X 46mm. From 1991 -1997 irradiation of 673 cans of MoO_3 , 240 cans of tellurium, 940 cans of sulphur, 46 cans of iridium, 1300 miscellaneous and 1300 service irradiations were carried out in CIRUS.

DHRUVA

Dhruva reactor, with maximum thermal power of 100MW, is natural uranium fuelled, heavy water moderated and cooled reactor. The maximum flux (at full power) in this reactor is $1.8 \times 10^{14} \text{ n/cm}^2/\text{sec}$. Although Dhruva reactor has irradiation facilities similar to Cirus, presently irradiation is carried out in

tray rod only. In Dhruva reactor 2600 cans of MoO_3 , 1350 cans of Te, 800 cans of sulphur, 350 cans of iridium, 1550 miscellaneous irradiation and 150 service irradiation were carried out during the period 1991-2001.

Production of Certain Medical Isotopes

The irradiated target is transferred to chemical processing plant in lead flasks. Processing is done in air-tight aluminium boxes fitted with remote handling tongs and other gadgets. The box is maintained at a negative pressure of 25-30mm WG to avoid release of radioactivity into the laboratory atmosphere.

Iodine-131

It is obtained by the irradiation of natural Te in the reactor. The production of this isotope is done on a weekly basis with about 60g of target Te for each batch giving a yield of 15-20 Ci of ^{131}I . A wet process of oxidation with $\text{H}_2\text{CrO}_4 + \text{H}_2\text{SO}_4$ mixture followed by reduction with oxalic acid is utilized for the separation of this isotope from the target. ^{131}I released is absorbed in Na_2SO_3 solution and supplied as Na^{131}I in alkaline sulphate solution. ^{127}I (stable) and ^{129}I ($T_{1/2}=1.6 \times 10^7 \text{ yr}$) are also produced from ^{126}Te and ^{128}Te during the irradiation of natural Te and presence of these isotopes of iodine leads to a reduction in the specific activity of product ^{131}I . This method yields large quantities of highly acidic, active liquid waste which poses post-production handling problems. An alternative method for the production of this important isotope through a dry distillation route using irradiated TeO_2 is being studied now. This process will result in higher concentration of ^{131}I solution with elimination of highly acidic, active liquid waste.

Phosphorus-32

This is obtained by the neutron irradiation of natural sulphur. Sulphur, after irradiation is distilled under vacuum to leave phosphorus in the flask. This phosphorus is leached with dil.HCl and then purified for removal of cationic impurities by passage through Dowex 50x8. The product ^{32}P is supplied as $\text{H}_3^{32}\text{PO}_4$ solution(Ortho phosphoric acid). In a batch, about 2-3Ci ^{32}P is produced fortnightly from 200g sulphur. In terms of weight, about 10-15 μg of

TABLE 2.

| Year | Medical Isotopes ¹³¹ I, ⁹⁹ Mo, ³² P, ¹⁵³ Sm, ⁵¹ Cr | Industrial tracers ²⁴ Na, ⁸² Br, ²⁰³ Hg, ¹⁹⁸ Au | Miscellaneous isotopes |
|---------|--------------------------------------------------------------------------------------------------------------|------------------------------------------------------------------------------------------------|------------------------|
| 1992-93 | 3020 Ci | 66 Ci | 40 Ci |
| 1994-95 | 2935 Ci | 40 Ci | 18 Ci |
| 1998-99 | 4057 Ci | 59 Ci | 23 Ci |
| 2000-01 | 3402 Ci | 75 Ci | 33 Ci |

phosphorus is separated from bulk of sulphur. Whereas the theoretical specific activity of this isotope is 9200Ci/mMole, we are presently able to achieve product quality with specific activity in the range of 3000-5000Ci/mMole. While this has been found to be acceptable for medical and agricultural uses, nucleotide labeling requires higher specific activity (>7000Ci/mMole) and attempts are on for improving the specific activity.

Molybdenum-99

There are two ways for production of ⁹⁹Mo isotope: (1) by the fission of Uranium and (2) by the neutron absorption by natural molybdenum.

While the first method gives a product with very high specific activity, the latter process is fairly easy to adopt and is presently being followed. The natural MoO₃ on irradiation forms ⁹⁹Mo. The production process involves dissolution of the irradiated target in NaOH solution at ~60°C followed by filtration after cooling. This isotope is also processed on a weekly basis (25-30Ci/week) with specific activity ranging from 300-400mCi/g of Mo with ~135g of irradiated MoO₃ used in each batch. The daughter product of ⁹⁹Mo, namely ^{99m}Tc finds extensive application in diagnostic imaging studies. The excellent coordination chemistry of technetium makes it possible to form a variety of organ specific compounds which are used in the medical field.

Chromium-51

This isotope is produced in the reactor by the Szilard-Chalmer's process during the irradiation of potassium chromate. The difference in the valency state of ⁵¹Cr produced (+3) state is utilized in effecting chemical separation of the product from the target material containing Cr in +6 state. A typical batch production for this isotope is carried

out with ~30g of irradiated K₂CrO₄ yielding ~200-300mCi of ⁵¹Cr.

Production data for major radioisotopes [1992-2001] is presented in Table 2.

Industrial Tracers

Isotopes like ²⁴Na, ⁴⁶Sc, ⁸²Br, ¹⁹⁷Hg and ²⁰³Hg find extensive applications as industrial tracers. Pioneering contribution has been made for the development of suitable production methods for these radionuclides and their applications in industry for trouble-shooting and process control. The areas of radioactive tracer applications in industry include (1) studies on RTD in process vessels, (2) mixing and blending studies, (3) wear rate measurement, (4) leak detection and blockage location in buried pipelines and other industrial systems, (5) sediment transport (6) material inventory, and (7) effluent dispersion investigations.

The radioisotope tracers are produced, processed and supplied to customers as per their request. ⁸²Br is supplied as NH₄⁸²Br for aqueous studies whereas it is supplied as p-di-bromo-benzene (Br-82) for organic studies. Similarly, ¹³¹I can be supplied as Na¹³¹I or CH₃¹³¹I depending upon the use. Mercury-203, in the elemental form, is used in mercury inventory studies in alkali industries and has got excellent export potential. 3-5Ci (111-185GBq) of this isotope is exported to European countries annually after meeting the local demand of about 3 Ci (111GBq).

Iridium-192 Sources

Production of Industrial radiography Sources

Gamma Radiography using ¹⁹²Ir sealed sources is a useful tool in the non-destructive testing

technology. Annually 750 sources with an activity of 30,000 Curies are being used for the above application. Natural iridium in the form of metal pellets is irradiated in the research reactors to form ^{192}Ir with the required specific activity. Pre irradiation handling involves packing of the iridium pellets in aluminium foil and sealing in the aluminium can with minimum shielding to the inner pellets.

The irradiated can is brought to the hot cell and can is cut open with a tube cutter inside the hotcell. The activity range of the pellets is measured and required number of pellets is dispensed in the stainless steel capsule. Welding of these capsules is carried out using Tungsten inert gas (TIG) welding. These capsules are cleaned, decontaminated, tested for surface contamination and leakage. The activity of the capsules are measured, crimped and loaded in the respective pigtails and cameras.

Atomic Energy Regulatory Board (AERB) has prescribed certain performance classification requirements, which will take care of the possible accidental conditions. Dummy capsules are tested for the parameters, viz., high temperature, low temperature, temperature quenching, high pressure, low pressure, impact, puncture and vibration tests. The ^{192}Ir source capsule has passed all the tests and is accorded performance classification E65515. The activity of each source varies from 10 Ci to 60 Ci. Around 30,000 Ci of ^{192}Ir activity is being supplied annually in 750-800 sources during the last 10 years.

^{192}Ir wire for Brachytherapy

^{192}Ir in the form of 0.3 mm diameter wire comprising of Iridium-Platinum alloy wire of 0.1 mm dia (with Ir-25 % and Pt 75%) sheathed in pure platinum of 0.1 mm thick is used for the treatment of cancer by brachytherapy. The requirement of the activity is 1 mCi/cm to 7 mCi/cm depending of the size and location of the cancerous tissue. This activity is supplied in lengths of 50 Cm or 100 Cm in the coil form. These wires are irradiated in Dhruva reactor in low flux positions. This wire is coiled and sealed in an aluminum container and is irradiated in the reactor. After the irradiation, loose contamination on the wire is checked, activity of the wire is measured and supplied to the hospitals.

Around 15-19 Ci of ^{192}Ir activity in the form of wire in 60-70 meters length is being supplied annually for brachytherapy.

Conclusions

The present requirement of radioisotopes for different applications in medicine, industry, agriculture and research in our country is being met by the effective utilization of the research reactors in Trombay, mainly Dhruva. While shortly CIRUS reactor is likely to be available for regular use, the need for an additional reactor dedicated for radioisotope production is being keenly felt. In order to enter into assured commitment for radioisotope supply for international market and to meet the continuous increase in the indigenous demands for use in medicine and industry, a new research reactor with higher neutron flux ($\geq 5 \times 10^{14} \text{ n.cm}^{-2}.\text{s}^{-1}$) and dedicated for radioisotope production will be highly desirable for the future. Certain emerging needs for radionuclides like ^{188}W - ^{188}Re meant for specific medical applications and which require higher neutron flux for production, can be also obtained from the new high flux reactor. The indigenous capability built and nurtured at BARC/BRIT can thus continue to contribute to meeting the national demands, apart from leading to possible exports.

Acknowledgements

Radioisotope production programme has been an on-going activity of our Department for more than four decades and many eminent scientists have made invaluable contributions in this regard. The names of Dr. V.K. Iya, Shri T.S. Murthy, Shri R.H. Krishnan, Shri V.C. Nair and Shri S.R.K. Iyer, who were responsible for development/ institution of many of the production processes / practices, deserve a special mention. A number of persons past and present, have contributed for the successful maintenance of an uninterrupted supply of a variety of radiochemicals to the end users and we express our sincere thanks to all of them. The authors sincerely thank Dr. N. Ramamoorthy, Chief Executive, BRIT and Associate Director, Isotope Group, BARC for his keen involvement in the radiochemicals programme and for always extending valuable support and advice.

Prospects and Challenges in Production of Radionuclides for Therapy



Dr. Meera Venkatesh is the Head, Radiopharmaceuticals Chemistry Section, Radiopharmaceuticals Division, BARC and General Manager, Quality Control, Medical and Biological Products Programme, Board of Radiation and Isotope Technology. She has been chiefly interested in radiolabelled bio-molecules, radioimmunoassays and radiopharmaceutical chemistry. Dr. Meera has served as an IAEA expert and as an invited associate professor at the University of Missouri, Columbia, USA. She is a recognised guide for M.Sc. and Ph.D. She has published over 80 papers in the international journals, international and national symposia/conferences and has authored a few invited articles.

Dr. M.R.A. Pillai is the Head, Radiopharmaceuticals Division, BARC and Senior General Manager, Medical and Biological Products Programme, Board of Radiation and Isotope Technology. His research interests include radioimmunoassay, monoclonal antibodies, production of isotopes and radiopharmaceuticals chemistry. He has worked as a Visiting Professor in the University of Missouri-Columbia, USA and was a technical cooperation expert for IAEA in Algeria, Ethiopia, Sri Lanka and Egypt. He is a guide for M.Sc. And Ph.D. of the University of Mumbai. He is one of the Founder Fellows of the Indian College of Nuclear Medicine and currently Secretary, Society of Nuclear Medicine. Dr. Pillai has co-authored a book, contributed chapters in books and Encyclopaedia, edited several monographs, published about 90 papers in international journals and presented over 100 papers in national international conferences.



Dr. N. Ramamoorthy is presently Associate Director, Isotope Group, BARC and Chief Executive of Board of Radiation and Isotope Technology (BRIT). Dr. Ramamoorthy's research interests include radiopharmaceuticals chemistry and production of reactor and cyclotron based radioisotopes. Dr. Ramamoorthy has served as a technical cooperation expert for IAEA in Iran, Uganda, Libya and Turkey and as a Visiting Assistant Professor in the University of Missouri-Columbia, USA. Dr. Ramamoorthy is a research guide for M.Sc. and Ph.D. Degrees in Chemistry of the University of Mumbai, a Member of Editorial Committee of the Indian Journal of Nuclear Medicine, a Founder Fellow of Indian College of Nuclear Medicine and a Fellow of Maharashtra Academy of Sciences. Dr. Ramamoorthy has published about 140 papers in international journals, national and international symposia, co-authored a book and a manual and contributed chapters in several books / manuals.

Dr. V. Meera, Dr. M.R.A. Pillai and Dr. N. Ramamoorthy, Isotope Group, Bhabha Atomic Research Centre, Mumbai 400 085 and Board of Radiation in Isotope Technology, Mumbai, E-mail: meeraav@apsara.barc.ernet.in, ambi@magnum.barc.ernet.in, cebrit@britatom.com

Introduction

Treatment of cancer using beams of radiation from external sources such as ^{60}Co (teletherapy), is well established and known. However, use of radiolabelled bio-molecules for therapeutic purposes by administration into the body was limited to the use of ^{131}I for treatment of thyroid disorders such as hyperthyroidism and thyroid cancers, for the past several decades. In the recent times, there has been phenomenal change in the modalities of treatment of cancer. Use of radionuclide based preparations '*in-vivo*' is one of the promising modalities for cancer therapy.

Although the basic principle of cell damage due to particulate radiations has been known since long and several groups have been reviewing the suitability of various beta and alpha emitting radionuclides for therapy of different types of tumors [1-6], the progress was very slow. Knowledge and the availability of bio-active molecules that can target tumors/cancer lesions in the recent times, has been a major factor responsible for the development in this area. Currently, antibodies, peptides and many smaller bio-molecules have been shown to target tumours, resulting in active research in this area of therapeutic radiopharmaceuticals.

Radionuclide Characteristics

One of the important considerations in the development of therapeutic radiopharmaceuticals is the radionuclide to be employed. Selection of a radionuclide is guided by characteristic radiation emitted, its energy, abundance, half-life etc. As a thumb rule, beta emitters with half-lives between a few hours to a few days are preferred. Presence of a small component of gamma (< 200 keV) is an additional advantage since one could image and ensure/ monitor the localisation of the radiopharmaceutical. The choice of the radionuclide will also depend on the actual therapeutic effect envisaged. For example, when a large organ or a lesion is to be treated, the radiations will have to be better penetrating (highly energetic) while if the organ/lesion is small, particularly in the vicinity of other critical organs, the range of radiations should be smaller. The list of potential therapeutic

radionuclides is quite large, while the ones that are actually widely used are limited.

In the Indian context, radionuclides and radiopharmaceuticals are being produced and supplied to the user laboratories/clinics/hospitals since several decades. In the recent past, novel therapeutic radiopharmaceuticals have been developed and are currently being supplied to hospitals. The radionuclides for therapy are selected after consideration of important factors such as availability of the target nuclide, capture cross-section for its production, the requirements of purity, specific activity and the amount of the radionuclide required, the feasibility of labeling the bio-molecule with the radionuclide and so on. Using the medium flux nuclear reactors that are available for production of radionuclides, several therapeutic radionuclides could be prepared and used. Table 1 lists most of the novel radionuclides under consideration/experimentation currently. The prospects appear very bright for therapy using a wide variety of radionuclides listed. However, in practice, there are several challenges to be met at every stage beginning with production to realization of the therapeutic effect.

As we see from Table 1, all the potential therapeutic radionuclides are particle emitters – beta, alpha or Auger electron. The ranges of these particles in tissue decides the use to which they can be put to and in order to achieve the therapy aimed, the particle energy/range should match the final location of the radiopharmaceutical molecule in the tissue. The adjoining figure depicts the dependence of range of tissue penetration with the energy of the beta particles/Auger electrons.

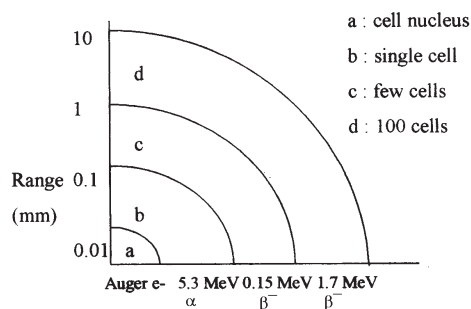


TABLE 1. Radionuclides for therapeutic applications

| Radionuclide | T _{1/2} | Mode of decay | Particle, Energy | Route of Production |
|--------------------------------------------------|------------------|----------------|---------------------------|----------------------------------------------------------------------------------------------------------------------------------------------------------|
| Auger/Conversion electrons | | | | |
| ¹²⁵ I | 60 d | E.C. | Auger e ⁻ | ¹²⁴ Xe(n,γ) ¹²⁵ Xe $\xrightarrow{\text{E.C.}}$ ¹²⁵ I |
| ^{117m} Sn | 14 d | I.T. | conversion e ⁻ | ¹¹⁶ Sn(n,γ) ^{117m} Sn |
| β ⁻ emitters E _β (Max) MeV | | | | |
| ³² P | 14.3 d | β ⁻ | 1.71 | ³² S(n,p) ³² P |
| ⁸⁹ Sr | 50.5 d | β ⁻ | 1.49 | ⁸⁸ Sr(n,γ) ⁸⁹ Sr |
| ⁹⁰ Y | 2.67d | β ⁻ | 2.28 | ⁸⁹ Y(n,γ) ⁹⁰ Y ; ⁹⁰ Sr(β ⁻) ⁹⁰ Y (Generator) |
| ¹⁰⁵ Rh | 2.4 d | β ⁻ | 0.6 | ¹⁰⁴ Ru(n,γ) ¹⁰⁵ Ru $\xrightarrow{\beta^-}$ ¹⁰⁵ Rh |
| ¹⁵³ Sm | 1.95 d | β ⁻ | 0.8 | ¹⁵² Sm(n,γ) ¹⁵³ Sm |
| ¹⁶⁶ Ho | 1.1d | β ⁻ | 1.6 | ¹⁶⁵ Ho(n,γ) ¹⁶⁶ Ho |
| ¹⁶⁹ Er | 9.4 d | β ⁻ | 0.34 | ¹⁶⁸ Er(n,γ) ¹⁶⁹ Er |
| ¹⁷⁵ Yb | 4.2 d | β ⁻ | 0.5 | ¹⁷⁴ Yb(n,γ) ¹⁷⁵ Yb |
| ¹⁷⁷ Lu | 6.74 d | β ⁻ | 0.5 | ¹⁷⁶ Lu(n,γ) ¹⁷⁷ Lu |
| ¹⁸⁶ Re | 3.77 d | β ⁻ | 1.08 | ¹⁸⁵ Re(n,γ) ¹⁸⁶ Re |
| ¹⁸⁸ Re | 17 h | β ⁻ | 2.13 | ¹⁸⁶ W(n,γ) ¹⁸⁷ W(n,γ) ¹⁸⁸ W(β ⁻) ¹⁸⁸ Re; (Generator) ¹⁸⁷ Re(n,γ) ¹⁸⁸ Re |
| α emitter E _α (Ave) MeV | | | | |
| ²¹¹ At | 7.2 h | α, , E.C. | 6.8 | ²⁰⁹ Bi(α,2n) ²¹¹ At |

For example, if a molecule labelled with ¹²⁵I localises on the tumour cell wall, there will be no therapeutic effect as the deleterious effect of the shower of Auger electrons will never reach the DNA or cell nucleus. On the other hand, if the molecule were to enter the cell and reside on the DNA backbone, the therapeutic effect is achieved very effectively without disturbing the other healthy cells! Similarly the alpha emitters will need to localize very close to the target tissue; or else there will be more damage than therapy!

Reactor Production Considerations

Although several radionuclides are identified as potential therapeutic nuclides, not all have been employed to formulate radiopharmaceuticals, often due to unfavourable production route or half life which result in very poor yields and difficult logistics. The Auger/conversion electron emitters, barring ¹²⁵I, which are accelerator produced and the

alpha emitters are seldom possible to be produced and supplied on a regular basis. Nuclear reactors provide the only economic means of large scale production of therapeutic radionuclides, which are always needed in larger quantities. Appropriate mechanised/remote handling process gadgets would be essential for this purpose apart from other requirements.

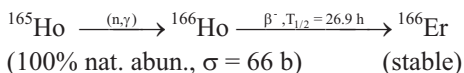
In practice, the preference in terms of features such as half-life may vary between a well developed country with excellent transport facilities and one with moderate facilities. In a country like India, half-life of a few days may be more advantageous than a few hours, avoiding waste as well as the requirement of heavy shielding to transport much higher amounts of activity than what would be used on the patient!

An attempt is made here to look at some of the radionuclides from the point of producing them and

supplying them as labelled molecules keeping in mind the Indian context.

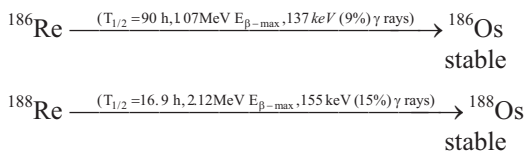
Some Major Therapeutic Radionuclides

¹⁶⁶Ho



¹⁶⁶Ho is an ideal therapeutic radionuclide being explored for various therapeutic applications. The salient features of ¹⁶⁶Ho are emission of β^- rays with E_{max} of 1.85 MeV (8-9 mm maximum soft tissue penetration), emission of 81 keV γ rays (6%) suitable for monitoring the injected radiopharmaceutical and possibility of producing high specific activity & high radionuclidic purity grade ¹⁶⁶Ho in adequate quantities by irradiating natural Ho target in reactors with medium thermal neutron flux. Typically, 5-6 mg of Ho₂O₃ irradiated at neutron flux of $3 \times 10^{13} \text{ n/cm}^2/\text{s}$ for 7 days yields 30-40 GBq (800-1080 mCi) of ¹⁶⁶Ho with a specific activity of $\sim 7.5 \text{ GBq/mg}$ (200 mCi/mg) after a cooling period of 6 hours. Formation of ^{166m}Ho ($T_{1/2} = 1200 \text{ y}$) along with ¹⁶⁶Ho has been cited as one disadvantage. However, our own repeated experiments have yielded ¹⁶⁶Ho without any contamination with ^{166m}Ho since the radioactivity due to ^{166m}Ho produced will be insignificant in short irradiations owing to its very long half life although the cross sections are nearly equal.

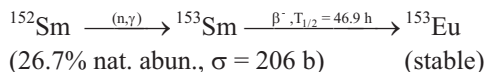
^{186/188}Re



Both ¹⁸⁶Re and ¹⁸⁸Re are potential therapeutic radionuclides owing to their favorable decay characteristics. Radionuclides of Re are often preferred for therapy owing to their chemical similarity with Tc since generally the actual therapy with a radiopharmaceutical is preceded by a study with a diagnostic nuclide, most often ^{99m}Tc, to ensure that the bio-molecule indeed homes in the target organ. Despite the attractive features of the rhenium radionuclides, their use is still very limited due to the unfavourable production conditions associated.

Typically, irradiation of natural rhenium metal for ~ 7 days at a flux of $3 \times 10^{13} \text{ n/cm}^2/\text{s}$, $\sim 80 \text{ mCi/mg}$ of ¹⁸⁶Re could alone be produced after a cooling period of a week. ¹⁸⁸Re: ¹⁸⁶Re ratio is nearly 3:2 at EOB and in order to avail nearly pure ¹⁸⁶Re (i.e. with $< 5\%$ ¹⁸⁸Re) a cooling period of minimum 5 d ($\approx 7 T_{1/2}$ of ¹⁸⁸Re) is necessary. This amounts to uneconomical utilisation requiring handling of large amounts of ¹⁸⁶Re activity. Alternately, enriched ¹⁸⁵Re target can be used to more effectively utilise the reactor irradiation capability, especially for large scale production of ¹⁸⁶Re. The problems associated with ¹⁸⁸Re production and ¹⁸⁸W-¹⁸⁸Re generator are discussed later.

¹⁵³Sm



¹⁵³Sm is a very useful radionuclide for various therapeutic applications because of its ideal radionuclidic characteristics such as 46.9 h half life, 810 keV $E_{\beta-\text{max}}$ (soft tissue range 3.5 mm) and 103 keV (28.3%) γ photon. Moreover ¹⁵³Sm can be produced in adequate specific activity by irradiating the natural Sm₂O₃ target in a reactor with acceptably high radionuclidic purity. The specific activity and radionuclidic purity could be enhanced further by the use of enriched ¹⁵²Sm₂O₃ target whenever required for specific applications.

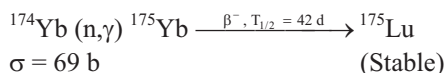
The typical yield of ¹⁵³Sm for 7 d irradiation at a thermal neutron flux of $3 \times 10^{13} \text{ n/cm}^2/\text{s}$ is 11 GBq/mg (300 mCi/mg) when using natural targets and around 44 GBq/mg (1200 mCi/mg) with enriched targets. The epithermal neutron activation leads to the higher yields. The average level of radionuclidic impurity burden at 2 days after production are 0.37 kBq (10 nCi) ¹⁵⁴Eu, 5.55 kBq (150 nCi) ¹⁵⁵Eu and 37 kBq (1 μCi) ¹⁵⁶Eu per 37 MBq (1 mCi) of ¹⁵³Sm in case of natural Sm target. In the case of enriched ¹⁵²Sm (98%) target, the level of ¹⁵⁴Eu is expectedly similar, while ¹⁵⁵Eu and ¹⁵⁶Eu burden are negligible. The criteria on the tolerance limits of the Eu radionuclides would hence set the stipulations of whether natural target be used or enriched.

¹⁷⁷Lu

¹⁷⁷Lu is another radioisotope with very good potential for use in *in vivo* therapy. ¹⁷⁷Lu decays with a half-life of 6.74 d by emission of β^- particles with E_{\max} of 497 keV (78.6%), 384 keV (9.1%) and 176 keV (12.2%) to stable ¹⁷⁷Hf. It also emits γ photons of 113 keV (6.4%) and 208 keV (11%), ideally suited for imaging. Although the physical half life of ¹⁷⁷Lu is relatively longer (compared to ¹⁵³Sm or ¹⁸⁶Re), it is within reasonable limits for therapeutic purpose and will in addition provide logistic advantages for facilitating supply to far off places. ¹⁷⁷Lu can be produced in reactors with moderate to high thermal neutron flux, either by irradiation of Lu₂O₃ target (natural ¹⁷⁶Lu, 2.6% or ¹⁷⁶Lu enriched) or by irradiation of Yb₂O₃ target followed by radiochemical separation of ¹⁷⁷Lu from Yb isotopes. Direct (n, γ) activation of natural Lu₂O₃ powder leads to ¹⁷⁷Lu of low specific activity which could be enhanced manifolds by using enriched ¹⁷⁶Lu target and by increasing duration of irradiation. On the other hand, second route gives high specific activity (no carrier added) ¹⁷⁷Lu. However, in this technique radiochemical separation of ¹⁷⁷Lu activity from irradiated Yb₂O₃ target is very crucial because of the radionuclidic purity requirement.

The typical yield of ¹⁷⁷Lu from natural as well as enriched targets for 7 d irradiation in Dhruva reactor are 4 GBq/mg (148 mCi/mg) and 100 GBq/mg (3.7 Ci/mg), respectively, again aided by contribution of epithermal neutron activation. The radionuclidic purity of ¹⁷⁷Lu produced from either natural or enriched target is ~100% as ascertained by analysing the γ ray spectrum. There is a possibility of formation of ^{177m}Lu ($T_{1/2}$ = 160.5 d) on thermal neutron bombardment of Lu₂O₃ target (low cross-section σ = 7 barns). Trace level of ^{177m}Lu activity is assessed by recording γ ray spectrum (at 128, 153, 228, 378, 414, 418 keV) of a sample aliquot, initially having high radioactive concentration, after complete decay of ¹⁷⁷Lu activity. The average level of radionuclidic impurity burden due to ^{177m}Lu was found to be 5.5 kBq of ^{177m}Lu/ 37 MBq of ¹⁷⁷Lu (150 nCi/1 mCi) at EOB. Here too, the limits of tolerance for ^{177m}Lu in ¹⁷⁷Lu would in turn define the irradiation target and conditions.

¹⁷⁵Yb



Ytterbium-175 is yet another potential radioisotope having excellent properties suitable for therapy. ¹⁷⁵Yb decays ($T_{1/2}$ 4.2 d, 80% β^- , $E_{\beta-\max}$ 480 keV, s 113 keV-1.9%, 282 keV-3.1%, 396 keV-6.5%) to stable ¹⁷⁵Lu. As in ¹⁷⁷Lu, longer half life provides logistic advantage for transportation. Ytterbium-175 can be produced by thermal neutron bombardment of natural ytterbium target. The radionuclidic impurities formed on irradiation of natural ytterbium target include ¹⁶⁹Yb (¹⁶⁸Yb (n, γ) 2300 b) and ¹⁷⁷Lu (¹⁷⁶Yb (n, γ) 2.4 b) and ¹⁷⁷Yb (¹⁷⁷Lu β^- , $T_{1/2}$ 1.9 h). Among these, ¹⁶⁹Yb ($T_{1/2}$ = 32 d) decays by electron capture process (100% K electron capture) followed by the emission of Auger electrons of low yield and the principal γ photons are of reasonably low energy [177 keV (22.5%), 197 keV (35.9%)], but somewhat in higher abundance than desired. It is hence envisaged that the presence of low amounts of ¹⁶⁹Yb should not cause any serious problem in the *in vivo* application of ¹⁷⁵Yb. On the other hand, the presence of ¹⁶⁹Yb will be useful in extended studies of the pharmacological characteristics of the ¹⁷⁵Yb-labelled radiopharmaceuticals in biological systems. ¹⁷⁷Lu is the other radionuclidic impurity which is itself a potential therapeutic radionuclide. The radionuclidic characteristics of ¹⁷⁷Lu as well as its chemical properties are very similar to those of ¹⁷⁵Yb. Hence, the presence of ¹⁷⁷Lu in very small quantities in the ¹⁷⁵Yb produced should not restrict the use of the latter in the *in vivo* therapy. It is also feasible to separate ¹⁷⁷Lu from the ¹⁷⁵Yb. Typically, 1200 GBq/g (35 Ci/g) of ¹⁷⁵Yb can be produced with >95% radionuclidic purity (with ~3% of ¹⁶⁹Yb and ~2% of ¹⁷⁷Lu) by irradiating natural Yb₂O₃ target at a thermal neutron flux of 310^{13} n/cm²/s for a period of 5 days.

Radionuclides of Difficult Production Logistics

There are a few radionuclides which have excellent physico-chemical properties for therapy while their production in reasonable quantities demand special facilities/conditions. Some of these are discussed below.

^{117m}Sn

^{117m}Sn with 13.6 d half-life, 86.3% E_γ of 159 keV and copious conversion electron emission has been advocated by the Brookhaven National Laboratories for very efficacious bone pain treatment as the marrow can be almost completely spared of radiation dose deposition, tissue range being just 0.2-0.3 mm. However, ¹¹⁶Sn present at 14.8% abundance has low neutron absorption cross-section of only 0.006 b. Thus the activation yields are very low in medium flux reactors and unlikely for large scale deployment.

⁸⁹Sr

⁸⁹Sr with a half life of 50.5 d and E_{β-max} of 1.49 MeV being a calcium analog is preferred for bone pain palliation in terminally ill cancer patients. Despite the very high abundance of ⁸⁸Sr in natural Sr (82.6%), the very low neutron absorption cross-section (0.0058 b) warrants deployment of neutron flux of > 510¹⁴ n/cm²/s for production of meaningful quantities of ⁸⁹Sr. Hence Centres with very high flux reactors (Belgium, USA etc.) hold the monopoly of its production.

¹⁸⁸Re from ¹⁸⁸W-Re generator

As mentioned earlier, ¹⁸⁸Re (T_{1/2} 16.9 h, E_{β-max} 2.13 MeV and 15% E_γ 155 keV) is an ideal therapeutic radionuclide. For a generator system, its precursor ¹⁸⁸W (T_{1/2} 69.4 d) is obtained by successive neutron capture of ¹⁸⁶W (28.6% abundance, σ 38 b and then 70 b). Predictably a high flux reactor with > 510¹⁴ n/cm²/s neutron flux would alone lead to large scale production of ¹⁸⁸W. Alternate means of accessing ¹⁸⁸Re warrants use of enriched ¹⁸⁷Re targets and short frequent irradiation cycles placing a higher demand on reactor irradiation facility making it very expensive.

⁹⁰Y

⁹⁰Y (T_{1/2} 2.7 d, E_{β-max} 2.3 MeV) is yet another radionuclide widely used for therapy, particularly for large organ irradiation such as liver cancers, radiation synovectomy of knee joints etc. due to 12 mm tissue range. ⁹⁰Y too can be obtained from two different modes; either from a ⁹⁰Sr-⁹⁰Y generator or neutron capture of ⁸⁹Y. ⁹⁰Sr (T_{1/2} 28.6 y, E_{β-max} 0.55 MeV) itself is a major fission product in nuclear

reactors which could be separated and purified from the high level waste. However, this is a challenging job requiring handling of large amounts of radioactive waste. Moreover, the tolerance limits for ⁹⁰Sr is extremely low (< 2 μCi in a dose of 30-50 mCi of ⁹⁰Y) since it is a very long lived nuclide which will localise in the skeleton being calcium analog. Thus, the technique for separation of ⁹⁰Y from ⁹⁰Sr has to be extremely efficient. The quality assurance methods to ensure ⁹⁰Sr levels lower than permissible levels in the ⁹⁰Y also need to be well developed which is a challenging task as both ⁹⁰Sr and ⁹⁰Y do not have any gamma emission. Process Development Division, BARC has successfully demonstrated the separation of ⁹⁰Sr from the high level waste and the ⁹⁰Y could be used to satisfaction in many radiopharmaceutical preparations. However, regular production and supply of such ⁹⁰Sr-⁹⁰Y generators would be a capital intensive challenging task. The alternate route of producing ⁹⁰Y by neutron irradiation of ⁸⁹Y suffers from the disadvantages of many other nuclides listed above. Although ⁸⁹Y is present in 100% abundance, the σ is just 1.3 b resulting in poor yields. Also ⁸⁹Y(n,p)⁸⁹Sr reaction occurs concurrently and separation of ⁸⁹Sr (T_{1/2} 50.5 d) adds to the complexity of radiochemical processing.

Other Miscellaneous Radionuclides

¹⁶⁹Er, ¹⁰⁵Rh, ¹²⁵I [10] etc. – belong to a category wherein the use is limited to few special needs or the process is so complicated that other radionuclides would cater to the needs. ¹⁶⁹Er (T_{1/2} 9.4 d, E_{β-max} 343 keV) is used for radiation synovectomy of phalangeal (finger) joints due to the very low beta energies. The quantities needed are low and the activation of natural Er (26.8% ¹⁶⁸Er, σ 1.95 b) target leads to several other unwanted Er radionuclides of which one leads to a long lived daughter. Thus ¹⁶⁹Er necessarily needs to be produced by irradiating enriched ¹⁶⁸Er target. ¹⁰⁵Rh T_{1/2} 35.4 h, E_{β-max} 0.6 MeV) is produced by irradiation of ¹⁰⁴Ru (nat. ab. 18.7 %, σ 0.32 b followed by its decay (T_{1/2} 4.4h). Although the radionuclide can be obtained in “no-carrier added” form, the chemical processing is lengthy and involves oxidation and sublimation of ruthenium oxide which have limited its use. Use of ¹²⁵I (T_{1/2} 60 d, Auger electron emitter) for therapy is again limited to molecules that can be targeted into the cell or even better the cell nucleus. Such

molecules are very few such as analogues of uridine, being tested for their efficacy. ^{125}I as well as ^{103}Pd find use as brachytherapy sources in some cancers such as ocular cancer and prostate cancers. ^{103}Pd is accelerator produced while ^{125}I needs special set-up in the reactor for compressed gas irradiation with on-line processing facilities, since ^{124}Xe (σ 110 b) has to be irradiated to get ^{125}I .

Quality Control Aspects of Targets

In general, lanthanide targets need to be ascertained for their purity in terms of the activation products formed upon exposure to the reactor neutrons. Even small traces of other lanthanide contaminants could lead to unfavourable radionuclide impurities in the product of interest. Due to similarity in chemistry and in general short $T_{1/2}$, post-irradiation radiochemical processing is not an easy option to follow.

The following aspects assume significance and determine the extent of utilisation of nuclear reactors for the production of therapeutic radionuclides and products labelled with them.

- Activation yield,
- Specific activity of the product
- Radionuclidic purity and characteristics of radionuclidic impurities
- Chemical characteristics of radionuclide element
- Simplicity of post-irradiation handling
- Target – purity, availability and cost

Conclusion

India ranks high in the list of nations capable of producing large quantities of such therapeutic radionuclides. In order to enhance the reliability of product availability and to meet pre-committed supply schedules with near zero failure rate, two reactors working in tandem mode would be ideal. Dhruva has been the mainstay of India's radioisotope production programme, while Cirus is expected to continue to play a good supportive role.

Considering the age of these reactors and the envisaged demands of therapeutic radionuclides in the immediate as well as distant future, an additional reactor with higher flux and greater dedicated operation towards radioisotope production would be essential. This warrants augmentation of reactor irradiation capability, direct delivery of irradiated cans from the reactor to the hot cells at production laboratories, flexible irradiation schedules and remote handling and processing of the radionuclides in the hot cells. A dedicated reactor with all the above mentioned facilities would indeed be needed to stride into the world of therapeutic radiopharmaceuticals.

The new reactor facility would not only ensure keeping India in the forefront of production and application of radioisotopes, but also open up possible avenues for exports to other countries in Asia and also Europe.

References

1. Radionuclides for Therapy, Proceedings of the 4th Bottstein Colloquium, Wurenlingen/Villigen, Switzerland, 1986, Eds. P.A. Schubiger and P.H. Hasler, Roche editon, Bases.
2. W.A. Volkert, W.F. Goeckeler, G.J. Erhardt and A.R. Ketrang, J. Nuclear Medicine, 32 (1991) 174.
3. D. Scott Wilbur, Antitbody, Immuno-conjugates and Radiopharmaceuticals, 4 (1991) 85.
4. M.R. Zalutsky, in Hadron therapy in oncology, Eds. U. Amaldi and B. Larsson, Elsevier Science, 1995.
5. S.M. Qaim, Radiochimica Acta, 89 (2001) 297.
6. V.J. Lewington, European J. of Nuclear Medicine, 20 (1993) 66.
8. N. Ramamoorthy, P. Saraswathy, M.K. Das, K.S. Mehra and M. Ananthakrishnan, Nuclear Med. Comm., 23 (2002) 83.
9. M. Venkatesh, V. Pandey, P.S. Dhami, R. Kannan et.al., Radiochim Acta, 89 (2001) 413.
10. B. Grazman and D.E. Troutner, Applied Radiation and Isotopes, 39 (1988) 257.